PERFORMANCE ANALYSIS OF METAL HYDRIDE-BASED HYDROGEN STORAGE SYSTEM

NUR AIN AMIRAH BINTI RUSMAN

DISSERTATION SUBMITTED IN FULFILMENT OF THE REQUIREMENTS FOR THE DEGREE OF MASTER OF ENGINEERING SCIENCE

FACULTY OF ENGINEERING
UNIVERSITY OF MALAYA
KUALA LUMPUR

2018

UNIVERSITY OF MALAYA

ORIGINAL LITERARY WORK DECLARATION

Name of Candidate: (I.C/Passport No:)

Matric No:

Name of Degree:

Title of Project Paper/Research Report/Dissertation/Thesis (“this Work”):

Field of Study:

I do solemnly and sincerely declare that:

(1) I am the sole author/writer of this Work;
(2) This Work is original;
(3) Any use of any work in which copyright exists was done by way of fair dealing and for permitted purposes and any excerpt or extract from, or reference to or reproduction of any copyright work has been disclosed expressly and sufficiently and the title of the Work and its authorship have been acknowledged in this Work;
(4) I do not have any actual knowledge nor do I ought reasonably to know that the making of this work constitutes an infringement of any copyright work;
(5) I hereby assign all and every rights in the copyright to this Work to the University of Malaya (“UM”), who henceforth shall be owner of the copyright in this Work and that any reproduction or use in any form or by any means whatsoever is prohibited without the written consent of UM having been first had and obtained;
(6) I am fully aware that if in the course of making this Work I have infringed any copyright whether intentionally or otherwise, I may be subject to legal action or any other action as may be determined by UM.

Candidate’s Signature Date:

Subscribed and solemnly declared before,

Witness’s Signature Date:

Name:

Designation:

PERFORMANCE ANALYSIS OF METAL HYDRIDE-BASED HYDROGEN STORAGE SYSTEM

ABSTRACT

Energy is one of the basic requirements in our daily lives. The world's energy demand is continuously increasing over the years due to the ever-increasing growth in the human population as well as economic development. At present, approximately 90% of energy demand are fulfilled by fossil fuels. With the rising demands of energy throughout the globe, it can be expected that the availability of fossil fuels is depleting at an alarming rate since fossil fuels are non-renewable sources of energy. In addition, fossil fuels are the main contributor of greenhouse gas emissions and therefore, they have a detrimental impact on human health and environment in the long term. Hence, there is a critical need to develop alternative sources of energy in replacement of fossil fuels. For that reason, hydrogen fuels have gained much interest among researchers all over the world since they are clean, non-toxic and renewable energy source. However, the greatest challenge in using hydrogen fuels lies in the development of hydrogen storage systems, especially for on-board applications. Current technologies used for hydrogen storage include high-pressure compression at about 70 MPa, liquefaction at cryogenic temperature (20 K) and absorption into solid state compounds. Among the three types of hydrogen storage technologies, the storage of hydrogen in solid state compounds appears to be the most feasible solution since it is a safer and more convenient. Because of that, hydrogen stored in solid state as metal hydride has been studied for this project. In this project, a three-dimensional dynamic simulation for metal hydride based hydrogen storage tank was performed using Computational Software COMSOL 5.1a Multiphysics. The software is used to simulate the charging process in the metal hydride container that is able to represent the system's behavior. The model consists of a system of partial differential equations (PDE) describing three dimensional heat and mass transfer of hydrogen in a porous matrix and has been implemented in a finite element program that allows obtaining results on the charging variables at different studied scenarios. The model is validated against published data and later the simulation result is compared with experimental data to validate experimentally the numerical simulation. The effects of different parameters such as porosity (ε), permeability (K), metal thermal conductivity (k_m), hydrogen absorption constant on metal (c_a), activation energy (E_a) and heat transfer coefficient (h_{ct}) on the metal hydride behavior during hydrogen gas absorption are investigated. The validation of the mathematical model is concluded to achieve a good agreement between all the data while the simulation and experimental results show agreement with each other having small deviation between $0.0 \sim 2.5\%$. Lastly, the sensitivity analysis indicated that the effective thermal conductivity was the most sensitive parameters for this system while other parameters such as porosity, permeability and heat transfer coefficient carried little effect on the system.

Keywords: Energy, Hydrogen storage, Metal hydride, Absorption, COMSOL Multiphysics

ANALISI PRESTASI SISTEM PENYIMPANAN HIDROGEN BERASASKAN HIDRIDA LOGAM

ABSTRAK

Tenaga adalah salah satu keperluan asas dalam kehidupan seharian manusia. Sejak beberapa tahun kebelakangan ini, permintaan dunia terhadap tenaga terus meningkat disebabkan oleh pertumbuhan masyarakat serta pembangunan ekonomi yang semakin pesat. Pada masa ini, kira-kira 90% daripada permintaan terhadap tenaga dipenuhi oleh bahan api fosil. Dengan permintaan tenaga yang semakin meningkat di seluruh dunia, dijangkakan bahawa ketersediaan bahan api fosil akan semakin berkurang pada kadar yang membimbangkan kerana bahan api fosil adalah sumber tenaga yang tidak boleh diperbaharui. Selain itu, bahan api fosil adalah penyumbang utama pelepasan gas rumah hijau yang membawa kesan yang buruk kepada kesihatan manusia dan alam sekitar untuk jangka masa panjang. Oleh itu, terdapat keperluan kritikal untuk membangunkan sumber tenaga alternatif untuk menggantikan bahan api fosil. Disebabkan itu, hidrogen sebagai sumber bahan api telah mendapat perhatian di kalangan penyelidik di seluruh dunia kerana ianya bersih, tidak toksik dan sejenis sumber tenaga yang boleh diperbaharui. Walau bagaimanapun, cabaran yang paling besar dalam menggunakan bahan api hidrogen terletak pada pembangunan sistem penyimpanan hidrogen, terutama untuk aplikasi system pengangkutan. Teknologi semasa yang digunakan untuk penyimpanan hidrogen sekarang adalah termasuk mampatan tekanan tinggi pada kira-kira 70 MPa, pencairan pada suhu kriogenik (20 K) dan penyerapan ke dalam sebatian pepejal. Antara tiga jenis teknologi penyimpanan hidrogen, penyimpanan hidrogen dalam keadaan sebatian pepejal muncul sebagai penyelesaian yang paling boleh dilaksanakan kerana ia adalah lebih selamat dan lebih mudah. Disebabkan itu, hidrogen yang disimpan dalam keadaan pepejal sebagai hidrida logam telah dikaji dalam projek ini. Dalam projek ini, simulasi dinamik tiga dimensi untuk tangki simpanan hidrogen berasaskan logam hidrida telah dilaksanakan dengan menggunakan perisian pengiraan Multiphysics COMSOL 5.1a. Perisian ini digunakan untuk mensimulasikan proses penyerapan hidrogen dalam logam hidrida yang mampu mewakili kelakuan sistem. Model ini merangkumi sistem persamaan pembezaan separa (PDE) yang menggambarkan pemindahan haba dan jisim hidrogen dalam tiga dimensi dalam matriks berliang. Model ini disahkan dengan data yang pernah diterbitkan oleh penyilidik sebelum ini dan keputusan simulasi kemudian dibandingkan dengan data eksperimen untuk mengesahkan simulasi berangka. Selepas itu, kesan parameter yang berbeza seperti keliangan (ε), kebolehtelapan (K), kekonduksian terma logam (k_m), pemalar hidrogen berterusan pada logam (c_a), tenaga pengaktifan (E_a) dan pekali pemindahan haba (h_{ct}) Semasa penyerapan gas hidrogen disiasat. Selain itu, penyelidikan ini juga akan memberi tumpuan kepada pengoptimuman parameter operasi untuk prestasi sistem hidrida logam. Pengesahan model matematik disimpulkan untuk mencapai persetujuan yang baik di antara semua data sementara hasil simulasi dan percubaan menunjukkan kesepakatan antara satu sama lain dengan sisihan kecil antara 0.0 ~ 2.5%. Akhir sekali, analisis kepekaan menunjukkan bahawa kekonduksian terma yang berkesan adalah parameter yang paling sensitif untuk sistem ini sementara parameter lain seperti keliangan, kebolehtelapan dan pekali pemindahan haba membawa sedikit kesan ke atas sistem.

Kata kunci: Tenaga, Peyimpanan hidrogen, Hidrida logam, Penyerapan, COMSOL Multiphysics

ACKNOWLEDGEMENTS

First and foremost, I would like to acknowledge the assistance and guidance of my supervisor, Associate Prof. Ir. Dr. Mahidzal Bin Dahari, who allowed me to work on his project and helped guide me through my research. I want to thank him for his patience with me and willingness to spend additional time helping me complete this thesis. I also would like to express my gratitude to the University Malaya (UM) Hydrogen Fuel Cell laboratory for giving me the opportunity to do the necessary research work while providing me with all the necessary resources and elements. Lastly, I would like to thank my family, especially my parents for their encouragements and my dear friends for their active assistance.

TABLE OF CONTENTS

performance analysis of metal hydride-based hydrogen storage system iii

analisi prestasi sistem penyimpanan hidrogen berasaskan hidrida logam v

Acknowledgements vii

Table of Contents viii

List of Figures xiii

List of Tables..xvi

List of Symbols and Abbreviations xvii

CHAPTER 1: INTRODUCTION..1

1.1 Energy ……………………………………………………………………..1

1.2 Hydrogen as Clean Energy 2

1.3 Hydrogen Storage 4

1.3.1 Compressed Gas Hydrogen 5

1.3.2 Cryogenic Liquid Storage..5

1.3.3 Physical Storage with High Surface Area Material (Adsorbed hydrogen) 6

1.3.4 Chemical Storage in Solid State Material (Metal Hydrides)......................7

1.4 Hydrogen Storage Target..8

1.5 Problem Statement..9

1.6 Research Objectives..10

1.7 Scopes 10

1.8 Thesis Outlines 11

CHAPTER 2: LITERATURE REVIEW..13

2.1 Metal Hydrides 13

2.2 Hydrides Material Review..14

2.2.1 Intermetallic Compound 14

2.2.1.1 AB_5- type alloys 15

2.2.1.2 AB-type alloys 16

2.2.1.3 AB_2-type (Laves phase) alloys 17

2.2.1.4 AB_3-type alloys 17

2.2.1.5 A_2B-type alloys 17

2.2.1.6 Solid solution alloys 18

2.2.2 Complex Hydrides 18

2.2.2.1 Alanates 19

2.2.2.2 Borohydrides 23

2.2.2.3 Nitrides 27

2.2.3 Chemical hydrides 28

2.2.3.1 Ammonia Borane 28

2.2.4 Magnesium-based Alloys 29

2.3 Fundamentals of Metal/Hydrogen Interactions 30

2.3.1 Thermodynamics of Metal/Hydrogen Interactions 30

2.3.2 Kinetics of Metal Hydrides 33

2.4 Metal Hydrides Modelling Review 37

2.4.1 One Dimensional Approach: Model Limitations 37

2.4.2 Two and Three-Dimensional Models 40

CHAPTER 3: METHODOLOGY 43

3.1 Introduction 43

3.2 Description of Dynamic Model 44

3.2.1 Model Assumption 45

3.2.2 Governing Equations 45

3.2.2.1 Mass conservation 46

3.2.2.2 Momentum conservation 47
3.2.2.3 Energy conservation 47
3.2.3 Initial Conditions 48
3.2.4 Boundary Conditions 49
3.2.5 Implementation of System into COMSOL Multiphysics 49
3.2.5.1 Physics Mode 49
3.3 Validation of Mathematical Model 51
3.3.1 Overview of the Model 51
3.3.1.1 Geometry 52
3.3.1.2 Material 52
3.3.1.3 Parameters used in Simulation 53
3.4 Validation of Actual Simulation 53
3.4.1 Overview of the Model 54
3.4.1.1 Geometry 54
3.4.1.2 Material 55
3.4.1.3 Parameters used in Simulation 56
3.4.1.4 Mesh Sensitivity Analysis 57
3.4.2 Experimental Set Up 57
3.5 Sensitivity Analysis of Metal Properties 60
3.6 Optimization on Metal Hydrides System 61

CHAPTER 4: RESULT AND DISCUSSION 62
4.1 Introduction 62
4.2 Modelling Results 62
4.2.1 Pressure 62
4.2.2 Temperature 63
4.2.3 Metal Hydrides Density 64

4.3 Validation of Mathematical Model 65

4.3.1 Temperature Evolution 65

4.3.2 Equilibrium Pressure as a Function of hydrogen/ metal (H/M) 66

4.4 Actual Simulation 67

4.4.1 Mesh Sensitivity Analysis 67

4.4.2 Actual Simulation Results 71

4.4.2.1 Temperature 71

4.4.2.2 Mass of Hydrogen Absorbed 74

4.5 Validation of Actual Simulation 77

4.5.1 Temperature 77

4.5.2 Mass of Hydrogen Absorbed 78

4.6 Sensitivity Analysis 79

4.6.1 Porosity (ε) 80

4.6.2 Permeability 82

4.6.3 Thermal Conductivity (k_m) 83

4.6.4 Hydrogen Absorption Constant on Metal (c_a) 85

4.6.5 Activation Energy (E_a) 86

4.6.6 Heat Transfer Coefficient (h) 88

4.7 Effect of operating condition 89

4.7.1 Charging pressure 89

4.7.2 Bed Temperature 91

CHAPTER 5: CONCLUSION & RECOMMENDATION 94

5.1 Conclusion 94

5.2 Recommendation 96

References 97

List of Publications and Papers Presented 107

LIST OF FIGURES

Figure 2.1: (a) Phase diagram showing the transformation from α-phase to β-phase for metal hydride; (b) Van’t Hoff plot derived from isotherms for various temperatures (Züttel, 2003)........31

Figure 2.2: Simplified one-dimensional potential energy curve (Züttel, 2003)........34

Figure 3.1: Geometry of metal hydride tank in COMSOL........52

Figure 3.2: Geometry of the actual metal hydride tank in COMSOL........55

Figure 3.3: Hydrogen test rig located at Hydrogen Fuel Cell laboratory of University of Malaya (UM)........58

Figure 3.4: Simple experimental set up diagram........58

Figure 3.5: MH-350 Metal Hydride Canisters........60

Figure 4.1: Relative gas pressure inside the canister over time. Point located r = 0 mm, z = 30 mm........63

Figure 4.2: Temperature inside the canister over time. Point locate r = 25 mm, z = 30 mm........64

Figure 4.3: Metal hydride density over time. Point located r=0, z=0........65

Figure 4.4: (a) Temperature evolution profiles obtained by Wang et al. (2009); (b) Temperature evolution profiles obtained in this project........66

Figure 4.5: (a) The equilibrium pressure as a function of the H/M atomic ratio and temperature for hydrogen absorption by Mellouli et al. (2010) (b) The equilibrium pressure as a function of the H/M atomic ratio and temperature for hydrogen absorption this project........66

Figure 4.6: The characteristics of each types of mesh (a) Extra coarse; (b) Coarser; (c) Coarse; (d) Normal; (e) Fine; (f) Finer; (g) Extra fine........68

Figure 4.7: Density of metal hydrides bed for different types of mesh size at point r = 0 mm, z = 150 mm........69

Figure 4.8: Temperature of metal hydrides canister for different types of mesh size at point r = 0 mm, z = 150 mm........70

Figure 4.9: Temperature of metal hydride canister over time. Point located r = 0 mm, z = 322 mm........72

Figure 4.10: Temperature profiles in half of a cross-section of the hydrogen storage canister at (a) 0 s; (b) 100 s; (c) 200 s; (d) 300 s; (e) 400 s; (f) 500 s and (g) 600 s 74

Figure 4.11: Mass of hydrogen gas absorbed over time. Point located at r = 0 mm, z = 150 mm 75

Figure 4.12: Density distribution in half of a cross-section of the hydrogen storage vessel at (a) 0 s, (b) 100 s, (c) 200 s, (d) 300 s, (e) 400 s, (f) 500 s and (g)600 s 76

Figure 4.13: Temperature comparison between simulation and experimental data at point r = 0 mm, z = 322 mm........ 77

Figure 4.14: Comparison of hydrogen mass absorbed between simulation and experimental data at point r = 0 mm, z = 150 mm 79

Figure 4.15: Density of metal hydride over time at different porosity values. Point located at r = 0 mm, z = 150 mm........ 81

Figure 4.16: Temperature of metal hydride canister over time at different porosity values. Point located r = 33 mm, z = 150 mm........ 82

Figure 4.17: Density of metal hydride over time at different permeability values. Point located at r = 0 mm, z = 150 mm 83

Figure 4.18: Temperature of metal hydride canister over time at different permeability values. Point located r = 33 mm, z = 150 mm 83

Figure 4.19: Density of metal hydride over time at different thermal conductivity values. Point located at r = 0 mm, z = 150 mm........ 85

Figure 4.20: Temperature of metal hydride canister over time at different thermal conductivity values. Point located r = 33 mm, z = 150 mm 85

Figure 4.21: Density of metal hydride over time at absorption rate constant values. Point located at r = 0 mm, z = 150 mm 86

Figure 4.22: Temperature of metal hydride canister over time at different absorption rate constant values. Point located r = 33 mm, z = 150 mm 86

Figure 4.23: Density of metal hydride over time at different activation energy values. Point located at r = 0 mm, z = 150 mm........ 87

Figure 4.24: Temperature of metal hydride canister over time at different activation energy values. Point located r = 33 mm, z = 150 mm........ 87

Figure 4.25: Density of metal hydride over time at different heat transfer coefficient values. Point located at r = 0 mm, z = 150 mm........ 88

Figure 4.26: Temperature of metal hydride canister over time at different heat transfer coefficient values. Point located r = 33 mm, z = 150 mm 89

Figure 4.27: Figure 4.27: Density of metal hydride over time at different charging pressure values. Point located at r = 0 mm, z = 150 mm 90

Figure 4.28: Temperature of metal hydride canister over time at different charging pressure values. Point located r = 33 mm, z = 150 mm 90

Figure 4.29: Density of metal hydride over time at different bed temperature values. Point located at r = 0 mm, z = 150 mm 92

Figure 4.30: Temperature of metal hydride canister over time at different bed temperature values. Point located r = 33 mm, z = 150 mm 92

LIST OF TABLES

Table 1.1: General characteristics of basic hydrogen storage methods 4

Table 1.2: Summary of targets for hydrogen storage systems set by DOE 8

Table 3.1: Table of physics mode and implementation of governed equations 51

Table 3.2: List of parameters used in simulation for **LaNi5** system 53

Table 3.3: List of properties of $Ti_{0.99}Zr_{0.01}V_{0.43}Fe_{0.09}Cr_{0.05}Mn_{1.5}$ alloy 56

Table 3.4: List of parameters and operating conditions used in the simulation 56

Table 3.5: List of parameters used in the parametric studies for each parameter. 61

Table 3.6: Operating value used in the optimization studies for charging pressure and temperature 61

Table 4.1: Density values of metal hydrides bed for different types of mesh size at point r = 0 mm, z = 150 mm 69

Table 4.2: Temperature values of metal hydrides canister for different types of mesh size at point r = 0 mm, z = 150 mm 70

Table 4.3: Summarization of total mesh size and solution time of each mesh type 71

Table 4.4: Temperature comparison between simulation and experimental data at point r = 0 mm, z = 322 mm 78

Table 4.5: Comparison of hydrogen mass absorbed between simulation and experimental data at point r = 0 mm, z = 150 mm 79

LIST OF SYMBOLS AND ABBREVIATIONS

General symbols

c	Heat capacity	$\mathrm{J/kg.K}$
Ca	Absorption constant	s^{-1}
d	Diameter	m
E	Energy	$\mathrm{J/mol}$
Ea	Activation energy	$\mathrm{J/mol}$
$\vec{g}$	Gravity	ms^{-2}
h	Heat Transfer Coefficient	$\mathrm{W/m^2.K}$
k	Thermal conductivity	$\mathrm{W/m.K}$
K	Permeability	m^2
m	Mass	g
M	Molar weight	$\mathrm{g/mol}$
$\vec{n}$	Normal vector unit	-
P	Pressure	$bar/\ Pa$
Q	Heat	J
R	Gas constant	$\mathrm{J/mol.K}$
S	Source Term	$-$
t	Time	s
T	Temperature	$\mathrm{K/\ ^\circ C}$
$\vec{u}$	Velocity	ms^{-1}

Greek letters

ΔH	Reaction enthalpy	$\mathrm{J/mol}$

ΔS	Reaction entropy	$\mathrm{J/mol.K}$
ε	Porosity	$-$
μ	Hydrogen dynamic viscosity	$\mathrm{Pa.s}$
π	Pie	$-$
ρ	Density	$\mathrm{kg/m^3}$

Sub-/ Superscripts

0	Initial
amb	Ambient
atm	Atmosphere
C	Chemisorbed
D	Dissociation
e	Effective
eq	Equilibrium
ext	Exterior
g	Gas
h	Hydrogen
in	Inlet
m	Metal
p	Particle
P	Physisorbed
ref	Reference
sat	Saturated
T	Energy (source term)

Abbreviations

DAE	Differential Algebraic Equation
DOE	Department of Energy
MH	Metal Hydride
ODE	Ordinary Differential Equation
SEM	Scanning Electron Microscope
UM	University Malaya

CHAPTER 1: INTRODUCTION

1.1 Energy

The world energy demand is increasing with the increase in human population and pursuit of higher standards of living (Baladincz & Hancsók, 2015). To meet the human needs for energy, a large amount of fuel is widely utilized from various fossil resources (Ashraful et al., 2014). This results in the risen of all types of fossil fuels production in the late 20th and early 21st centuries (Kontorovich et al., 2014). Fossil fuels, mainly petroleum-based liquid fuels, natural gas and coal, are important for global energy demands, accounting for more than 80% of the world global primary energy consumption (Mohr et al., 2015). Therefore, human society, with its expansion and high technological development, is very dependent on petroleum fuel for its activities (Banković-Ilić et al., 2014).

Unfortunately, the production and utilization of fossil fuel cause environmental problems, for example, rising carbon dioxide levels in the atmosphere. Carbon dioxide is the main greenhouse gas, and about 75% of the carbon dioxide emission is due to the burning of fossil fuels. Emissions of carbon dioxide have been the topic of worldwide debate in regard to the sustainability of energy and stability of the global climate (Ball & Wietschel, 2009). During the next decades, the most challenging environmental tasks is to reduce the impacts of global warming from the burning of fossil fuels (Hoel & Kverndokk, 1996).

It is undeniable that combustion of fossil fuels has caused serious detrimental environmental consequences. Due to their non-renewable nature, fossil fuels are projected to be exhausted in the near future as it takes millions of years to form with limited reserves and high prices. This situation has worsened with the rapid rise in energy demand with significant worldwide population growth (Ashraful et al., 2014). Since fossil fuels are a limited resource, it can be predicted that by 2020–2030 mankind has to face the challenges arising from the sustainability of conventional oil production.

In conclusion, the world is moving toward an energy crisis with the depletion of conventional, non-renewable, fossil- based fuel, which forcing the human society to look for other alternatives. The depleting of fossil fuel based energy has triggered research and development works on alternative source for reliable, environmentally friendly and yet economically feasible renewable energy (Issariyakul & Dalai, 2014).

1.2 Hydrogen as Clean Energy

With the existed energy crisis, clean energy technologies, such as biofuels, wind, solar, hybrid electric, geothermal, and hydrogen has grown worldwide interest in recent years (Garland et al., 2012). However, for this type of energy sources, a safe and clean energy carrier is needed to ensure an environmentally friendly energy system. With the development of the proton exchange membrane (PEM) fuel cell, hydrogen has been seen as a potential solution for this crisis. Proton exchange membrane (PEM) fuel cell which is fuelled by hydrogen and oxygen, is harmless to the environment as it produces only water (Mao et al., 2012).

Assuredly, hydrogen is regarded as a promising solution for the current energy crisis (Orhan & Babu, 2015) and has attracted worldwide attention as a safe and clean energy carrier (Nath et al., 2015), (Klindtworth et al., 2018). Across the world, interest in hydrogen has been growing as a potential fuel for transportation and medium for energy storage (Ehret & Bonhoff, 2015). Such interest is primarily due to the potency of hydrogen for replacing fossil fuels in the transport sector and at the fact that hydrogen can be stored over for a long period of time (López González et al., 2015).

Most of world hydrogen productions are mainly from the non-renewable energy sources (S. Sharma & Ghoshal, 2015). However, hydrogen as energy carrier can be produced from both renewable and non-renewable sources. Unlike petroleum, which is non-renewable and produce pollutants, hydrogen can be generated from renewable energy sources and is free from pollutants, as its only produces water (Orhan & Babu, 2015). For long term sustainable hydrogen production, hydrogen can be produced from various renewable primary energy sources such as solar, wind, biogases, industrial waste streams and nuclear power (Brouwer, 2010). In short, hydrogen from renewable sources is regarded as a potential replacement for common fossil energy carriers (Tietze & Stolten, 2015).

Hydrogen has unique features that make it a promising secondary energy carrier. This includes the fact that it can be generated from and converted into electrical energy and is environmentally friendly since its production, storage and transportation do not produce any pollutants (Sherif et al., 2005). Hydrogen is very volatile and, possibly, it is very quickly dissipated in the surroundings. It is also practically impossible to make hydrogen explode except for a much reduced spaces (Cipriani et al., 2014). Besides, hydrogen is the lightest element in the periodic table of element, not toxic, nor corrosive and the most abundant element in the universe (Winter, 2009).

Hence, it is hopeful to promote a " hydrogen economy ", where hydrogen can be expected to substitute oil and natural gas in many applications, including transportation and heating (Shinnar, 2003). According to the approach of ‘hydrogen economy’, hydrogen can become the main secondary energy carrier at the end of the 21st century and will gradually replace fossil fuels (Marchenko & Solomin, 2015). The role of hydrogen in sustainable energy economy which requires full attention in terms of policy studies, researches and developments, as well as commercialization of the potential technologies (Andrews & Shabani, 2012).

Unfortunately, due to its gaseous property of low density, storage of hydrogen remains a big challenge (Mori & Hirose, 2009). Hydrogen storage system is regarded as one of the greatest obstacles, particularly for mobile application which must be resolved before an economically and technically viable hydrogen fuel system can be produced. Without an efficient storage system, 'hydrogen economy' will be a challenging task to be accomplished (Ball & Wietschel, 2009).

1.3 Hydrogen Storage

Hydrogen storage is often considered as the most crucial issue in order to obtain a 'hydrogen economy' free of environmental pollution and fossil fuel (Aceves et al., 2013). In order to meet the vehicle restrictive volume constraints, further compressing of the gaseous fuel is required for the hydrogen storage system. At the same time, the storage system must not badly affect the performance, design, and utility of the vehicle. At present, several methods are being considered to store hydrogen, e.g., high-pressure gas compression, cryogenic liquefaction, physically adsorbing porous materials and chemical solid storage materials (Paggiaro et al., 2010), (Zheng et al., 2012). Four basic methods that are used for hydrogen storage are being discussed in this chapter. General characteristics of the basic hydrogen storage methods are given in Table 1.1 (Demirbas, 2007).

Table 1.1: General characteristics of basic hydrogen storage methods

Storage Method	Pressure (bar)	Temperature (K)	Max capacity (wt. %)
Compressed Gas Hydrogen	800	298	13
Cryogenic Liquid Hydrogen	1	21	100
Physically Adsorbed Hydrogen	70	65	14
Chemical Storage (Metal Hydride)	1	298-500	2-18

1.3.1 Compressed Gas Hydrogen

Hydrogen act as a gas at room temperature and atmospheric pressure so it can be compressed at high pressure, typically 350-700 bars, in a vessel capable of high pressure (Hua et al., 2011). One of the advantages of hydrogen compression is that it provides fast transfer rates during refuelling and discharging process (Maus et al., 2008). Besides, the compressed hydrogen gas can be stored at an ambient temperature, thus avoiding costly thermal insulation (Ananthachar & Duffy, 2005). At present, compressed gas cylinder is the most commonly used hydrogen storage methods on vehicles (Züttel, 2003).

However, there are several issues with the current compressed hydrogen gas system. Apparently, the overall efficiency of this method is reduced as there are large energy losses during the compression of hydrogen. For instance, for compression to 800 bars, the energy loss is usually in the order of 12-16% (Westerwaal & Haije, 2008). Besides, compressed hydrogen storage system has relatively low volumetric density compared to other methods and stores the substantial mechanical compressive energy (~ 0.6kWh/kg H2), which can be abruptly discharged in case of vessel breakdown (Aceves et al., 2006; Paggiaro et al., 2010).

1.3.2 Cryogenic Liquid Storage

In a highly insulated vacuum vessel, hydrogen can be stored as liquid at very low temperatures (20K) through liquefaction (Ananthachar & Duffy, 2005). Liquefaction of hydrogen allows higher storage density and represent the ideal solution when a huge scale of hydrogen storage and long distance transportation is required (Trevisani et al., 2007). Other benefits of liquid hydrogen is it has high energy mass ratio which is three times that of gasoline and high volumetric density at low pressure, which allows light, compact and safe vehicular storage at considerably low cost (Aceves et al., 2013).

The liquid hydrogen technology has grown significantly in recent years, allowing fast (3 min) refuelling without any losses of evaporation and with very low rate of heat transfer from the environment to the storage vessels (~ 1W in H_2 tank 5 kg). However, even at this very low rate of heat transfer, evaporation losses remain a problem, as hydrogen must be released from a full container after 3-5 days of inactivity (Aceves et al., 2006). The storage vessel usually suffers liquid hydrogen losses due to cryogen boil-off caused by heat flow into the vessel from the higher surrounding temperature (Ho & Rahman, 2008).

Another disadvantage of liquid hydrogen storage is that it requires huge amounts of energy for the liquefaction process (up to 40% of the lower heating value) which reduces the overall efficiency of the system (Wolf, 2002). Therefore, cryogenic liquid hydrogen storage method is limited only to applications where the hydrogen cost is disregarded and the hydrogen gas is for short period usage (Schlapbach & Züttel, 2001).

1.3.3 Physical Storage with High Surface Area Material (Adsorbed hydrogen)

Another possible method to store hydrogen is by physically adsorbing molecular hydrogen on material with a high surface area (Ross, 2006). The most popular material for physical hydrogen storage are of carbonaceous nature, especially activated carbon and carbon nanotubes (Georgakis et al., 2007). Physical storage with porous material offers another alternative for safe hydrogen storage with high thermodynamic energy efficiency and considerably lower storage pressure (S. J. Yang et al., 2012). For physically adsorbing method, material with high specific surface area and slit pore nano-structure is preferred as the main mechanism of hydrogen uptake is the monolayer adsorption (Zhou et al., 2006).

Although this storage method has considerable advantages compared to other conventional methods, effective storage of hydrogen is challenging because of its extremely low density (Ho & Rahman, 2008). In fact, compared to conventional storage methods such liquid and gas storage, physically adsorbing porous material is heavier due to the weight of the storage material. Other drawback of physical storage is that the adsorption mechanism rely on van der Waals interactions, which are intrinsically low-energy (S. J. Yang et al., 2012). Because of the weak van der Waals interaction, significant adsorption can only be observed at low temperature, which is less than 273 K (Züttel, 2003).

1.3.4 Chemical Storage in Solid State Material (Metal Hydrides)

Hydrogen can be chemically stored in solid material by incorporation into the crystal structure of the storage material itself. Certain materials such as metals and alloys have the ability to absorb hydrogen under moderate pressure (<1000psia) at low temperatures, forming reversible hydrogen compounds called metal hydrides. Hydrogen can be discharged from metal hydrides material by reducing pressure and by applying heat to the system (Blackman et al., 2006). In order to satisfy all the conditions need for practical solid-state hydrogen storage system, the chemical adsorbing hydrogen materials should have high volumetric density, fast kinetic and low thermodynamic.

It has been proven that metal hydride as solid-state hydrogen storage offers a number of advantages over compressed hydrogen gas and cryogenic hydrogen liquid methods (P. Wang & Kang, 2008). Some of the advantages are that metal hydrides are capable of storing large amounts of hydrogen (high volumetric hydrogen storage densities) and they are inherently safer compared to mechanical hydrogen storage methods (Hong & Song, 2013). Metal hydrides appear to be the safest method of storing hydrogen since metal hydrides can be operated at relatively low temperatures and pressures typical of fuel cell vehicles and the release of hydrogen from metal hydrides is an endothermic process (R. K. Jain et al., 2007). Different materials that are used for chemical hydrogen storage will be discussed in much more detail in Chapter 2.

1.4 Hydrogen Storage Target

It is expected that the "hydrogen economy" will require two types of hydrogen storage systems, for stationary and mobile applications, including transportation. Each system has its own constraints and requirements; however it is evident that mobile applications are far more demanding (Agrawal et al., 2005). The on-board hydrogen system required light, compact, safe and affordable containment and should meet the target set by the United States Department of Energy (US DOE) for hydrogen powered vehicles in order to compete with other commercialized vehicles in the market. The use of the targets for hydrogen storage system set by the US DOE is to guide researchers and developers by specifying system operating conditions in order to develop commercially practical hydrogen storage systems.

Research is still ongoing to synthesize metal hydrides materials which will fulfil the targets for hydrogen storage systems set by the US DOE for on-board vehicular applications (Sai Raman et al., 2002). The reader may refer to the Reference (Srinivasa Murthy & Anil Kumar, 2014) for a detailed treatment on the targets set by the US DOE and only a brief summary is given in Table 1.2.

Table 1.2: Summary of targets for hydrogen storage systems set by DOE

Parameter	Unit	2017 goal	Ultimate
System gravimetric capacity	%	5.5	7.5
System volumetric capacity	kg H_2/ L system	0.04	0.07
Operating temperature	°C	40/60	40/60
Cycle life	cycles	1500	1500
System fill time (5 kg)	min	3.3	2.5

Currently, there are no metal hydrides systems or materials which can meet the entire above goals concerning the system gravimetric and volumetric capacity as well as reaction kinetics and thermodynamics for practical on-board hydrogen storage systems for mobile applications.

1.5 Problem Statement

Although there has been considerable research activities on the development of potential metal hydrides materials, there are still no materials which can fulfil all of the targets for hydrogen storage systems set by the US DOE, particularly for on-board vehicular applications. To date, most of the hydrogen storage alloys can effectively store about 1wt% to 3wt% of hydrogen only, which are insufficient for on-board vehicular applications.

Besides, there are still a number of issues associated with the metal hydrides system for hydrogen storage, i.e. slow reaction kinetics, low reversibility and high dehydrogenation temperatures (Ma et al., 2013). Much effort is being made to synthesize metal hydrides materials with low thermodynamics, fast reaction kinetics and high gravimetric hydrogen storage capacities (Principi et al., 2009). Although there is a lot of pressure to find metal hydrides materials that can meet or indeed exceed, the target set by US DOE, one must realize the importance of taking into account both the material itself and the final term use for application specific target.

Many experimental and theoretical studies have been conducted in the past which focus on the heat and mass transfer aspects of metal hydrides systems for various applications (Patil & Ram Gopal, 2013). It has been proved that the poor heat and mass transfer aspects of metal hydrides beds are one of the major disadvantages of metal hydrides for hydrogen storage systems. Therefore, a research project consists of simulation analysis of metal hydrides properties for hydrogen storage is suggested. This research project main purposed is to observe and analyse the effect of metal hydrides properties for hydrogen storage system during the absorption process especially in term of mass and heat transfer.

1.6 Research Objectives

The main objective of this study is to observe and analyse the metal hydrides behaviour for solid-state hydrogen storage system during the absorption process. The following sub-objectives are defined within the frames of the main objective:

1. To simulate and validate a three-dimensional (3D) metal hydrides hydrogen storage system with published and experimental data using COMSOL Multiphysics 5.1 software.
2. To validate the three-dimensional model with published data and simulation result with experimental data.
3. To perform a sensitivity analysis on different metal hydrides properties in order to determine their influence on the absorption process.
4. To perform an optimization study on the effect of operating parameter on metal hydrides system.

1.7 Scopes

The scopes of this research are mainly focused on the analysis of metal hydrides bed behaviour for solid-state hydrogen storage system during the hydrogen absorption process and the effect of different metal hydrides properties on the performance of metal hydrides system in terms of heat and mass transfer aspects as stated in the objectives. In order to achieve the objectives stated in Section 1.5, the following activities are carried out.

1. A thorough literature review of current developments of different types of metal hydrides material for solid-state hydrogen storage system is summarized.
2. Three-dimensional (3D) metal hydrides hydrogen storage system using COMSOL Multiphysics 5.1 software is conducted to analyze the hydrogen absorption process

numerically in order to understand how the absorption process works. The three-dimensional model later is validated against published data while the simulation results are compared with experimental data collected from the Hydrogen Fuel Cell laboratory.

3. Series of parametric studies by modifying preperties of material are performed to investigate the effects and consequences of different material properties on the metal hydride based hydrogen storage system. The properties studied are porosity (ε), permeability (K), metal thermal conductivity (k_m), hydrogen absorption constant on metal (c_a), activation energy (E_a) and heat transfer coefficient (h).
4. Optimization study has been performed in order to determine the optimum operating condition such as charging pressure and bed temperature in terms of absorption efficiency.

1.8 Thesis Outlines

This research consists of 5 chapters. The contents of each chapter are described briefly below:

CHAPTER 1 is the introductory chapter, which gives a background of study and an introduction of hydrogen and the main idea and project aim and research objectives are presented as well.

CHAPTER 2 is the literature review and it shows the previous study of chemical storage in solid state materials, thermodynamics and kinetics of metal hydrides as well as the review on metal hydrides modelling.

CHAPTER 3 describes the research methodology. In this chapter the method of conducting the research has been illustrated.

CHAPTER 4 presents the experimental and simulation results with their respective discussion as well.

CHAPTER 5 where the main conclusions and contributions of the project are summarized and the aim of this chapter is to clarify the findings of this research and suggestions for the future works.

CHAPTER 2: LITERATURE REVIEW

2.1 Metal Hydrides

Materials such as metals and alloys can form metal hydrides by reacting with hydrogen which leads hydrogen into a solid state storage system under moderate temperature and pressure. Using metal hydride as hydrogen storage which requires absorption and desorption step. Hydrogen can be released from metal hydrides either by an increase in temperature or a decrease in external pressure (I. P. Jain et al., 2010). Generally, metals and alloys can reversibly form metal hydrides reversibly according to the following reaction:

$$M + \frac{x}{2}H_2 \leftrightarrow MH_x \tag{2.1}$$

Where M denotes the metal. Metal hydrides consist of metal atoms that include a host lattice for hydrogen atoms. Metal and hydrogen normally create two different types of hydrides, α-phase where only some hydrogen is absorbed and β-phase where hydrogen is completely absorbed. Hydrogen stored in metal hydrides depends on different parameters with some mechanistic steps. Different metals have different ability to release hydrogen as the ability which depends on surface structure, morphology and purity (Sakintuna et al., 2007).

Hydride formation is an exothermic reaction due to lower entropy of the hydride compared to the hydrogen in metal and gaseous phases. Consequently the hydrogen desorption reaction is endothermic, therefore heat is needed to discharge the hydrogen. An optimum hydrogen-storage material, should possess the following properties; high mass and volumetric capacity, low desorption temperature and pressure, low heat of formation in order to minimize the energy required for hydrogen release, low heat dissipation during the exothermic hydride formation, minimum energy loss during hydrogen absorption and desorption, fast kinetics, good reversibility and cycle ability, low cost and high safety (George & Saxena, 2010).

At present, the main materials for metal hydrides are intermetallic compounds (AB_5, AB_2, AB and A_2B), which has a hydrogen storage capacity of 1.5, 2.0, 1.8 and 3.0 wt%, respectively. Solid solution alloys are also available such as vanadium-based solid solution alloys with body-centred cubic structures and Mg-based alloys, which have a hydrogen storage capacity of approximately 2 and 5 wt% respectively. To date, most of the hydrogen storage alloys can effectively store about 2 to 3 wt% of hydrogen, but this is insufficient for on-board vehicular applications based on the targets set by the US DOE. Metal hydrides composed of lightweight elements such lithium, boron, nitrogen, magnesium and aluminium have shown great potential for use as hydrogen storage materials (Wu et al., 2013). Complex hydrides are the only group of metal hydrides having high volumetric and gravimetric hydrogen storage densities (Varin et al., 2006).

2.2 Hydrides Material Review

Owing to the considerable number of articles pertaining to hydrogen storage materials available in the literature, it is deemed useful to highlight and summarize the various types of metal hydrides materials for solid-state hydrogen storage applications. The summarized storage materials comprise of intermetallic compounds (AB_5, AB, AB_2, A_2B and AB_3-type alloys, as well as solid solution alloys), complex hydrides (alanates, borohydrides and nitrides), chemical hydrides and Mg-based alloys. The characteristics, advantages and disadvantages of each type of metal hydride are discussed.

2.2.1 Intermetallic Compound

Intermetallic compounds have gained prominence in recent years due to their widespread use in the development of hydrogen-absorbing metal alloys (Gasiorowski et al., 2004). The applications of intermetallic compounds are numerous, which include hydrogen storage systems, nickel metal hydride (NiMH) battery electrodes, hydrogen purification systems, hydrogen sensors and catalysts, heat pumps, as well as cooling systems (Falahati & Barz, 2013). Intermetallic compounds are attractive for the development of metal hydrides since they are capable of absorbing large quantities of hydrogen. Moreover, they are available in abundance and they come in a variety of compositions. In general, hydrogen reacts with intermetallic compounds, producing crystalline or amorphous solid solutions of hydrogen in the respective compounds or in the hydrides formed (Palewski et al., 2005).

The resultant hydrides are called intermetallic hydrides. The common formula for intermetallic hydrides is $A_mB_nH_x$. The properties of the intermetallic compounds are determined by the interaction between the interstitial hydrogen atoms and the metal atoms and therefore, they are largely dependent on the crystal structure of the compounds. AB_5 ($CaCu_5$ structure), AB_2 (Laves phase), AB (CsCl relative structure), A_2B (AlB_2 relative structure) and vanadium-based solid solution alloys are among the important types of intermetallic compounds (Pan et al., 2003). It has been shown that AB_5, AB_2 and A_2B-type alloys have excellent hydrogen absorbing properties (Okada et al., 2002).

2.2.1.1 AB_5- type alloys

AB_5-type intermetallic compounds composed of rare earth metals and d-metals have gained much interest in the last decade because of their hydrogen storage capabilities (Borzone et al., 2013). AB_5-type intermetallic compounds with $CaCu_5$ structures remain the most promising compounds owing to their high hydrogen absorption/desorption capacities, good cyclic abilities, low equilibrium pressures, fast kinetics and good resistance to impurities. However, the gravimetric hydrogen storage capacity of the intermetallic hydrides produced from these compounds is rather low, with a value less than 1.5 wt%, due to the limitations of the $CaCu_5$-type hexagonal structures (Pan et al., 2003).

$LaNi_5$-based hydrides are example of AB_5-type alloys that has been widely investigated for use as potential hydrogen storage materials because of their fast kinetics as well as their ability to store hydrogen reversibly at ambient conditions (V. K. Sharma & Anil Kumar, 2014), (Prigent et al., 2012). Typical $LaNi_5$-based hydrides can release about 0.9 wt% of hydrogen at 100°C. The exact amount of hydrogen released can reach up to 1.2 wt%, with a maximum theoretical value of 1.5 wt% for on-board vehicular applications (Georgiadis et al., 2009). However, $LaNi_5$-based hydrides are very costly and they have low theoretical hydrogen storage capacities. Hence, there is a critical need to develop other cost-effective materials with high hydrogen storage capacities (Zhu et al., 2011).

2.2.1.2 AB-type alloys

AB-type alloys are among the desirable materials in the development of intermetallic hydrides because of their light molar mass and high weight capacities. TiFe alloys with cubic CsCl-type structures are the most well-known alloys of this class and they are capable of absorbing hydrogen reversibly up to 1.9 wt% (Ćirić et al., 2012). TiFe alloys are able to absorb and desorb hydrogen provided that the conditions are favourable. These conditions include fast absorption/desorption kinetics and high hydrogen absorption capability at a hydrogen atom-to-metal atom (H/M) ratio of 1 near ambient conditions (Endo et al., 2013). The TiFe alloy produces TiFeH and $TiFeH_2$ hydrides and more importantly, it is inexpensive compared to the $LaNi_5$ alloy (Principi et al., 2009), (Islam et al., 2018). However, TiFe alloy suffers from poor absorption/desorption kinetics, low hydrogen storage capacity (less than 2 wt%), high equilibrium pressure and complicated activation procedure (Ćirić et al., 2012).

2.2.1.3 AB_2-type (Laves phase) alloys

In AB_2-type alloys, A represents titanium (Ti) or zirconium (Zr), whereas B represents a transition metal. AB_2-type (Laves phase) alloys composed of rare earth metals and non-magnetic metals appeared to be simpler intermetallic compounds compared to those containing transition metals (Orgaz, 2001). However, the use of rare earth metal-based hydrides is rather limited since rare earth metals are very costly. For this reason, several attempts have been made to synthesize cost-effective intermetallic hydrides without the need for rare earth metals (Maeda et al., 2013).

Unlike AB_5-type alloys, AB_2-type alloys are more capable of forming a new phase at high pressures – however, this is negated by the fact that the properties of these alloys are easily hampered by the presence of contaminants (Principi et al., 2009). Hence, the surface reactions of the alloys need to be improved in order to overcome this problem. This can be done by substituting certain elements in the alloys with other elements which will increase the surface area and catalytic properties of the alloys (Young et al., 2013).

2.2.1.4 AB_3-type alloys

AB_3-type alloys (where A = La, Ce, Y) have been studied extensively as potential hydrogen storage materials in recent years due to their interesting properties for electrochemical applications (Denys et al., 2007). However, the hydrogen storage capacity is rather low for AB_3-type alloys. $LaNi_3$ is an example of an AB_3-type alloy which reacts with hydrogen during the hydrogenation process to produce the amorphous hydride, $LaNi_3H_5$ (Latroche & Percheron-Guégan, 2003).

2.2.1.5 A_2B-type alloys

A_2B alloys are composed of an alkali earth metal (A) and a transition metal (B). Ti_2Ni alloys have gained much attention from scientists and researchers among all A_2B-type of alloys because of their desirable structural, magnetic and hydrogen storage properties.

The partial substitution of Ti with Zr in Ti_2Ni alloys increases the hydrogen desorption capacity and cyclic ability of the substituted alloys. The stability of the substituted alloys also decreases compared to the parent alloys which results in lower crystalline temperatures (Zhao et al., 2012).

2.2.1.6 Solid solution alloys

It has been reported in previous studies that vanadium-based solid solution alloys with body-centred cubic (BCC) structures have high gravimetric hydrogen storage capacities up to 4 wt%, low hydrogen absorption/desorption temperatures, fast diffusion rates and rapid activation. However, these alloys are still considered to be unsatisfactory for commercial on-board vehicular applications due to their poor initial activation and low absorption capacities. A large number of studies have been conducted over the years in order to improve the kinetic and electrochemical properties of vanadium-based solid solution alloys by implementing methods such as element substitution, annealing treatment and surface modification (Yanzhi Wang et al., 2009).

Ti-based alloys with BCC structures such as Ti-V-Cr, Ti-V-Mn and Ti-Cr-Mo alloys have high hydrogen storage capacity of almost 2 wt% and fast hydrogenation kinetics near ambient conditions (Okada et al., 2002), (Endo et al., 2013). Pickering et al. (2013) discovered that $Ti_{0.5}V_{0.5}Mn$ alloys have fast absorption/desorption kinetics and high reversible hydrogen capacities up to 1.9 wt% at a temperature and pressure of 260 K and 35 MPa, indicating that these alloys are potential hydrogen-absorbing materials.

2.2.2 Complex Hydrides

Complex hydrides composed of light elements such as lithium (Li) and sodium (Na) which have gained significance as hydrogen storage materials since conventional metal hydrides are mostly composed of heavy elements in the Periodic Table of Elements. Lightweight complex hydrides emerge as potential candidates for hydrogen storage applications due to their high hydrogen storage capacities, high hydrogen storage densities, as well as mild dehydrogenation pressures and temperatures (S. Srinivasan et al., 2008).

Even though complex hydrides have high energy densities, they are difficult to handle safely and they may decompose into highly stable elements, which are very challenging to refuel with hydrogen on board a motor vehicle (Ley et al., 2014). More importantly, most of these complex hydrides do not fulfil the targets set by the US DOE since they have high thermodynamic stability and slow kinetics during hydrogen cycling (Huang et al., 2006). However, these problems can be compensated to a certain extent by thermodynamic destabilization, which involves the addition of a new element into the system by means of cation or anion substitution, or the addition of reactive hydride composites. Nanoconfinement or the addition of catalysts can also be used for thermodynamic destabilization (Albanese et al., 2013).

2.2.2.1 Alanates

Complex aluminium hydrides (also known as complex aluminohydrides or alanates) are hydrogen storage materials in which the evolution of hydrogen takes place upon contact with water (Schuth et al., 2004). Aluminium is a good hydride destabilizing component and it has been studied extensively in the development of alkali metal and alkaline earth metal-based complex hydrides (Kumar et al., 2013). Alkali metal and alkaline earth metal-based complex aluminium hydrides, $MAlH_4$ (where M = Na, Li, K), have shown to be good potential candidates for hydrogen storage materials at mild pressures and temperatures (S. S. Srinivasan et al., 2004).

These hydrides have been widely studied since they have high theoretical hydrogen capacities up to 10.4 wt% (Iosub et al., 2009). Unlike conventional metal hydrides, $MAlH_4$ desorbs through chemical decomposition – a process which begins with melting of the hydride, followed by the formation of an intermediate tri-alkali metal, hexahydroaluminate (M_3AlH_6) (Gross et al., 2002). The decomposition process takes place in a three-step reaction, which is given by Equations (2.2), (2.3) and (2.4).

$$M\mathrm{AlH}_4(s) \rightarrow M\mathrm{AlH}_4(\mathrm{l}) \tag{2.2}$$

$$M\mathrm{AlH}_4(1) \rightarrow \frac{1}{3}M_3\mathrm{AlH}_6 + \frac{2}{3}\mathrm{Al} + \mathrm{H}_2 \tag{2.3}$$

$$\frac{1}{3}M_3\mathrm{AlH}_6 \rightarrow M\mathrm{H} + \frac{1}{3}\mathrm{Al} + \frac{1}{2}\mathrm{H}_2 \tag{2.4}$$

The decomposition temperature of these complex hydrides can be reduced to room temperature by using a suitable metal catalyst (Wiench et al., 2004). Much efforts have been given to synthesize mixed alanate compounds which have good thermodynamic and kinetic properties (Akbarzadeh et al., 2009).

(a) *Sodium alanates*

Sodium aluminium hydrides or sodium aluminohydrides (more commonly known as sodium alanates, $NaAlH_4$) are metal hydrides that have high hydrogen storage capacities. $NaAlH_4$ appear to be viable hydrogen storage materials since they have high hydrogen content up to 5.6%, as well as desirable operating pressures and temperatures. In addition, $NaAlH_4$ are inexpensive and easily acquired in bulk (Tang et al., 2007).

However, the main disadvantage of $NaAlH_4$ is the decomposition process of the hydrides which takes place in a two-step reaction, as represented by Equations (2.5) and (2.6) (Mosher et al., 2007). In the first step, the $NaAlH_4$ decomposes into an intermediate compound (Na_3AlH_6) and metallic Al, and the evolution of hydrogen takes place in this step. The evolution of hydrogen continues in the second step, whereby the Na_3AlH_6 decomposes to form NaH and metallic Al. The first and second reaction releases 3.70 and 1.85 wt% of hydrogen, respectively (Thomas et al., 2002).

$$\mathrm{NaAlH_4} \leftrightarrow \frac{1}{3}\mathrm{Na_3AlH_6} + \frac{2}{3}\mathrm{Al} + \mathrm{H_2} \tag{2.5}$$

$$\mathrm{Na_3AlH_6} \leftrightarrow \mathrm{NaH} + \mathrm{Al} + \frac{3}{2}\mathrm{H_2} \tag{2.6}$$

Even though $NaAlH_4$ offer a number of advantages over conventional metal hydrides, these hydrides suffer from poor reversibility, severe dehydrogenation conditions (temperature: 473–673 K; pressure: 10–40 MPa) and slow kinetics (Bogdanović et al., 2009). Hence, the use of $NaAlH_4$ for reversible on-board vehicular applications may prove to be an insurmountable obstacle in attaining the targets set by the US DOE for hydrogen storage systems. This necessitates the addition of a suitable catalyst in order to achieve the desired performance during the absorption/desorption process (Eberle et al., 2006).

(b) *Lithium alanates*

Lithium aluminium hydrides or lithium aluminohydrides (more commonly known as lithium alanates, $LiAlH_4$) have been widely investigated for use as potential hydrogen storage materials because of their high hydrogen capacities up to 10.6 wt% (Vittetoe et al., 2009). Unlike $NaAlH_4$, $LiAlH_4$ decomposes into LiH and Al in a three-step reaction, which is given by Equations (2.7), (2.8) and (2.9). However, it shall be noted that the hydrogenation process takes place at very high pressures. In the first step, $LiAlH_4$ decomposes into Li_3AlH_6, Al and H_2 at temperatures above 413 K. For second step, the Li_3AlH_6 dissociates further into LiH, Al and H_2 at temperatures above 463 K. In the third step, the final decomposition of $LiAlH_4$ takes place at temperatures higher than 673 K, and these temperatures are extremely high for on-board vehicular applications (Xiong et al., 2007).

$$3\mathrm{LiAlH_4} \rightarrow \mathrm{Li_3AlH_6} + 2\mathrm{Al} + 3\mathrm{H_2} \tag{2.7}$$

$$\mathrm{Li_3AlH_6} \rightarrow \mathrm{3LiH} + \mathrm{Al} + \frac{3}{2}\mathrm{H_2} \tag{2.8}$$

$$\mathrm{3LiH} + \mathrm{3Al} \rightarrow \mathrm{3LiAl} + \frac{3}{2}\mathrm{H_2} \tag{2.9}$$

The first, second and third reaction releases approximately 5.3, 2.6 and 3.6 wt% of hydrogen, respectively. However, the third reaction is generally not considered due to the extremely high temperatures (Vittetoe et al., 2009). Even though $LiAlH_4$ are kinetically stable, they are very thermodynamically unstable for hydrogen storage since they decompose easily below room temperature (Schuth et al., 2004), (Bogdanović et al., 2009), (Barkhordarian et al., 2007). In addition, $LiAlH_4$ cannot be dehydrogenated within the range of practical pressures due to their poor thermodynamic properties (Akbarzadeh et al., 2009). Therefore, $LiAlH_4$ are not practical for on-board hydrogen storage application.

(c) *Calcium alanates*

Calcium aluminohydrides (more commonly known as calcium alanates, $Ca(AlH_4)_2$) can be synthesized from alkaline earth hydrides and $AlCl_3$ using a simple ball milling process. However, this process leads to the formation of alkaline earth chloride as a by-product, which is difficult to be removed from the hydrides (Schuth et al., 2004). Alternatively, $Ca(AlH_4)_2$ can be synthesized by a metathesis reaction between $CaCl_2$ and $NaAlH_4$ at a molar ratio of 1:2. However, $Ca(AlH_4)_2$ suffer from similar issues as with other alanates since they are thermodynamically unstable at ambient conditions and they decompose exothermically into CaAlH, Al and H_2. It shall be noted that $Ca(AlH_4)_2$ are not suitable for reversible hydrogen storage applications since the first reaction is exothermic (Akbarzadeh et al., 2009).

During the decomposition of $Ca(AlH_4)_2$, the $CaAlH_5$ slowly desorb hydrogen at 373 K and transform into $Ca_3(AlH_6)$. The nature of the decomposition process of $CaAlH_5$ is inherently complex and therefore, a more detailed study is needed to gain insight into this process, particularly with regards to the first and second reactions. The third reaction, which produces CaH_2 and Al, indicated favourable candidate for hydrogen storage material, with a moderate decomposition pressure and temperature (Iosub et al., 2009).

(d) *Potassium alanates*

Potassium aluminohydrides (more commonly known as potassium alanates, $KAlH_4$) have been shown to be prospective materials for hydrogen storage applications. The main advantage of these hydrides is that they are capable of absorbing and releasing hydrogen without the need for a catalyst. However, the disadvantage of these materials is that their theoretical hydrogen storage capacity is lower than that for NaAlH, with a value of only 4.3 wt% in the first and second reactions. In addition, the final reaction is irreversible. This is undesirable, considering that $KAlH_4$ can be easily handled, and the operating pressure in the first and second reactions is less than 1 MPa. However, the operating temperature of these hydrides is considerably high for on-board hydrogen storage applications, with a range of 573–623 K (Bogdanović et al., 2009).

2.2.2.2 Borohydrides

Tetrahydroborates are the highest hydrogen-containing compounds among hydrogen storage materials with high hydrogen content. Hydroborates are among the rare metal hydrides that can be dissolved in water without any danger and this unique property is attributed to their stability. The simpler anion family of hydroborates (typically known as complex metal borohydrides, MBH_4) is the more common group of hydrogen-containing compounds (Laversenne). Alkali-transition metal borohydrides have gained much interest among scientists and researchers worldwide due to their high gravimetric hydrogen storage densities and tuneable properties (Choudhury et al., 2009), (Nickels et al., 2008). The decomposition of borohydrides differs from the decomposition of alanates since there are no hexahydride intermediate products formed during the process. Binary metal hydride and elemental boron are the final products of the decomposition process. The decomposition process of complex metal borohydrides is given by Equations (2.10) and (2.11).

$$\mathrm{M(BH_4)n} \rightarrow \mathrm{nMH} + \mathrm{nB} + \frac{3}{2}\,\mathrm{nH_2} \qquad (2.10)$$

$$\mathrm{nMH} + \mathrm{nB} \rightarrow \mathrm{nB} + \mathrm{nM} + \frac{1}{2}\,\mathrm{nH_2} \qquad (2.11)$$

$LiBH_4$, $NaBH_4$, $Mg(BH_4)_2$ and $Ca(BH_4)_2$ have been shown to be great prospective hydrogen storage materials among all complex metal borohydrides owing to their high gravimetric and volumetric hydrogen storage densities (George & Saxena, 2010). However, there are a couple of issues associated with these borohydrides which need to be addressed in order to realize their full potential. Firstly, these borohydrides have high thermodynamic stability, which is impractical for on-board hydrogen storage applications. Secondly, these borohydrides form borane, which is an undesirable volatile by-product, and they have slow kinetics (Barkhordarian et al., 2007). For these reasons, complex metal borohydrides are not recommended for reversible hydrogen storage applications. However, the thermodynamics and kinetics of these materials can be improved by implementing destabilization techniques or doping the materials with other materials (Choudhury et al., 2009).

(a) *Lithium borohydrides*

Lithium borohydrides ($LiBH_4$) are compounds that have high gravimetric and volumetric hydrogen storage capacity of 18.5 wt% at room temperature (Arnbjerg et al., 2009). $LiBH_4$ was first synthesized in 1940 by reacting ethyl lithium with diborane (B_2H_6) (Ichikawa et al., 2005). In $LiBH_4$, four hydrogen atoms are covalently stabilized as $[BH_4]^-$

anion, and this anion is combined with a counter-cation, Li^+ (Nakamori & Orimo, 2004). The thermal decomposition of $LiBH_4$ is given by the following equation:

$$\mathrm{LiBH_4} \rightarrow \mathrm{LiH} + \mathrm{B} + \frac{3}{2}\,\mathrm{H_2} \tag{2.12}$$

In general, the hydrogenation of $LiBH_4$ is a difficult process due to the high thermodynamic stability of the materials resulting from strong B-H interactions (Choudhury et al., 2009). The activation energy needed to dissociate hydrogen from $LiBH_4$ is roughly 180–200 $kJmol^{-1}$ of hydrogen, which is very high (P. Wang & Kang, 2008). In addition, $LiBH_4$ have a high enthalpy of decomposition (-67 $kJmol^{-1}$) and thus, a high decomposition temperature (Ravnsbæk et al., 2009). $LiBH_4$ begin to release hydrogen at temperatures above 593 K, and the overall decomposition process takes place within a temperature range of 673–873 K. The total amount of hydrogen desorbed is only around 50% of the theoretical capacity (Schuth et al., 2004). Hence, $LiBH_4$ are not suitable for on-board hydrogen storage applications since the decomposition temperature is too high and the process is irreversible in practical conditions. However, the thermodynamic properties and decomposition conditions of the compounds can be altered by the addition of a catalyst (Bogdanović et al., 2009).

(b) *Zinc borohydrides*

In recent years, a new class of transition-metal complexes, zinc borohydrides ($Zn(BH_4)_2$), have gained attention as potential hydrogen storage materials due to their high theoretical hydrogen storage capacities of up to 8.4 wt% (S. Srinivasan et al., 2008). $Zn(BH_4)_2$ can be synthesized by a metathesis reaction between $NaBH_4$ and $ZnCl_2$ in a suitable solvent such as diethyl ether. However, it has been shown that it is difficult to remove the solvent completely without causing decomposition of the $Zn(BH_4)_2$ (Jeon & Cho, 2006). $Zn(BH_4)_2$ decompose thermally and release hydrogen according to the stoichiometric reactions given by Equations (2.13) and (2.14).

$$\mathrm{Zn(BH_4)_2(solid) \rightarrow Zn(BH_4)_2(liquid)} \quad (2.13)$$

$$\mathrm{Zn(BH_4)_2(solid) \rightarrow Zn + B_2H_6 + H_2} \quad (2.14)$$

$Zn(BH_4)_2$ melt at a temperature around 358 K in Ar-rich environment. However, $Zn(BH_4)_2$ decompose slowly into diborane (B_2H_6), H_2 and Zn as well as traces of B at a temperature range of 631–686 K. In addition, $Zn(BH_4)_2$ are unstable since they decompose readily at room temperature even though the decomposition process is endothermic (Jeon & Cho, 2006). The decomposition of $Zn(BH_4)_2$ not only releases hydrogen, but also considerable amounts of boron hydrogen (BH) compounds. The decomposition temperature of $Zn(BH_4)_2$ can be reduced by the addition of a catalyst. Doping $Zn(BH_4)_2$ with a nanomaterial reduces the decomposition temperature by 293 K and detains the evolution of boranes (Choudhury et al., 2009).

(c) *Sodium borohydrides*

Sodium borohydrides ($NaBH_4$) are complex metal borohydrides with high reversible hydrogen storage capacities of up to 10.8 wt%. Hydrogen can only be released from $NaBH_4$ by hydrolysis (reaction with water), which is an irreversible process. In the absence of a catalyst or additive, the thermodynamic properties of $NaBH_4$ are deemed inappropriate for hydrogen storage applications since the decomposition temperature is extremely high, with a value of 673 K (Schuth et al., 2004). Furthermore, the traces of BH compounds formed during the thermal decomposition process are not only damaging to the membranes of the fuel cells, but they are also toxic to the catalysts in the fuel cells (Bogdanović et al., 2009).

(d) *Calcium borohydrides*

Calcium borohydrides ($Ca(BH_4)_2$) cannot be synthesized from elements at a temperature and pressure range of 573–673 K and 20–35 MPa. $Ca(BH_4)_2$ are favourable materials for hydrogen storage applications because they have high theoretical hydrogen capacities up to 8.3 wt%. However, $Ca(BH_4)_2$ are less stable compared to $LiBH_4$ since they have lower decomposition temperatures in their pure state. The decomposition of $Ca(BH_4)_2$ is given by Equation (2.15) (Barkhordarian et al., 2007):

$$CaH_2 + MgB_2 + 4H_2 \rightarrow Ca(BH_4)_2 + MgH_2 \quad (2.15)$$

2.2.2.3 Nitrides

A number of studies have shown that metal-nitride-based systems (simply known as metal-N-H systems) composed of amide and binary hydrides have gained significance as candidate materials for on-board hydrogen storage applications owing to their capability in releasing hydrogen in appropriate conditions. It shall be noted that the binary hydrides used in these systems are compounds formed between hydrogen and an active metal from the Periodic Table of Elements, which is typically an alkali metal or alkaline earth metal (Xiong et al., 2007).

(a) *Lithium nitrides*

Similar to lithium borohydride ($LiBH_4$), two hydrogen atoms are covalently stabilized in lithium amide ($LiNH_2$) as $[NH_2]^-$ anion and this anion combines with the counter-cation, Li^+. Even though mixtures of lithium amide and lithium hydride ($LiNH_2$ + LiH) are able to store hydrogen at high gravimetric hydrogen storage capacities, they are impractical for on-board hydrogen storage applications because of their high decomposition temperatures. The reaction between $LiNH_2$ and LiH at a ratio of 1:1 results in the formation of lithium imide (Li_2NH), whereas the reaction between Li_2NH, LiH and H_2 results in the formation of lithium nitride (Li_3N). These reactions are given by Equation (2.16).

$$LiNH_2 + 2LiH \Leftrightarrow Li_2NH + LiH + H_2 \Leftrightarrow Li_3N + 2H_2 \quad (2.16)$$

Both of these reactions release up to 5.2 wt% of hydrogen. It shall be noted that the desorption of $LiNH_2$ generally occurs above 473 K in vacuum conditions (Nakamori & Orimo, 2004).

2.2.3 Chemical hydrides

Differ than conventional metal hydrides, chemical hydrides are typically composed of lighter elements (Smythe & Gordon, 2010). This result in higher gravimetric hydrogen storage capacities, along with ease of hydrogen release which is similar to complex hydrides (Hwang et al., 2010). Chemical hydrides can exist in either solid or liquid state, and can be heated directly, passed through a catalyst-containing reactor, or combined with water (i.e. hydrolysis) or other reactants to produce hydrogen. Unlike reversible complex hydrides, chemical hydrides are irreversible and generally intended as ‘‘one-way’’ single-use fuels. Besides, the left-over by-product must be removed from the vehicle for off-board regeneration (J. Yang et al., 2010). Among chemical hydrides, ammonia borane (AB) is reported as a potential material for hydrogen storage due to its high hydrogen capacity.

2.2.3.1 Ammonia Borane

Ammonia borane (NH_3BH_3 or simply known as AB) has garnered considerable attention from scientists and researchers due to their favourable properties which can be exploited for on-board hydrogen storage applications (Kang et al., 2012). According to Lee and McKee (2009), NH_3BH_3 has high hydrogen content up to 19.6 wt% and it is really stable in basic or neutral aqueous solutions. However, NH_3BH_3 suffers from a number of disadvantages: (1) NH_3BH_3 hydrolyses easily in acids (Lee & McKee, 2009), (2) the synthesis of NH_3BH_3 is a complex process, and (3) the decomposition of NH_3BH_3 results in the formation of B_2H_6 impurities. In spite of these drawbacks, NH_3BH_3 is still one of the leading materials for hydrogen storage with assured stability (K. Wang et al., 2013). The exothermic decomposition of NH_3BH_3 is a multi-step reaction which is given by Equations (2.17), (2.18) and (2.19) (P. Wang & Kang, 2008).

$$\mathrm{xNH_3BH_3(solid) \rightarrow [NH_2BH_2]_x + xH_2(gas)} \tag{2.17}$$

$$\mathrm{[NH_2BH_2]_x \rightarrow [NHBH]_x + xH_2(gas)} \tag{2.18}$$

$$\mathrm{[NHBH]_x \rightarrow BN + xH_2(gas)} \tag{2.19}$$

In addition, the rate of hydrogen released from NH_3BH_3 is sluggish at moderate temperatures below 373 K. The hydrogen gets entrapped by the discharge of harmful by-products due to energy barriers and side reactions. Various techniques have been proposed and implemented to overcome these issues, which include the addition of catalysts or chemical promoters which will improve the hydrolysis reactions, as well as chemical modifications of NH_3BH_3 by the substitution of its amine protonic hydrogen with metal cations (Kang et al., 2012).

2.2.4 Magnesium-based Alloys

Magnesium-based alloys have been studied extensively during the last 30 years for use as hydrogen storage materials (Andreasen, 2008) due to the following reasons: (1) Mg-based alloys have favourable hydrogenation properties, (2) Mg-based alloys are lightweight materials for solid-state hydrogen storage applications (Aburto & Orgaz, 2007), and (3) Mg-based alloys have high hydrogen storage capacities up to 7.6 wt% as well as good kinetics (de Castro et al., 2004), (Dornheim et al., 2007). More importantly, Mg is inexpensive and it is available in abundance within the Earth's crust (Shao et al., 2008), (Zhang et al., 2018). Mg-based alloys also have excellent heat resistivity, good recyclability, and they are capable of forming solid solutions and compounds with other elements in their equilibrium states (Liang, 2004). However, Mg-based alloys have poor thermodynamic and kinetic properties due to the strong bonding between Mg and hydrogen (Ponthieu et al., 2014). Hence, a high decomposition temperature (~573 K) is required to evolve the absorbed hydrogen due to the poor thermodynamics and slow hydrogen absorption/desorption kinetics of Mg-based hydrides (Kalisvaart et al., 2010).

There are three factors that inhibit the hydrogen absorption/desorption kinetics of Mg (Liu et al., 2014). The first factor is the formation of a magnesium oxide (MgO) layer, resulting from oxidation of the Mg surface. This layer forms a barrier which cannot be penetrated by hydrogen. However, the MgO layer can be broken down by performing several cycles of annealing at ∼673 K, which is a form of heat treatment, in both vacuum and hydrogen environments. The second factor is the limited dissociation rate of the hydrogen molecules on the Mg surface. However, the dissociation rate can be improved by the addition of a small amount of catalyst. The third factor is the low hydrogen mobility of the magnesium hydride (MgH_2) phase, which hinders further hydrogen absorption when the catalysed Mg begins to absorb hydrogen (Yermakov et al., 2006).

Much effort has been made to improve the hydrogenation properties and synthesize of Mg-based alloys that have higher reversible hydrogen storage capacities and lower stability than MgH_2 (Prigent & Gupta, 2007). A number of techniques have been devised to achieve this goal, which include alloying, surface modifications, doping the materials with catalysts, as well as the development of nanocrystalline and amorphous Mg-based alloys (Ouyang et al., 2014), (He et al., 2008).

2.3 Fundamentals of Metal/Hydrogen Interactions

2.3.1 Thermodynamics of Metal/Hydrogen Interactions

Materials such as metals and alloys can form metal hydrides by reacting with hydrogen but only a few of them are suitable as storage for hydrogen at moderate temperature and pressure.. Reaction of metals with hydrogen can be exothermic depending on the type of the hydrogen-metal (H-M) bond and the strength. The absorption process is reversible and can be defined by Equation 2.20.

$$\mathrm{M} + \frac{\mathrm{x}}{2}\mathrm{H}_2 \leftrightarrow \mathrm{MH}_\mathrm{x} \pm \Delta H \tag{2.20}$$

where M and H represents metal and hydrogen respectively, x is the non-stoichiometric coefficient, and ΔH is the reaction enthalpy. This reaction has an enthalpy change ΔH and an entropy change ΔS. The hydride formation is an exothermic reaction, since entropy of hydride is lower in comparison to metal and hydrogen gas,. Consequently the desoprtion reaction is endothermic, therefore heat is needed to discharge hydrogen. The thermodynamic aspects of this reaction can be expressed by pressure-composition isotherms. A schematic PCI curve is shown in Figure 2.1.

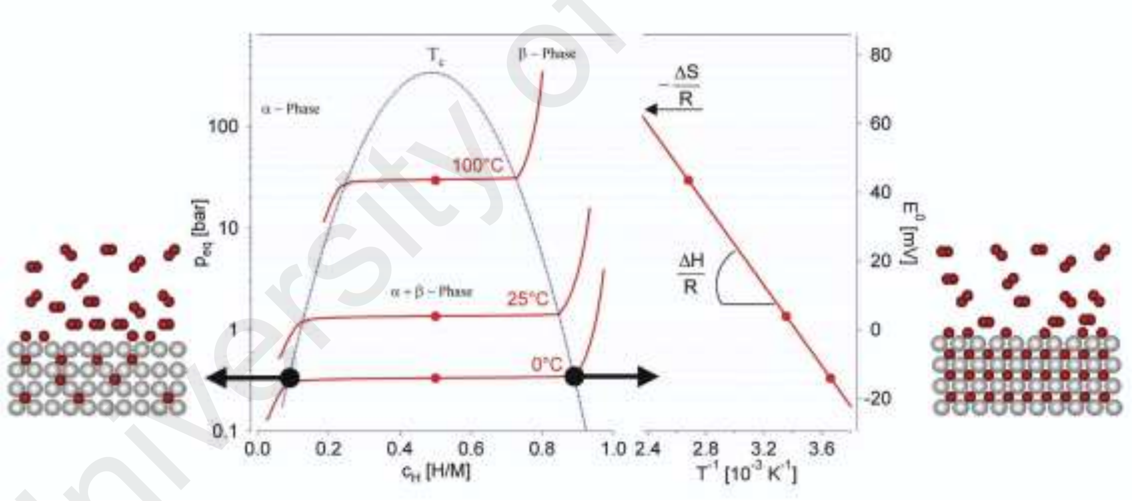

Figure 2.1: (a) Phase diagram showing the transformation from α-phase to β-phase for metal hydride; (b) Van't Hoff plot derived from isotherms for various temperatures (Züttel, 2003).

Figure 2.1 is an idealized description of the metal hydride behavior. Hydrogen molecule is first physisorbs onto the metal surface when they are in contact to form metal hydride and later split up into two hydrogen atoms. The hydrogen atoms then penetrate the metal to form a solid solution of dissolved hydrogen atoms in the metal lattice. This phase is normally called the alpha (α) phase, where the crystal structure similar to the bare metal is observed. When the pressure of the hydrogen increase, the concentration of hydrogen atoms dissolved into the metal will be in equilibrium with the gas phase increase. Then, a higher concentration phase (*β*) begins to form when the concentration of hydrogen atoms surpass a certain critical value where the H-H interaction becomes significant. As a result, the system possess three phases which are *α*, *β* and hydrogen gas phases as well as two components which are metal and hydrogen. From the Gibbs phase rule, the degree of freedom (*f*) is:

$$f = C - P + 2 \tag{2.21}$$

Where, *C* represents the components number and *P* denotes the phases number. Therefore, if the process is isothermal (constant temperature), the concentration in the two-phases region is increasing at a constant hydrogen pressure. When the *α* phase is completely dissapeared, the pure *β* phase will be obtained and the system now has two degree of freedom. The hydrogen pressure again increases with concentration when the hydrogen enters into solid solution in the *β* phase.

During the transformation from the *α* to *β* phase, both of the two phases are in equilibrium with each other as well as the gaseous hydrogen molecules. If the process takes place at a constant temperature (isothermal process), following the Gibbs' phase rule, the hydrogen equilibrium pressure on the metal surface is then set to a value depending on the specific metal hydride characteristics. This pressure is known as the equilibrium plateau pressure, because it appears as a plateau in a pressure composition isotherm (PCI). Derived from Van't Hoff equation, the equilibrium plateau pressure P_{eq} for this reaction is given by:

$$\ln \frac{P_{eq}}{P_0} = \frac{\Delta H}{R.T} - \frac{\Delta S}{R} \tag{2.22}$$

Where P_0 is the reference pressure, ΔH and ΔS are the enthalpy and entropy of the hydride formation (β phase), based on one mole of H_2. Generally, the ΔS change is primarily given by the hydrogen gas standard entropy loss as it enters the metal lattice. This suggests that the ΔS term can be assumed to be constant, although this is fairly correct for complex metal hydrides. The ΔH term indicates the metal hydrides bond stability. The enthalpy, ΔH of metal hydrides formation is negative in most cases, reflecting its exothermic properties and hence P_{eq} rises exponentially with temperature.

From Figure 2.1, it can be seen that in α phase, the amount of hydrogen in the metal is quite low compared to the actual metal hydride β phase where the amount of hydrogen is quite high. To refill a metal hydride tank, adequate hydrogen is charged at a pressure above P_{eq}. The metal within the tank will then absorb hydrogen until it is completely transformed to the β phase. By reducing the metal hydrides pressure or increasing the temperature, the hydride will discharge hydrogen gas and gradually change from β phase to α phase.

Therefore, the transition process from α phase to β phase, determined by the enthalpy and entropy of the hydride formation, is very important for any promising metal hydride-forming material. For a suitable practical applications, the transition pressure must be near to 1 bar at relatively low temperature (~ 373 K). Assuming that ΔS of gaseous hydrogen is 130 $Jmol^{-1}K^{-1}$, the ΔH of the hydride should be between -30 and -55 $kJmol^{-1}$ to achieve 1 bar hydrogen equilibrium between 313 K and 423 K, based on the Van't Hoff equation. Unfortunately, none of the existence hydrides with high hydrogen capacity has the required thermodynamic properties (Mao, 2011).

2.3.2 Kinetics of Metal Hydrides

Besides thermodynamic factors, the slow absorption kinetics of hydrogen is also an obstacle for practical applications of metal hydrides. It is crucial to fully understand the hydrogen sorption process in order to determine which step is the rate-limiting step. The hydrogen gas reaction with metals can be described as a simple one-dimensional potential energy curve term as shown in Figure 2.2.

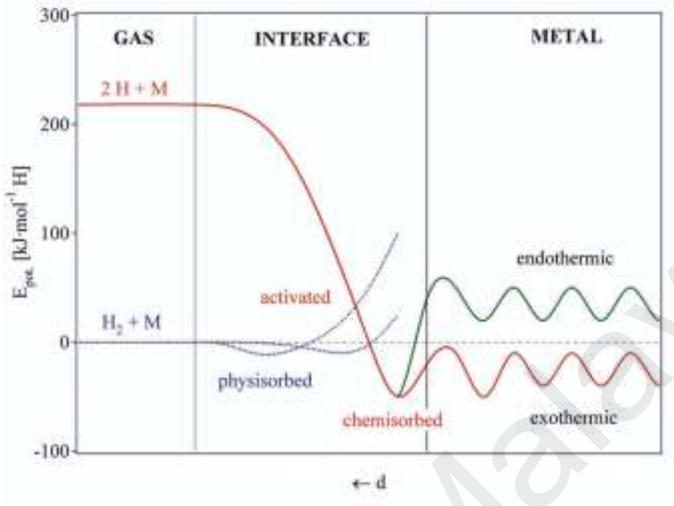

Figure 2.2: Simplified one-dimensional potential energy curve (Züttel, 2003)

As shown in Figure 2.2, far from the metal surface, the hydrogen molecule and two hydrogen atoms potential are splitted by the dissociation energy ($H_2 \rightarrow 2H, E_D = 435.99$ kJmol^{-1}). When the hydrogen molecule approaches the metal surface approximately one radius of hydrogen molecule (≈ 0.2 nm) from the metal surface, the first interaction between both of them is the Van der Waals force which leads to the physisorbed state ($E_P \approx 10$ kJmol^{-1}). Closer to the surface, for dissociation and formation of the hydrogen metal bond to occur, the hydrogen needs to surpass the activation obstacle.

The activation barrier height depends on the involved element surface. On the surface, the hydrogen atoms that shares electrons with the metal atoms are then in chemisorbed condition ($E_C \approx 50$ kJmol^{-1} H_2). The chemisorbed hydrogen atoms with high surface mobility then interacting with each other to form surface phases at adequately high coverage. For the final step, the chemisorbed hydrogen atom can enter the subsurface layer and eventually spread on the interstitial sites through the lattice of the host metal.

Hydride formation contains specific characteristic that makes this process different from other gas-solid reactions. One of the special characteristic is high diffusivity of hydrogen dissolved in the metal lattice. The other unique trait is that many metal-hydrogen interaction starts to fracture at the initial reaction stage. Besides, there are many factors that controlled the reaction rate of hydrogen. Briefly, the absorption and desorption process of hydrogen can be divided into several independent steps as proposed by (M. Martin et al., 1996) and listed below:

Hydrogen absorption	Hydrogen desorption
1. Physisorption of hydrogen molecules on the surface of the metal.	1. Hydride decomposition at the hydride/α-solid solution interface.
2. Chemisorption and dissociation of hydrogen molecules.	2. Diffusion of hydrogen atoms through the α-solid solution.
3. Surface penetration of the atomic hydrogen into the bulk and formation of α-solid solution.	3. Penetration of hydrogen atoms from bulk to the surface.
4. Diffusion of hydrogen atoms through the layer of α-solid solution, involving interstitial and vacancy mechanisms.	4. Recombination of chemisorbed hydrogen atoms into the H_2 molecules and the physisorption on the surface.
5. Hydride formation at the interface of the metal.	5. Desorption from the surface into the gaseous phase.

There are certain cases where the conditions may be more complicated, such as by the existence of subsurface sites with distinct absorption energy. During the hydrogen desorption, analogous steps can be distinguish. The kinetic curve has its own properties at each step that can be devised based on the amount of the fractional change over time. The overall kinetic is limited by the rate-limiting step which is the slowest process. The pressure and temperature influence on this curve also needs to be studied to infer the reaction rate-limiting step.

Physisorption of hydrogen is a rapid process, and hence usually not a rate-limiting process. For that reason, the surface equilibrium concentration can be assumed. Normally, the rate-limiting step in the hydrogen absorption process is either the hydrogen dissociation at the surface where surface concentration is important or the hydrogen diffusion through the hydride to the metal/hydride interface, or both. The system needs to be provided with sufficient activation energy for the dissociation to occur. For this circumstance, the dissociation or recombination reaction is slow and might be the rate-limiting step for the sorption process.

To enhance the rate-limiting step of physical and chemical sorption process, an appropriate catalyst may be available. Unfortunately, metal surfaces are usually not clean as it is passivated by oxygen, which inhibits the dissociation of hydrogen molecules and the diffusion of hydrogen atoms into the bulk. Conversely, if the thickness of the hydride layer increases (considering hydration occur from the outside to the core of the particle), the restriction due to the diffusion through the hydride layer can become significant. For detailed information on kinetic reaction, the apparent activation energy (E_a) can be calculated by using the same Arrhenius equation based on the isothermal dehydrogenation results:

$$K = Ae^{\left(\frac{-E_a}{RT}\right)} \tag{2.23}$$

Where K is the constant reaction rate (temperature dependent), A is a pre-exponential factor, E_a is the apparent activation energy, R is universal gas constant, and T is absolute temperature. Hence, it is crucial to figure out the value of K before determining the activation energy. Typically, K can be figured out by analysing the isothermal hydrogen sorption curves with suitable solid state kinetic rate expressions obtained from the solid state reaction mechanism model such as nucleation, geometric contraction, diffusion and reaction order models, which are based on different geometric particles and different driving forces. Several of different rate expressions have been obtained from these mechanisms.

2.4 Metal Hydrides Modelling Review

Metal hydride hydrogen storage system needs to have rapid charging and discharging rates in order to compete with other commercialize energy storage system such as gasoline tanks and batteries. Enhancing the reaction rate required the rate of heat transfer in the reaction bed to be improved. There are some improvements that can be applied to increase the heat and mass transfer in the metal hydride bed. To study the effect of heat and mass transfer on the reaction rates, a mathematical model can be constructed to illustrate the phenomena of heat and mass transfer in the metal hydride bed instead of depending on experimental study only. This section describes a number of the previous study involving the modelling and simulation of metal hydride tanks.

2.4.1 One Dimensional Approach: Model Limitations

One of the earlier one-dimensional mathematical model of metal hydrides is that of Lucas & Richards (1984). They developed a detailed one-dimensional mathematical model of a hydride bed which described the behaviour of the hydride bed during absoprtion and desorption processes. These processes had been solved analytically based on a one-dimensional transient heat conduction equation. Unlike the other hydride bed models previously studied in the literature, the model adopted in the study bed simulated an actual, commercially available hydrogen storage system rather than an abstract ideal situation. Therefore, this model provides an easy way to predict the time required to absorb or release a given amount of hydrogen. However, the model implemented by Lucas & Richards (1984) excluded the heat of reaction which was the main source of heat produced in the system. In conclusion, there was a large dispute observed between numerical and experimental results due to the oversimplified model.

Further investigations by using one-dimensional model are carried out by Mayer et al. (1987). They developed a one-dimenisonal mathematical model that was able to explain the transient heat and mass transfer reaction within metal hydride beds. The theoretical predictions of this model were compared with reaction rates and pressure-temperature distributions within the reaction beds where they were experimentally determined. The temperature profiles for z direction and the heat transfer by convection were excluded from the model. However, the experimental results clearly displayed that temperature variations occur not only with r direction but also with z direction. Therefore, it was concluded that it is important to consider the process along the z direction while the convective effect may also be significant in tanks where the charging pressure is high.

In the previous literature, only models with constant physical properties of hydrogen and metal hydride have been investigated. Da-Wen et al. (1988) felt that acquainting the heat and mass transfer characteristics of reaction beds is significant and that model with constant physical properties of hydrogen and metal hydrides could not present the practical systems well. Hence, in 1988, they created a one dimensional model which includes the effects of the effective thermal conductivity, the hydride physical properties and other operating conditions on the metal hydride bed. The results indicate that the reaction occurs throughout the hydride bed, but the major reaction take place in a rather narrow areas. They also found that the improvement of heat transfer in the metal hydride bed is extremely important in reducing the time taken for the reaction.

Then, in 1992, Ram Gopal & Srinivasa Murthy (1992) developed another one-dimensional heat and mass transfer model for metal hydrides beds with annular cylindrical geometry. They claimed that existed models were restricted to certain alloys only, and that a general work that predict the performance of different alloy systems were unavailable. Therefore, a one-dimensional model in dimensionless form, which covers a variety of alloys and operating parameters was created. As most works reported, Ram Gopal & Srinivasa Murthy (1992) concluded that the rate-controlling resistance to heat and mass transfer is the metal hydrides bed thermal resistance and the perfect approach to design a reactor is to enhance the heat transfer characteristics by minimizing the bed thickness and improving the bed conductivity. In 1993, Ram Gopal & Srinivasa Murthy (1993) developed another new one-dimensional model. To make sure the study was a generalised one, the input and output variables were combined into non-dimensional parameter and the properties as well as operating parameters is varied. The variation of the metal hydride properties and operating parameters was large so that the results could be used for a many alloys and systems. Again, they concluded that an enhancement in heat transfer is most important for metal hydride system.

By using a revised one-dimensional mathematical model, Gopal et al. (1995) has displayed a good comparison between numerical and experimental results. They investigated the effect of different cooling fluid temperatures on hydriding/dehydriding characteristics theoretically and experimentally and the results showed that higher heat and mass transfer rates could be achieved at lower cooling fluid temperature. Unfortunately, some inconsistency in the bed temperatures caused by the reactor thermal mass was observed. The conclusion of their study was that the presented model can only be used for beds with small thickness and for other mathematical model development, the effect of pressure drop and reactor thermal mass must be taken into account to correctly predict the hydride beds performance.

Therefore, it can be assumed that one-dimensional models may not be able to fully reflect the heat and mass transfer processes in the reaction beds because some of the important effects of the design and the system behavior prediction are mostly excluded. This leads researchers to develop other alternative such as two and three dimensional approach to this problem.

2.4.2 Two and Three-Dimensional Models

In 1989, Da-Wen et al. (1989) created a two-dimensional model as an extension for their previous one-dimensional model. The model contain the general equations for effective thermal conductivities and kinetics for metal hydrides beds as well as pressure-concentration-temperature (P-C-T) curves, thus forming a “more universal” model. The two-dimensional model has been validated against experimental results with constant and varying properties to observe which of the models is more accurate. Sun & Deng (1990) presented their model in more detail in 1990, and present a numerical solution based on finite difference approximations by using alternating-direction implicit method. There was good agreement between the numerical and experimental results.

In their series of papers, A. Jemni et al. (1995a, 1995b) created two dimensional mathematical model for heat and mass transfers during hydrogen sorption process within metal hydride bed. The numerical simulation showed that the reactor dimensions, the inlet pressure and temperature during absorption, and the heating fluid outlet pressure and temperature during desorption, were significant. They also concluded that the assumption of thermal equilibrium was not valid for the whole reactor and that the heat transfer by convection which could be neglected. This study indicated that enhancing the solid, effective thermal leads to substantial improvement in reactor performance.

Later, in 1997, Nasrallah & Jemni (1997) also validated the main assumptions commonly used by different authors in producing mathematical models for metal hydride reactions. The validation was done by comparing the numerical results with and without the use of the assumptions for LaNi5-hydrogen reactor. This study concluded that the assumption of local thermal equilibrium, negligible pressure variation and the effect of hydrogen concentration on equilibrium pressure were almost valid for all conditions. The conclusion is important as it allows authors to use the simplified model with given assumptions to correctly illustrate the heat and mass transfer process in the reactor.

However, even with the simplified mathematical model, there were some parameters that need to be precisely determined, including the effective thermal conductivity, equilibrium pressure, reaction kinetics and the conductivity between hydride beds and fluid around tank. Thus, to address this problem, an attempt was made in the next experimental study of Jemni et al. (1999) where the developed theoretical model was validated against experimental results. In this work, they determined all the parameters experimentally. As conclusion, they obtained good agreement between the experimental and the calculated results.

In 2000, Nakagawa et al. (2000) proposed a two dimensional mathematical model which described transient heat and mass transfer in metal hydride bed. They validated the assumptions of local thermal equilibrium and negligible convection effect on heat transfer in detail and also bring into account the influence of reacted fraction on thermophysical properties such as specific heat, thermal conductivity, and metal hydrides particle diameter. For this study, they came up with the same conclusion by A. Jemni et al. (1995a, 1995b) that temperature equilibrium between gas and solid did not occur throughout the bed but, almost true for the whole volume. Still, they noted that the convection only improved the hydriding process initially and caused a bad effect afterward.

In 2001, Mat et al. (2001) adopted the mathematical model from A. Jemni et al. (1995a) and applied it to the available experimental study in literature to investigate the basic mechanisms of hydride formation and the heat and mass transfer process which occur within the hydrides bed. It was observed that in the regions with lower equilibrium pressure, the hydride formation was enhanced where the hydride formation increased rapidly at the beginning and later started to slow down when the bed temperature increase due to the exothermic reaction. The model successfully predicted the experimental results. Afterwards, they extended the analysis to three-dimensional models which includes three-dimensional complex heat and mass transfer and chemical reaction in metal hydride (Aldas et al., 2002). The important founding of the analysis was that the main parameter in the absorption process was equilibrium pressure, which strongly depended on temperature as in the two-dimensional model. The important implication of this study was that the absorption process can be represented by a two-dimensional or three-dimensional model.

CHAPTER 3: METHODOLOGY

3.1 Introduction

In this chapter a three-dimensional mathematical model is presented for describing the absorption processes that take place in porous metal hydride compacts of cylindrical shape that conforms the actual setup used in the experiment. First, a series of equations governing the heat and mass transfer process as well as the initial and boundary conditions are discussed. These equations are first implemented in the COMSOL Multiphysics simulation using literature data from the references (Yun Wang et al., 2009) and (Nam et al., 2012) to validate the three-dimensional mathematical model.

After the mathematical model validation, these equations then implemented again in the COMSOL Multiphysics for the simulation of the three-dimensional model describing actual hydrogen storage canister used in the prior experiment. The simulation are conducted using identical conditions, as used in the previous experiment, and both of the simulation and experiment results are compared for validation purpose. The purpose of the simulation of the actual metal hydrides canister is to improve the understanding of the behavior of an actual metal hydride storage system. For instance, in metal hydride system, the canister is completely sealed, therefore it is impossible to observe the phenomena that are occurring within the canister.

Moreover, simulation is a flexible process which means that once the model is created, it can be easily utilized for other work conditions. Therefore, a parametric study is performed on the three-dimensional model describing actual hydrogen storage canister to study the effect and consequences of different metal hydrides properties on an actual metal hydrides storage system performance. Finally, a systematic optimization-based strategy for the design and operating conditions of metal hydride beds for hydrogen storage is performed to maximize the amount of hydrogen stored within the hydride.

Generally, this study focused on model validation and simulation of an actual AB_2 type metal hydrides canister, for which Ti-Mn based ($Ti_{0.99}Zr_{0.01}V_{0.43}Fe_{0.09}Cr_{0.05}Mn_{1}$) metal hydrides system is used in the experimental and simulation procedure.

3.2 Description of Dynamic Model

Metal hydrides bed is solid material with internal pore structures called porous media. Therefore, the mass and heat transfer aspects of metal hydrides bed are described through the mechanism of fluid flow and heat transfer in porous media.

In 1856, Darcy first quantified the relation between solid and liquid phases in porous media by identifying that the flow rate is proportional to the pressure gradient. The relationship can be applied for most porous media, but cannot be applied for non-Newtonian fluids, high velocity Newtonian liquids, and gases at very low or high velocities. Besides, the friction within the fluid and the momentum exchange between solid and fluid phases also neglected by Darcy.

In porous media, the molecules move follows the tortuous pathway in the void space (Truskey et al., 2004). There are two approaches that can describe the fluid flow in porous media which is to numerically solve the governed equation for fluid flow in individual pores or to assume that the porous medium is a homogenous material which is known as continuum approach. In the continuum approach, the volume fraction of the void space is assumed to be volumetric porosity, ε, and the volume fraction of the solid phase is $(1 - \varepsilon)$.

For the heat transfer mechanism, the equation that describes the first law of thermodynamics in a porous medium is used. The medium is adopted to be isotropic whereas radiation effects, viscous dissipation, and the work done by pressure changes are negligible for the sake of simplicity. Besides, there is local thermal equilibrium assumed so that the temperatures of the solid and gas phases inside the vessel are the same. In general, for heat transfer in porous medium, the overall thermal conductivity depends on the medium geometry. If the conduction of heat in the solid and gas phases occurs in parallel, then the efficient conductivity, k_e is the weighted arithmetic mean of the conductivities k_g and k_m where $k_e = \varepsilon k_g + (1 - \varepsilon)k_m$.

3.2.1 Model Assumption

The following assumptions are made for the flow and transport process in porous medium (Nasrallah & Jemni, 1997):

1. The gas phase (hydrogen) is treated as an ideal gas from thermodynamic view.
2. The solid phase (powdery metal alloy) is considered as an isotropic and homogenous porous medium.
3. The media (solid metal and hydrogen gas) is assumed to be in local thermal equilibrium. That means that the gas temperature and the metal temperature inside the vessel is the same.
4. The volumetric expansion of the metal hydride bed during absorption process is ignored.
5. The metal hydride properties such as porosity, permeability and thermal conductivity remain constant during the absorption process.

3.2.2 Governing Equations

Under these assumptions, the metal hydrides container is governed by the conservation equation of mass, momentum and thermal energy (Freni et al., 2009).

3.2.2.1 Mass conservation

Mass conservation equation for hydrogen gas is denoted by Equation (3.1):

$$\varepsilon \frac{\partial \rho_g}{\partial t} + \nabla\left(\rho_g \boldsymbol{u_g}\right) = -S_m \tag{3.1}$$

Where the gas density, ρ_g, can be expressed by Equation (3.2) (ideal gas law):

$$\rho_g = \frac{p_g . M_{H_2}}{R_g T} \tag{3.2}$$

The mass balance equation of the solid metal hydride then can be presented by Equation (3.3):

$$(1-\varepsilon)\frac{\partial \rho_m}{\partial t} = S_m \tag{3.3}$$

In Equations (3.1) and (3.3), ε represents the porosity of the metal hydride tank and S_m denotes the rate of hydrogen absorption per unit volume. Therefore, the volumetric mass source term, S_m, is zero in the expansion volume sub-region, but nonzero in the metal hydride sub-region. Then, S_m can be shown as follows (Jemni & Nasrallah, 1995).

$$S_m = C_a exp\left(-\frac{E_a}{R_g T}\right) In\left(\frac{P_g}{P_{eq}}\right)(\rho_{ms} - \rho_m) \tag{3.4}$$

Where C_a is absorption rate constant, E_a the activation energy, ρ_{ms} the density of metal hydride at the saturation state and P_{eq} the equilibrium pressure for hydrogen absorption that is greatly dependent on the temperature and H/M atomic ratio. Their correlation can be derived through van't Hoff's relationship as follows (Nam et al., 2012):

$$p_{eq} = p_{eq}^{ref}.exp\left(\frac{\Delta H}{R_g T} - \frac{\Delta S}{R_g}\right) = f\left(\frac{H}{M}\right).exp\left(\frac{\Delta H}{R_g T} - \frac{\Delta S}{R_g}\right) \tag{3.5}$$

3.2.2.2 Momentum conservation

Momentum balance equation consist of Darcy's term to describe the momentum transfer due to pressure gradient in the metal hydrides porous media. The hydrogen gas velocity ($\boldsymbol{u_g}$) which represent by Equation (3.6), can be computed using the Darcy's law (Jemni & Nasrallah, 1995):

$$\boldsymbol{u_g} = -\frac{K}{\mu_g}\nabla P_g \tag{3.6}$$

Where K is permeability, μ_g is hydrogen gas dynamic viscosity, P_g is gas pressure.

The solid permeability, K is given by the Kozeny – Carman's equation:

$$K = \frac{d_p^2 e^3}{150(1-\varepsilon)^2} \tag{3.7}$$

Where, d_p is the diameter of metal hydride particle.

3.2.2.3 Energy conservation

Assuming there is thermal equilibrium between the hydrogen gas and hydride bed, the energy equation is combined in the simulation instead of separate equations for the hydrogen gas and hydride bed which is denoted by Equation (3.8):

$$\left(\rho C_p\right)_e \frac{\partial T}{\partial t} + \left(\rho C_p\right)_g \left(\boldsymbol{u_g} \cdot \nabla \mathrm{T}\right) = \nabla \cdot (k_e \nabla \mathrm{T}) + S_T \tag{3.8}$$

Where, S_T is the heat source term given by Equation (3.9):

$$S_T = \zeta\left(\frac{\Delta H}{M_g}\right) = m\left(\Delta H - T\left(C_{pg} - C_{pm}\right)\right) \tag{3.9}$$

Considering only parallel heat conduction in solid and gas phases, the following expression for effective specific heat and thermal conductivity can be presented by Equation (3.10):

$$\left(\rho C_p\right)_e = \varepsilon\rho_g C_{pg} + (1-\varepsilon)\rho_s C_{pm} \tag{3.10}$$

The effective thermal conductivity is given by Equation 3.11:

$$k_e = \varepsilon k_g + (1-\varepsilon)k_m \tag{3.11}$$

The volumetric energy source term, S_T in Equation (3.8) denotes the heat release during the exothermic reaction of hydrogen absorption; therefore, the value is positive in the porous metal sub-region. Thus, S_T can be indicated as the product of the enthalpy change during hydrogen absorption (ΔH) and the volumetric hydrogen absorption rate, S_m, as shown by Equation (3.12).

$$S_T = S_m[\Delta H - T\left(C_{pg} - C_{pm}\right)] \tag{3.12}$$

3.2.3 Initial Conditions

Initially, the metal hydride canister is assumed to be in thermodynamic equilibrium, so the initial conditions are given by Equations (3.13)-(3.15):

$$T = T_0; \tag{3.13}$$

$$p = p_0; \tag{3.14}$$

$$\rho_m = \rho_{m,0} \tag{3.15}$$

where $\rho_{m,0}$ describes the initial hydrogen-empty metal hydride density. The initial value of hydrogen gas velocity is zero as hydrogen gas is absent in the metal hydride canister.

$$\boldsymbol{u_g} = 0 \tag{3.16}$$

3.2.4 Boundary Conditions

As for boundary conditions, no-slip velocity and no-flux condition are applied as the boundary walls are assumed to be impermeable. Therefore, the energy equation becomes as shown below where convection boundary condition is applied between the canister walls and exterior air.

$$k_e \frac{\partial T}{\partial \vec{n}} = h(T_{ext} - T) \tag{3.17}$$

Where $\vec{n}$ is the normal unit vector out of the vessel wall and T_{ext} is the exterior air temperature. Inlet conditions are enforced to the inlet region of computational domain according to the specified temperature and pressure.

3.2.5 Implementation of System into COMSOL Multiphysics

The governed mathematical equations are implemented into COMSOL Multiphysics software. COMSOL Multiphysics software uses the finite element method to solve the partial differential equations and time-dependent solver in the model since the dynamic conditions in the metal hydrides tank require time-dependent partial differential equation. The mathematical sorption model for porous metal hydrides compacts takes into account mass conservation of hydrogen-absorbed metal alloy, Darcy flow in the porous medium and heat generation by exothermic reaction during absorption. Besides, the COMSOL Multiphysics software enables the governing equations implementation by entering each differential equation as a separate physics mode, therefore permitting each one to have unique initial and boundary conditions.

3.2.5.1 Physics Mode

(a) *ODE and DAE Interfaces*

The Domain ODEs and DAEs interface, found under mathematic is used to add space-independent equations to domains. The field variables can represent additional states and the corresponding equations which can be ODEs, algebraic equations, and DAEs. In this study, it is used to simulate the mass conversation of hydrogen absorbed and is governed by Equation (3.3) and state variable ρ_m.

(b) *Darcy’s Law Interface*

The Darcy’s Law interface, located under the Porous Media and Subsurface Flow physics interface, is applied to model fluid flow through interstices in a porous medium. It is valid for low-velocity flows or media where the value of permeability and porosity are varied, and for which the pressure gradient is the major driving force and the flow is mostly determined by the frictional resistance within the pores. Set up multiple Darcy's Law interfaces to model multiphase flows involving more than one mobile phase. The Darcy's Law interface can be utilized for stationary and time-dependent analysis. This physic mode used for hydrogen flow in porous media is the combination of Equations (3.1) and (3.6) and the state variable p_g.

(c) *Heat Transfer Interface*

The Heat Transfer in Porous Media interface, located under Heat Transfer physics is used to simulate heat transfer by conduction, convection, and irradiation. On all domain, the Heat Transfer in Porous Media model is active by default. All functionality including other domain types, such as a solid domain, is also applicable. The temperature equation expresses in the porous media domain corresponds to the convection-diffusion equation with thermodynamic properties averaging models to account for both solid matrix and fluid properties. For this study, this physic mode is the final physics mode, which is for metal hydride energy conservation is governed by Equation (3.8) and the state variable is T.

The physics mode and implementation of governed equations into COMSOL Multiphysics simulation is summarized in the Table 3.1.

Table 3.1: Table of physics mode and implementation of governed equations

Purpose	Module	Application mode	Governed equation	State variable
Mass source term (Mass conservation)	Mathematics	ODE and DAE Interfaces ⇒Domain ODEs and DAEs (dode)	Eq. (3.2)	ρ_m
Fluid flow in porous media (Momentum conservation)	Fluid Flow	Porous Media and Subsurface Flow ⇒Darcy's Law Interface (dl)	Eq. (3.1) and Eq. (3.6)	p_g
Energy conservation	Heat transfer	Heat transfer in Porous Media (ht)	Eq. (3.8)	T

3.3 Validation of Mathematical Model

Numerical simulation is first conducted to validate the presented three-dimensional mathematical model for metal hydrides system. When a mathematical model of metal hydrides vessel is developed, it is significant to compare the model predictions to experimentally validated study. Jemni and Ben Nasrallah have carried out comprehensive modelling work, including experimental validation, and their experimental data have been used for model validation by other researchers such as Wang et al. (2009) and Nam et al., (2012).

Therefore, it is more convincing to compare the results of the model presented in this study with the experimentally validated model results from Wang et al. (2009) and Nam et al., (2012). The purpose of validating against experimentally validated model results and not directly against the experimental results is because the model results are more precise and based on a scenario that is easy to replicate while experimental results are usually limited

3.3.1 Overview of the Model

Since the mathematical model which has been presented in Section 3.2 is been validated with previous experimentally validated model results from Wang et al. (2009) and Nam et al., (2012), therefore the geometry, material and parameters used in the model simulation are implemented from them and will be explained further.

3.3.1.1 Geometry

The metal hydrides tank is simple cylindrical vessel identical to model geometry from Wang et al. (2009) and Nam et al., (2012) with geometrical dimensions as shown in Figure 3.1.

Figure 3.1: Geometry of metal hydride tank in COMSOL

3.3.1.2 Material

Regarding the metal inside the tank, $LaNi_5$ is used as the alloy material as reviewed from Wang et al. (2009) and Nam et al., (2012).

The reaction then is:

$$LaNi_5 + 3H_2 \leftrightarrow LaNi_5H_6 + \Delta H \quad (3.18)$$

3.3.1.3 Parameters used in Simulation

The kinetic parameters for Equation (3.1), thermal–physical properties of $\mathrm{LaNi_5}$ and $\mathrm{LaNi_5}$ hydride ($\mathrm{LaNi_5H_6}$), and operating conditions for the absorption process used in the simulation are given in Table 3.2.

Table 3.2: List of parameters used in simulation for $\mathrm{LaNi_5}$ system

Parameter	**Designation**	**Value**
Hydrogen absorption constant on metal alloy	Ca_h	$59.187\ \mathrm{s^{-1}}$
Hydrogen activation energy	Ea_h	$21179.6\ \mathrm{J/mol}$
Hydrogen heat capacity	c_{pg}	$14890\ \mathrm{J/kg.K}$
Metal heat capacity	c_{pm}	$419\ \mathrm{J/kg.K}$
Reaction enthalpy	ΔH	$29879\ \mathrm{J/mol}$
Reaction entropy	ΔS	$108\ \mathrm{J/mol.K}$
Porosity	ε	0.63
Heat transfer coefficient	h_{ct}	$1652\ \mathrm{W/m^2.K}$
Permeability	K	$1 \times 10^{-8}\ \mathrm{m^2}$
Hydrogen thermal conductivity	k_g	$0.1672\ \mathrm{W/m.K}$
Metal thermal conductivity	k_m	$3.18\ \mathrm{W/m.K}$
Hydrogen molar weight	M_g	$2\ \mathrm{g/mol}$
Metal molar weight	M_m	$432\ \mathrm{g/mol}$
Hydrogen dynamic viscosity	μ	$8.411 \times 10^{-6}\ \mathrm{Pa.s}$
Empty metal hydride density	ρ_{m0}	$4200\ \mathrm{kg/m^3}$
Saturated metal hydride density	ρ_{ms}	$4264\ \mathrm{kg/m^3}$
Atm pressure	p_{atm}	1 bar
Inlet pressure	p_{in}	10 bar
Reference pressure	p_{ref}	10 bar
Ambient temperature	T_{amb}	293 K
Reference temperature	T_{ref}	303 K
Gas constant	R	$8.314\ \mathrm{J/mol.K}$
Pie	π	3.142857143

3.4 Validation of Actual Simulation

For the actual simulation of real metal hydrides system, the three-dimensional model validated in the previous section is implemented into COMSOL Multiphysics using an actual hydrogen storage canister used in the prior experiment. In order to accurately present the actual simulation of the real metal hydrides tank, some experimental data is required. Some experimental data for the absorption of metal hydrides is available from previous study of other researcher's team which has been developed and performed in the Hydrogen Fuel Cell laboratory of Universiti Malaya (UM).

Therefore, the simulation is conducted using identical conditions, as used in the experiment, i.e.: geometry, material, operating condition in order to validate the computational simulation data with actual metal hydrides data. The objective of the validation is not to exactly match the values obtained by both methods, but to achieve the same tendency and the same orders of magnitude.

3.4.1 Overview of the Model

The distinct aspect between the model implemented in Section 3.3 and the final model, are the geometry, as well as the properties that come with it, for example material, parameters and operating condition as it is adapted from the actual hydrogen storage canister used in the prior experiment.

3.4.1.1 Geometry

At first, a simple cylinder identical to model geometry from Wang et al. and Nam et al. was drawn for model validation purpose, but lastly the actual geometry of the real metal hydride canister is implemented. To acquire that final geometry few measurements of the actual canister are taken and a three-dimensional solid geometry is created on COMSOL Multiphysics. The units are set on millimeters. The geometry dimensions of the metal hydrides canister is as shown in Figure 3.2.

Figure 3.2: Geometry of the actual metal hydride tank in COMSOL

3.4.1.2 Material

For this study, an AB_2-type (Laves phase) alloy is chosen for their excellent hydrogen-storage capacity and operating conditions. Most of the Laves phases exhibit high capacities, fast kinetics, long life and a relatively low cost in comparison to the $LaNi_5$-related systems. Therefore, a commercially available AB_2-type metal hydrides tank is selected from Horizon Fuel Cell Technologies. The definite composition of the alloy used in the hydride product is unknown, so a scanning electron microscope (SEM) which is used to analyze the samples. The electrons interact with the atoms in the sample, producing various signals that carry information about the sample's surface topography and composition. Based on the SEM result, $Ti_{0.99}Zr_{0.01}V_{0.43}Fe_{0.09}Cr_{0.05}Mn_{1.5}$ alloy is selected considering its similar element number. Some properties of this material are obtained from (Satheesh & Muthukumar, 2010) and shown in Table 3.3.

Table 3.3: List of properties of $Ti_{0.99}Zr_{0.01}V_{0.43}Fe_{0.09}Cr_{0.05}Mn_{1.5}$ alloy

Parameter	Designation	Value
Hydrogen absorption constant on metal alloy	Ca_h	$100s^{-1}$
Hydrogen activation energy	Ea_h	$28000\ \mathrm{J/mol}$
Metal heat capacity	c_{pm}	$500\ \mathrm{J/kg.K}$
Reaction enthalpy	ΔH	$20120\ \mathrm{J/mol}$
Reaction entropy	ΔS	$97.4\mathrm{J/mol.K}$
Porosity	ε	0.65
Convection coefficient	h_{ct}	$500\mathrm{W/m^2.K}$
Permeability	K	$1 \times 10^{-8}\mathrm{m}^2$
Metal thermal conductivity	k_m	$1.6\ \mathrm{W/m.K}$
Metal molar weight	M_m	$160.24\ \mathrm{g/mol}$
Hydrogen dynamic viscosity	μ	$9.5 \times 10^{-6}\mathrm{Pa.s}$
Empty metal hydride density	ρ_{m0}	$5500\ \mathrm{kg/m^3}$
Saturated metal hydride density	ρ_{ms}	$5563\ \mathrm{kg/m^3}$

3.4.1.3 Parameters used in Simulation

The parameters and operating conditions used in the simulation are listed in Table 3.4.

Table 3.4: List of parameters and operating conditions used in the simulation

Parameter	Designation	Value
Hydrogen absorption constant on metal alloy	Ca_h	$100s^{-1}$
Hydrogen activation energy	Ea_h	$28000\ \mathrm{J/mol}$
Hydrogen heat capacity	c_{pg}	$14290\ \mathrm{J/kg.K}$
Metal heat capacity	c_{pm}	$500\ \mathrm{J/kg.K}$
Reaction enthalpy	ΔH	$20120\ \mathrm{J/mol}$
Reaction entropy	ΔS	$97.4\mathrm{J/mol.K}$
Porosity	ε	0.65
Convection coefficient	h_{ct}	$500\mathrm{W/m^2.K}$
Permeability	K	$1 \times 10^{-8}\mathrm{m}^2$
Hydrogen thermal conductivity	k_g	$0.182\ \mathrm{W/m.K}$
Metal thermal conductivity	k_m	$1.6\ \mathrm{W/m.K}$
Hydrogen molar weight	M_g	$2\ \mathrm{g/mol}$
Metal molar weight	M_m	$160.24\ \mathrm{g/mol}$
Hydrogen dynamic viscosity	μ	$9.5 \times 10^{-6}\mathrm{Pa.s}$
Empty metal hydride density	ρ_{m0}	$5500\ \mathrm{kg/m^3}$
Saturated metal hydride density	ρ_{ms}	$5563\ \mathrm{kg/m^3}$
Atmospheric pressure	p_{atm}	1 bar
Inlet pressure	p_{in}	20 bar
Initial pressure	p_0	8 bar
Reference pressure	p_{ref}	20 bar
Ambient temperature	T_{amb}	305.15 K

Table 3.4 continued.

Parameter	**Designation**	**Value**
Inlet temperature	T_{in}	306.15 K
Initial temperature	T_0	293.15 K
Reference temperature	T_{ref}	293.15 K
Gas constant	R	8.314 J/mol. K
Pie	π	3.142857143

3.4.1.4 Mesh Sensitivity Analysis

Prior to analyzing solutions developed by the model, a mesh sensitivity analysis is conducted to ascertain that a suitable mesh size and solution time are utilized. The mesh sensitivity analysis is conducted by observing the effect of modifying the grid size on the evolution of temperature and density over time. The idea of this sensitivity analysis is to start with an extremely coarse mesh and refine it gradually in order to get a rather fine mesh where the meshes are generated by tetrahedral, creating a grid. The computational simulation will be simulated using all the developed meshes and then the optimum mesh for the absorption process is decided.

3.4.2 Experimental Set Up

As explained in Section 3.4 of the project, the experimental data for the validation purpose is collected from previous study of other researcher's team. The experiment has been developed and conducted using a test rig at the Hydrogen Fuel Cell laboratory of Universiti Malaya (UM). Figure 3.3 shows the actual hydrogen test rig located at Hydrogen Fuel Cell laboratory of Universiti Malaya (UM).

Figure 3.3: Hydrogen test rig located at Hydrogen Fuel Cell laboratory of University of Malaya (UM)

In order to briefly understand the experimental procedure, a simple diagram for the experimental set up is illustrated in Figure 3.3 and followed by a brief explanation of the experimental procedure.

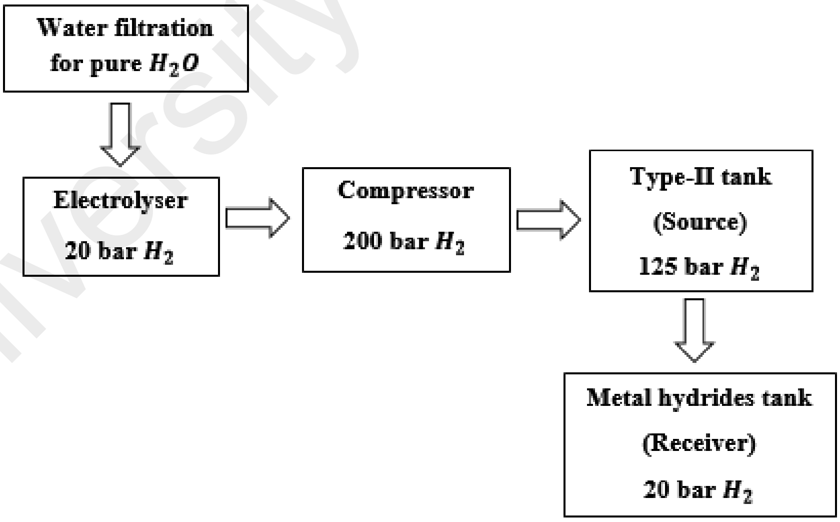

Figure 3.4: Simple experimental set up diagram

A simple diagram for the experimental procedure is shown on Figure 3.4. The diagram explains starting from the process of producing the hydrogen, compression of the gas and finally the storage system. Filtration of the tap water through the water filtration process produced demineralized water where the allowable conductivity was less than 5 μS. The pure water was supplied to the electrolyser which broke up the water into two gases, hydrogen and oxygen as shown in the equation below. The hydrogen gas produced from this process was 99.9 % pure.

$$H_2O + energy \rightarrow O_2(gas) + H_2(gas) \quad (3.2)$$

To summarized the process, the water inside electrolyser is separated by method of electrolysis. The products of the electrolysis, hydrogen and oxygen gas, entrains the electrolyte up to separating which separate the gas phase from excess liquid phase by method of weight separation. Water which is heavier than air and under the pressure of the separating vessel will fall back down to the bottom of the separating vessel, whereas the hydrogen and oxygen gas along with any other components that is carried by these gases will rise to the top of the vessel. Water that has fallen to the bottom of the vessel will again flow into the cell stack to go through electrolysis again.

Then, the hydrogen gas was supplied to the water piston jet compressor that was capable of compressing the gas up to 200 bar, but the maximum pressure of the hydrogen that mass flow meter can withstand was 125 bar. For the sake of compensating the mass flow meter limit, the hydrogen gas was compressed up to 125 bar only. Finally the gas was supplied to the storage cylinder type-II as a source tank. A 4 mm tubing was connected between both type-II and metal hydrides cylinders as the receiver. A globe valve was fitted at each cylinder and another globe valve was fitted at the coriolis mass flow meter for control during the experiment. The data collected during the experiment is recorded using Prolink software.

The metal hydrides canister used in the experiment is a commercial metal hydrides tank called MH-350 Metal Hydride Canisters. The MH-350 Metal Hydride Canisters are developed and manufactured by Horizon Fuel Cell Technologies and are designed with aluminum alloy as the canister material and AB_2 (Ti-Mn based) alloy for the hydrides bed material. This AB_2 alloy can be able to absorb hydrogen, expand and release heat until saturation. The internal pressure of the hydrides tank remains at 8 Bar at ambient temperatures of 20℃-25℃ . When the canister valve is opened and pressure is reduced, hydrogen gas will be released from the alloy material which will absorb heat. The rate of hydrogen release will be decreased if the rate of heat absorption decreases. The aluminum alloy which used for canister enclosure has excellent heat conductivity properties that can facilitate heat conduction of the alloy during gas intake and release processes. Figure 3.5 shows the geometry of the MH-350 Metal Hydride Canisters.

Figure 3.5: MH-350 Metal Hydride Canisters

3.5 Sensitivity Analysis of Metal Properties

After validating the actual simulation with experimental result, a sensitivity analysis on metal hydrides properties is performed to study the effect of metal hydrides properties on the behavior of the hydrogen storage system during the absorption process especially in term of mass and heat transfer. The metal properties sensitivity analysis is conducted by performing a parametric studies using computational simulation on variation of small and major influence parameters such as porosity (ε), permeability (K), metal thermal conductivity (k_m), hydrogen absorption constant on metal (c_a), activation energy (E_a) and heat transfer coefficient (h_{ct}). Table 3.5 shown the list of parameter values used in the parametric studies for each parameter. The parameter values are selected by reviewing others studies (Satheesh & Muthukumar, 2010), (Busqué Somacarrera, 2015).

Table 3.5: List of parameters used in the parametric studies for each parameter.

Parameter	**Values**				
Porosity ,ε	0.10	0.30	0.50	0.65	0.80
Permeability, K (m^2)	1×10^{-10}	1×10^{-8}	1×10^{-5}	1×10^{-3}	1.00
Thermal conductivity, k_m ($\mathrm{W/m.K}$)	0.10	1.00	1.60	6.50	10.00
Absorption constant , c_a (s^{-1})	1	10	50	100	305
Activation energy, E_a ($\mathrm{J/mol}$)	2000	2800	3500	5000	10000
Heat transfer coefficient, h_{ct} ($\mathrm{W/m^2.K}$)	10	50	200	500	1000

3.6 Optimization on Metal Hydrides System

Optimization of the operating condition used for a metal hydride based hydrogen storage system which can influence the gravimetric hydrogen storage density, and refueling time. Therefore, a study on the operating condition is presented to find the optimal operating strategy which includes operating pressure and temperature so as to minimize the storing time, while satisfying a number of operating constraints. To study the effect of pressure, five different pressure values are studied by keeping the other operating parameters as constant. The pressure values are varied from 10 to 50 bar as shown in Table 3.6. For temperature, the same procedure as pressure is used by varying the temperature value from 25 to 50 °C as illustrated in Table 3.6.

Table 3.6: Operating value used in the optimization studies for charging pressure and temperature

Parameters	**Values**				
Charging pressure (bar)	10	20	30	40	50
Temperature (°C)	25	33	40	43	50

CHAPTER 4: RESULT AND DISCUSSION

4.1 Introduction

In this chapter, the results from the three-dimensional simulation of metal hydrides bed using COMSOL Multiphysics are presented and discussed in detailed.

4.2 Modelling Results

As proposed in Chapter 3, the mathematical model obtained from Freni et al. (2009) is first simulated using the geometry, material and parameters from Yun Wang et al. (2009) and Nam et al. (2012) for metal hydrides absorption process. The purpose of the numerical simulation is to validate the presented three-dimensional mathematical model in Section 3.2 for metal hydrides system. The model is simulated considering an inlet pressure of 10 bar at a constant temperature of 30 ℃ over the time interval of 1500 s. The tank is considered initially at a temperature of 20 ℃ and a pressure of 0 bar. Modelling results include pressure, temperature, and density of metal hydrides during absorption process are illustrated below.

4.2.1 Pressure

In Figure 4.1, the graph illustrated the hydrogen gas pressure inside the canister during absorption process. Initially, the relative pressure of hydrogen gas is 0 bar which means that the pressure within the canister is atmospheric. As pressurized hydrogen starts to enter the canister immediately during charging process, a sharp pressure increase is observed until it gets the value of 10 bar. This is the hydrogen pressure value during the charging process. The final pressure of 10 bar is quickly achieved because pressure is a fast traveler, and so within a few seconds the canister is already pressurized completely.

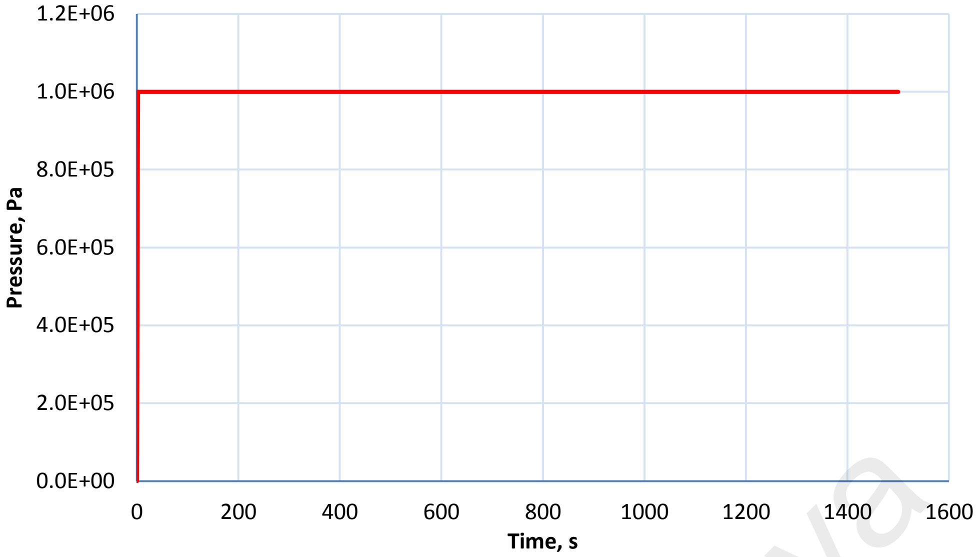

Figure 4.1: Relative gas pressure inside the canister over time. Point located r = 0 mm, z = 30 mm

4.2.2 Temperature

As shown in Figure 4.2, the temperature distribution inside the hydrides bed during absorption process is illustrated. From the simulation result, it can be observed that the temperature increase sharply at the beginning, which means that the hydrogen absorption reaction rate is fast at the initial stage. This is due to the abrupt discharge of heat which dominates over the rate of heat removal by heat convection with exterior air. Then, the temperature of the canister diminished gradually, due to slower absorption reaction resulting from an increase in equilibrium pressure which means the hydrogen absorption close to complete (Nam et al., 2012).

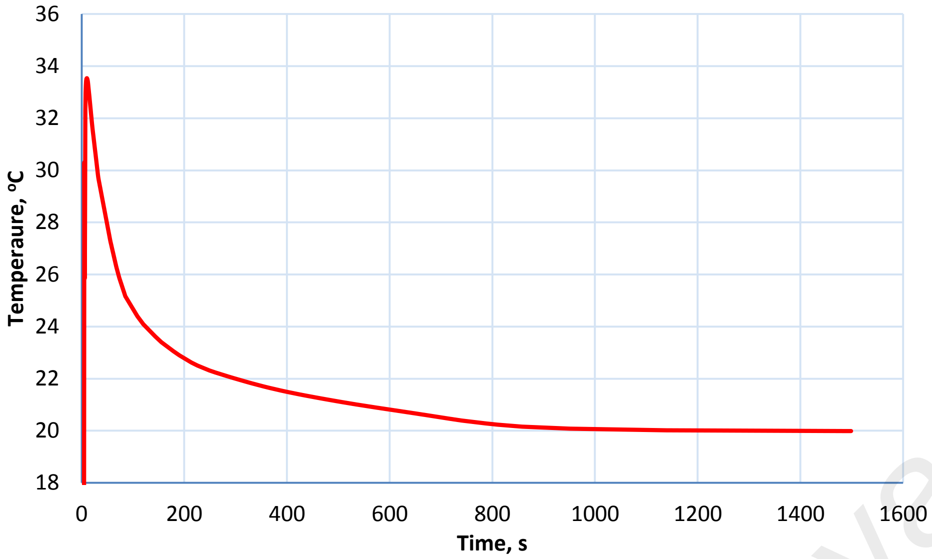

Figure 4.2: Temperature inside the canister over time. Point locate r = 25 mm, z = 30 mm

4.2.3 Metal Hydrides Density

The metal hydride density evolution over time is displayed in Figure 4.3. It can be observed that there is a sharp increase metal hydride density at the initial stage, which is due to the fast absorption reaction rate at the beginning where large amount of hydrogen is absorbed into metal to form metal hydride. The abrupt increase in density corresponds with the high temperature levels from Figure 4.2, because the chemical reaction occurred. Then, the density growth rate starts to slow down until the hydrides bed become saturated. When there are no more available void spaces for hydrogen to be absorbed, the saturated metal hydride density is achieved.

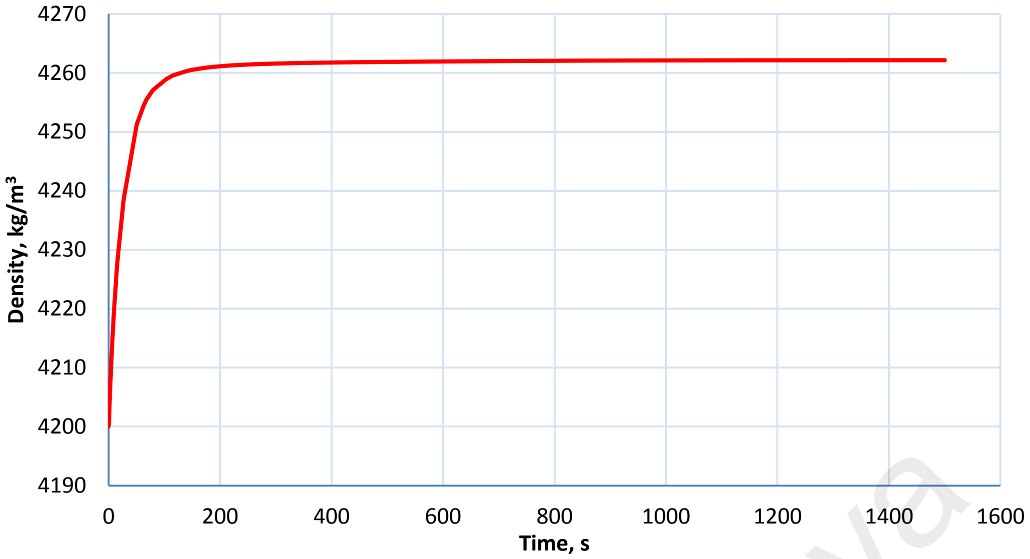

Figure 4.3: Metal hydride density over time. Point located r=0, z=0

4.3 Validation of Mathematical Model

The modelling result from Section 4.2 are then been validated with previous experimentally validated model results from Yanzhi Wang et al. (2009) and Nam et al. (2012). The validations focused on the temperature evolution of metal hydrides bed at six different points and the equilibrium pressure as a function of the hydrogen to metal atomic ratio and temperature for hydrogen absorption at T = 30 ℃.

4.3.1 Temperature Evolution

The first validation is to compare the evolution of temperature from this project with other published work. In the left plot, Figure 4.4 (a) there is an evolutions of temperatures at six different locations of the tank from the work of Wang et al. (2009). It can be observed that the evolution curve shape is almost similar in both plots, but on the right graph, the metal hydrides canister cooled down faster. This is due to some assumption done for missing information, as Wang et al. (2009) didn't provide all the required information.

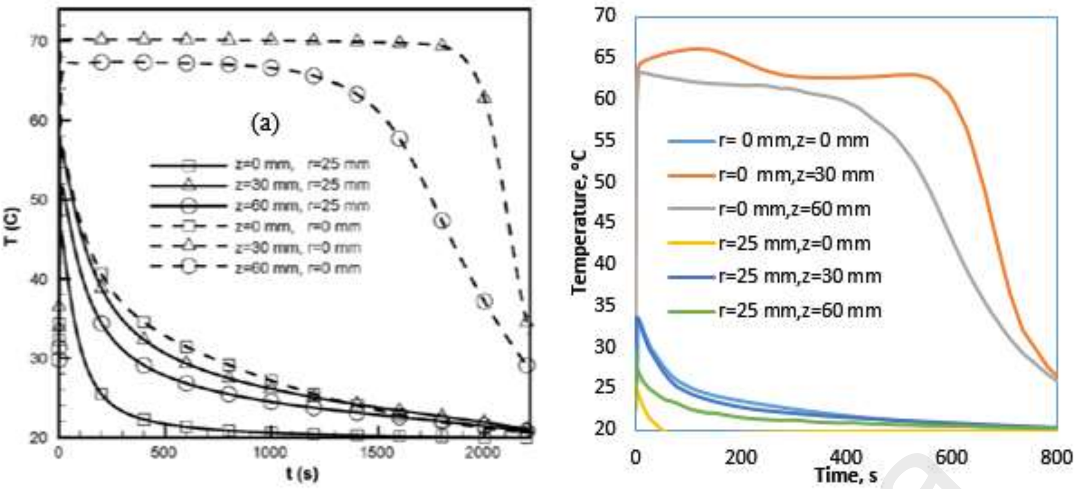

(a) (b)

Figure 4.4: (a) Temperature evolution profiles obtained by Wang et al. (2009); (b) Temperature evolution profiles obtained in this project

4.3.2 Equilibrium Pressure as a Function of hydrogen/ metal (H/M)

The next comparison will be focused on the equilibrium pressure as a function of the hydrogen/ metal (H/M) atomic ratio and temperature for hydrogen absorption at T=30 ℃. As it can be seen in the Figure 4.5(a) and (b), the shape of curve of both graph are very similar. The plot on the left is extracted from Nam et al. (2012) and the other is the one that has been obtained in this work.

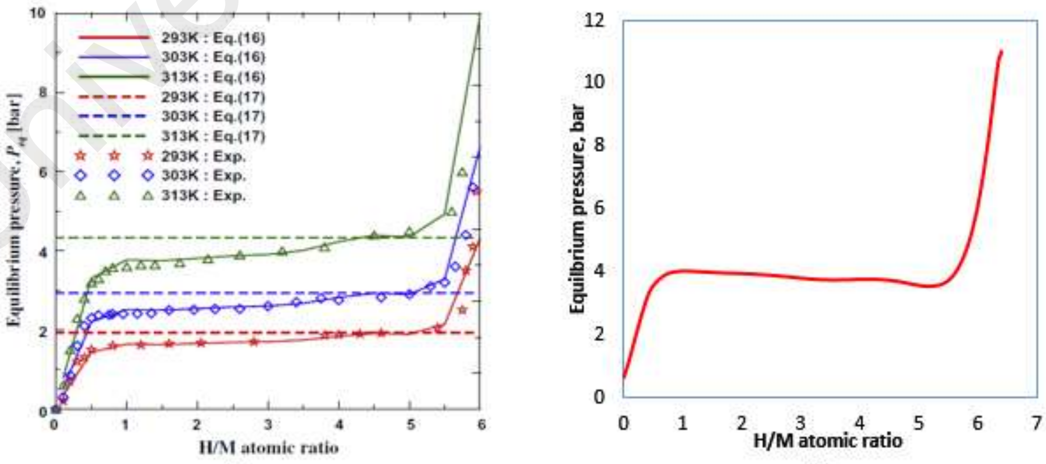

(a) (b)

Figure 4.5: (a) The equilibrium pressure as a function of the H/M atomic ratio and temperature for hydrogen absorption by Mellouli et al. (2010) (b) The equilibrium pressure as a function of the H/M atomic ratio and temperature for hydrogen absorption this project

4.4 Actual Simulation

After validation in Section 4.3, the three-dimensional model is further implemented into COMSOL Multiphysics using an actual hydrogen storage canister. The model is simulated considering the actual metal hydrides properties used in the prior experiment with an inlet pressure of 20 bar and temperature of 33 ℃ over the time interval of 600 s. The canister is considered initially at a temperature of 20 ℃ and a pressure of 8 bar. The purpose of this simulation is to study the behaviour of real metal hydrides system especially in terms of mass and heat transfer.

4.4.1 Mesh Sensitivity Analysis

Prior to implementing the actual simulation, a mesh sensitivity analysis is conducted to ascertain that a suitable mesh size and solution time are utilized. This sensitivity analysis is conducted by observing the effect of modifying the grid size on the evolution of temperature and density over time. The idea of this sensitivity analysis is to start with an extremely coarse mesh and refine it gradually in order to get a rather fine mesh where the meshes are formed by tetrahedral, creating a grid. The computational simulation will be simulated using all the developed meshes and then the optimum mesh for the absorption process is decided. The characteristics of the mesh are defined in Figure 4.6.

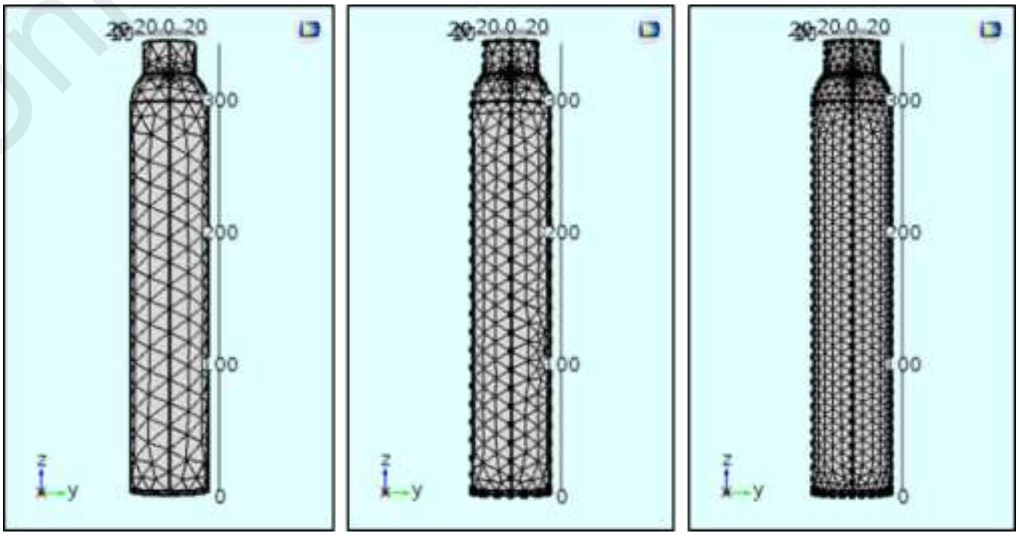

(a) (b) (c)

Figure 4.6 continued.

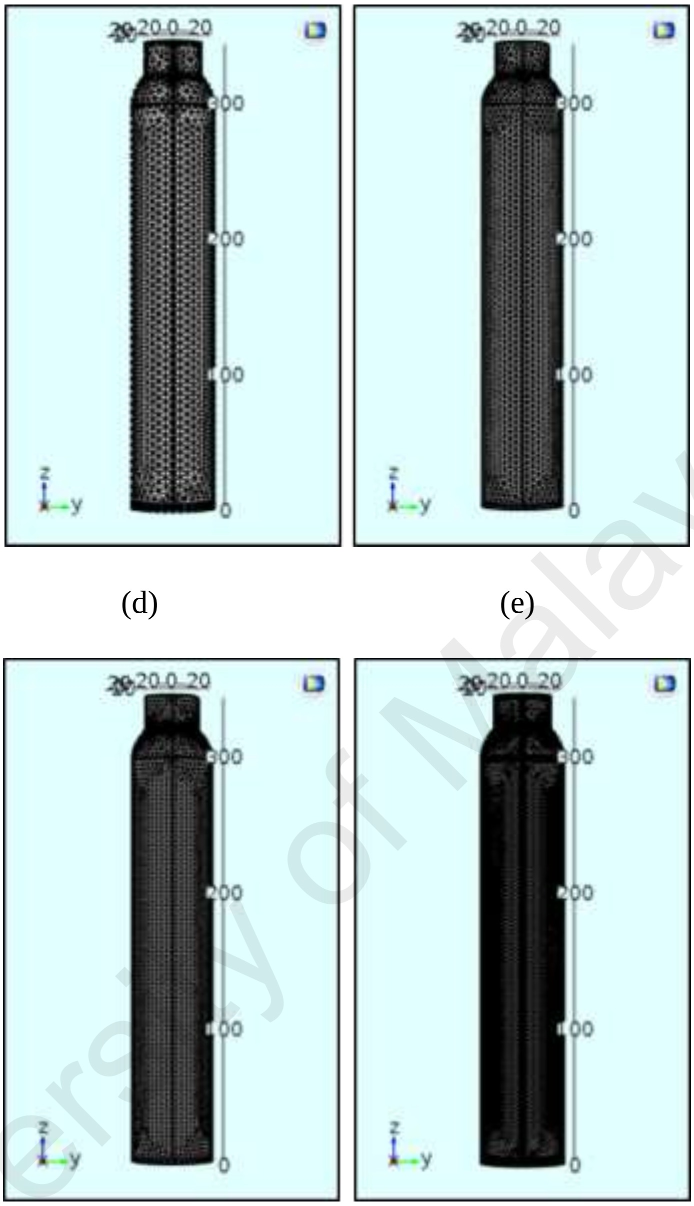

(d) (e)

(f) (g)

Figure 4.6: The characteristics of each types of mesh (a) Extra coarse; (b) Coarser; (c) Coarse; (d) Normal; (e) Fine; (f) Finer; (g) Extra fine

The results of the mesh analysis are given in terms of temperature and density as shown in Figure 4.7 and Figure 4.8 for simulation period of 300 s.

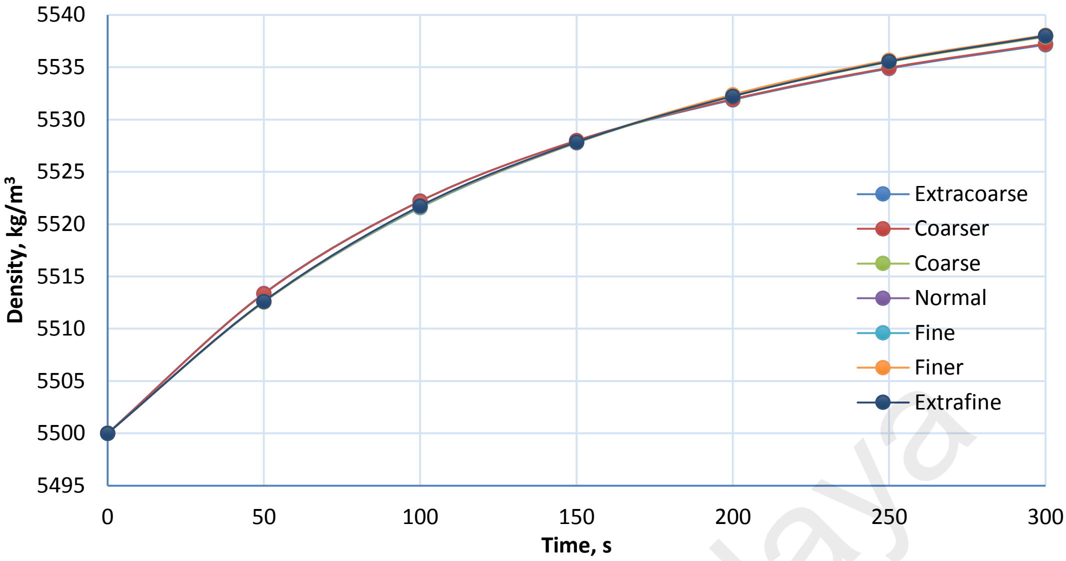

Figure 4.7: Density of metal hydrides bed for different types of mesh size at point r = 0 mm, z = 150 mm

Table 4.1: Density values of metal hydrides bed for different types of mesh size at point r = 0 mm, z = 150 mm

Time (s)	**Density (kg/m^3)**						
	Extra coarse	**Coarser**	**Coarse**	**Normal**	**Fine**	**Finer**	**Extra fine**
0	5500.00	5500.00	5500.00	5500.00	5500.00	5500.00	5500.00
50	5513.38	5513.34	5512.55	5512.61	5512.60	5512.61	5512.62
100	5522.21	5522.19	5521.58	5521.62	5521.61	5521.69	5521.74
150	5527.97	5527.99	5527.78	5527.79	5527.81	5527.82	5527.84
200	5531.89	5531.96	5532.23	5532.30	5532.35	5532.39	5532.23
250	5534.87	5534.96	5535.52	5535.58	5535.63	5535.67	5535.55
300	5537.15	5537.25	5537.93	5537.97	5538.03	5538.06	5538.00

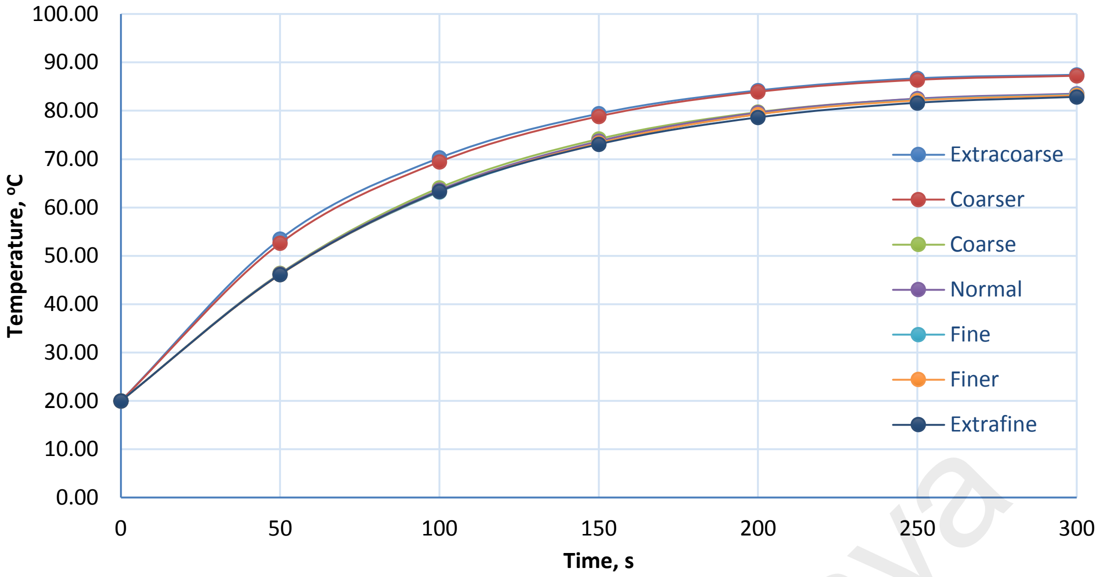

Figure 4.8: Temperature of metal hydrides canister for different types of mesh size at point r = 0 mm, z = 150 mm

Table 4.2: Temperature values of metal hydrides canister for different types of mesh size at point r = 0 mm, z = 150 mm

Time (s)	**Temperature (°C)**						
	Extra coarse	**Coarser**	**Coarse**	**Normal**	**Fine**	**Finer**	**Extra fine**
0	20.00	20.00	20.00	20.00	20.00	20.00	20.00
50	53.49	52.61	46.38	46.30	46.16	46.12	46.16
100	70.27	69.46	64.09	63.61	63.21	63.36	63.36
150	79.42	78.86	74.18	73.73	73.26	73.32	73.07
200	84.23	83.92	79.74	79.63	79.24	79.26	78.61
250	86.73	86.40	82.49	82.54	82.22	82.15	81.64
300	87.46	87.26	83.42	83.56	83.30	83.20	82.85

As shown in the Figure 4.7 and Figure 4.8, it can be seen that the different mesh size result in slightly different curves. The results attained from the normal, the fine, the finer and the extra fine mesh match closely and did not have much deviation from each other. The solving time for each of the simulations using different types of mesh sizes are also compared to optimize the time taken for the whole simulation. The total mesh size and solution time of each mesh are summarized in Table 4.3.

Table 4.3: Summarization of total mesh size and solution time of each mesh type

	Extra coarse	Coarser	Coarse	Normal	Fine	Finer	Extra fine
Domain Element	4144	7425	12983	32019	51969	86105	172750
Boundary Element	2054	3315	5166	10078	14878	21654	35280
Edge Element	412	537	680	918	1126	1410	2016
Solution Time (s)	71	92	150	461	776	1235	2523
DOF	16655	32351	66203	199685	342623	573109	1062004

4.4.2 Actual Simulation Results

Finally, after all the precise steps in the previous sections, the actual simulations are performed. The main parameters which are associated with the mass and heat transfer in the hydride bed include hydride bed temperature and the concentration of hydrogen in metal hydride. Therefore, the validations focused on the bed temperature and mass of hydrogen absorbed by the metal hydrides.

4.4.2.1 Temperature

As presented in Figure 4.9, it can be seen that the temperature evolution is quite different to the one obtained in Section 4.2. The first significant difference is the time scale. This is because for Section 4.2, the simulation time for absorption process was 1500 s, while for the actual process with the new conditions; the simulation time for the absorption process is only 600 s. However, it can be observed that the temperature pattern from this plot is similar to the temperature pattern from Figure 4.4 for r = 0 mm, z = 60 mm at the first 600 s.

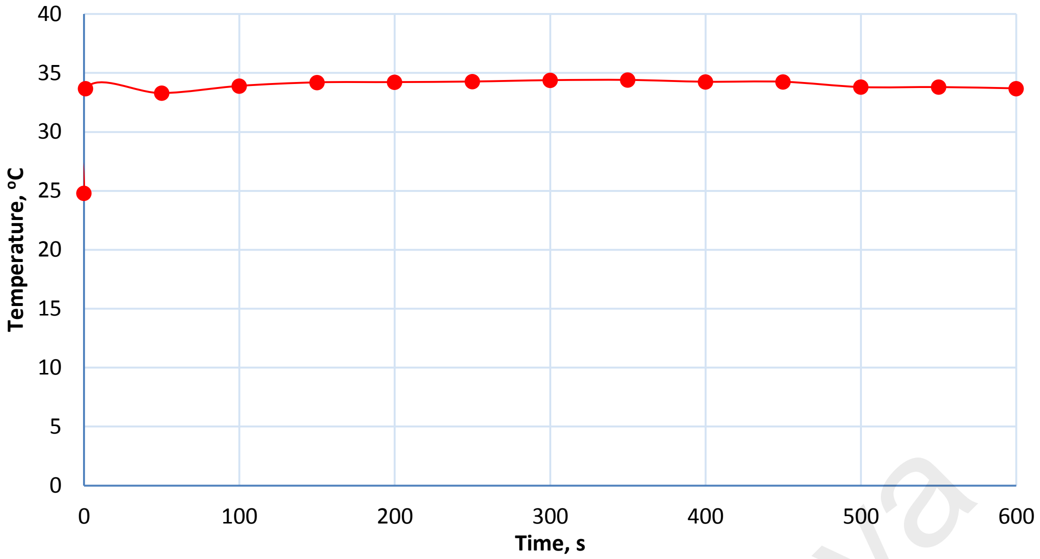

Figure 4.9: Temperature of metal hydride canister over time. Point located r = 0 mm, z = 322 mm

The temperature distributions in half a cross-section of the hydride canister at six different points are shown in Figure 4.10. At t=0 s, the canister is at its initial conditions but the canister temperature rapidly increase as the hydrogen absorption process proceeds. At t=100 s, the metal hydrides bed achieved its highest temperature on the metal hydride region which is the core region. This is mainly due to the fact that enormous void space available for rapid absorption reaction rate. It is noticed that the area near the wall is much colder than the core region. At t=200 s, the core region stil1 is at a high temperature, but the walls are starting to cool down due to the convection with surrounding exterior air. As time proceeds, the area close to the canister wall temperature is reduced to the outside temperature, which indicates that the absorption of metal hydride nearly complete and the absorption rate has decreased. However, the core region of the canister is still at higher temperature due to ongoing absorption reaction at a much higher rate in that region. It can likewise be mentioned that at t=500 s, some heat is being transmitted to the area between the void region and the metal hydride zone as the temperature has increased a little in that area. At t=600 s, the canister temperature seems to return to its initial value as the reaction has completed.

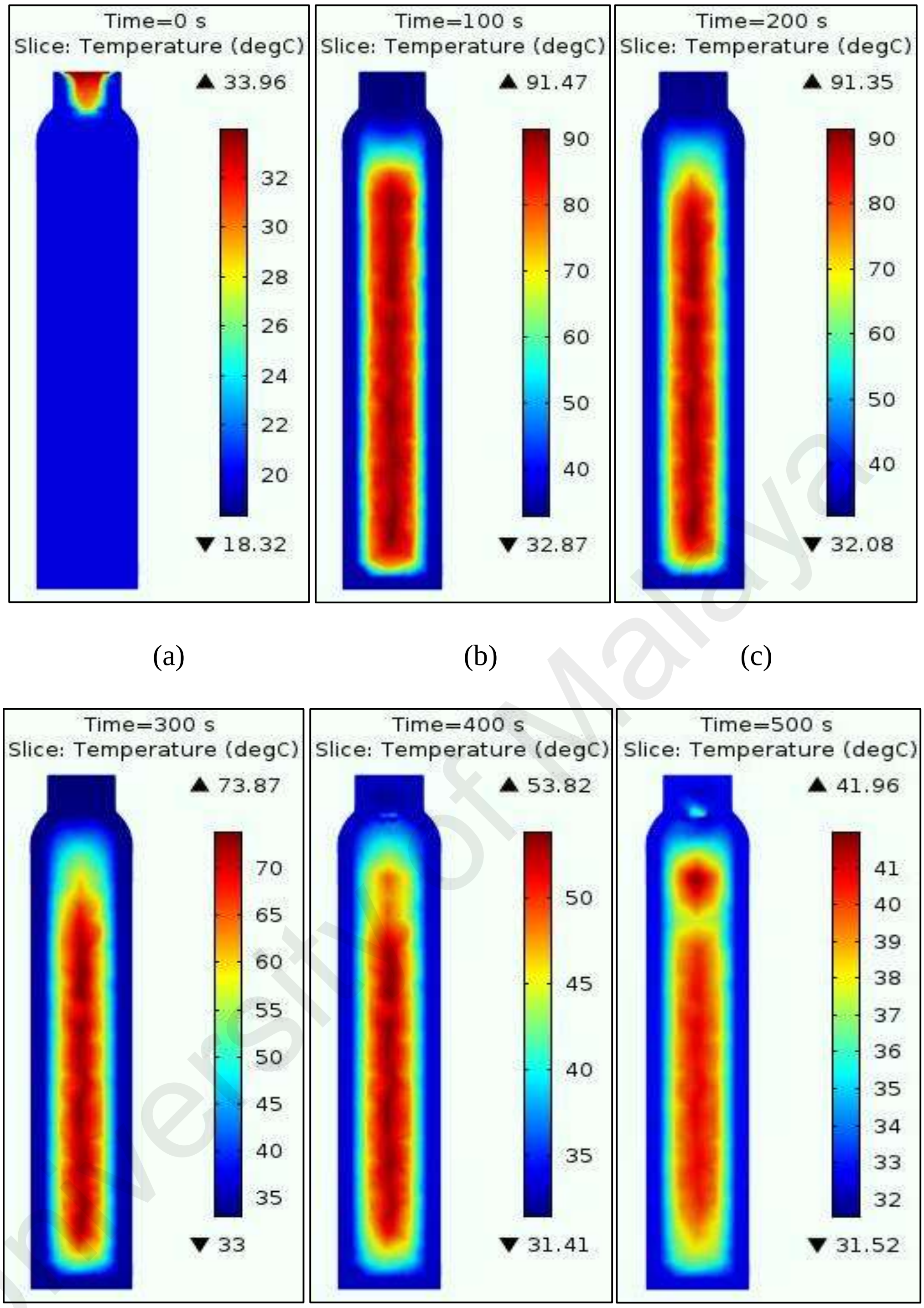
Time=0 s
Slice: Temperature (degC)
▲ 33.96
32
30
28
26
24
22
20
▼ 18.32
Time=100 s
Slice: Temperature (degC)
▲ 91.47
90
80
70
60
50
40
▼ 32.87
Time=200 s
Slice: Temperature (degC)
▲ 91.35
90
80
70
60
50
40
▼ 32.08
Time=300 s
Slice: Temperature (degC)
▲ 73.87
70
65
60
55
50
45
40
35
▼ 33
Time=400 s
Slice: Temperature (degC)
▲ 53.82
50
45
40
35
▼ 31.41
Time=500 s
Slice: Temperature (degC)
▲ 41.96
41
40
39
38
37
36
35
34
33
32
▼ 31.52

(a) (b) (c)

(d) (e) (d)

Figure 4.10 continued.

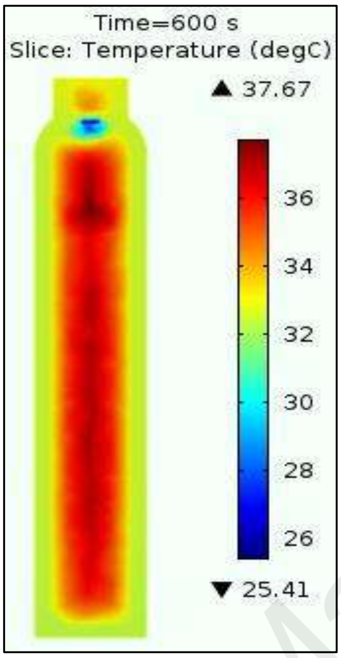

(g)

Figure 4.10: Temperature profiles in half of a cross-section of the hydrogen storage canister at (a) 0 s; (b) 100 s; (c) 200 s; (d) 300 s; (e) 400 s; (f) 500 s and (g) 600 s

4.4.2.2 Mass of Hydrogen Absorbed

In the next plot, Figure 4.11 shows the evolution of hydrogen gas absorbed over time. Similar to density evolution, it can be seen that at the first few seconds, the hydrogen mass absorbed increases with a sharp rise but then becomes more uniform. This is due to the charging process that becoming much slower after the first 100 s, because the hydrides density slowly starting to achieve the saturation value, which means that the canister is close to completely fill with hydrogen.

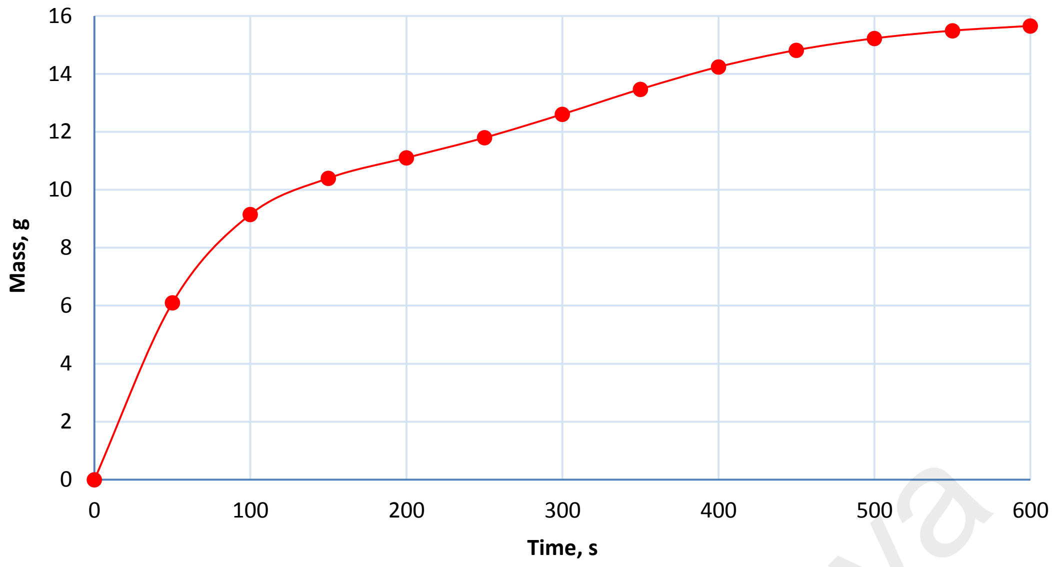

Figure 4.11: Mass of hydrogen gas absorbed over time. Point located at r = 0 mm, z = 150 mm

From Figure 4.10, it is observed that the bed temperature decreases continuously from the metal hydride core region to the convective wall in radial direction. It can be concluded that the amount of heat removal is very fast for the area close to the convective wall. Because of this, the core region of the metal hydride bed experiences high temperature resulting in a slower hydration rate as the metal hydride bed temperature strongly influences the hydride equilibrium pressure. Figure 4.12 illustrated the density distributions at the six time instants and reveals that the rate of hydrogen absorbed in the area near the convective wall is higher due to fast removal of the reaction heat. At 0 s, it shows that the density distribution is uniform, while higher values appear near the wall and the bed upper surface starting from 200 s but the spatial variation is fairly small in the hydride bed. At t=600 s, the hydride bed seems to reach to its saturated value as the reaction has completed.

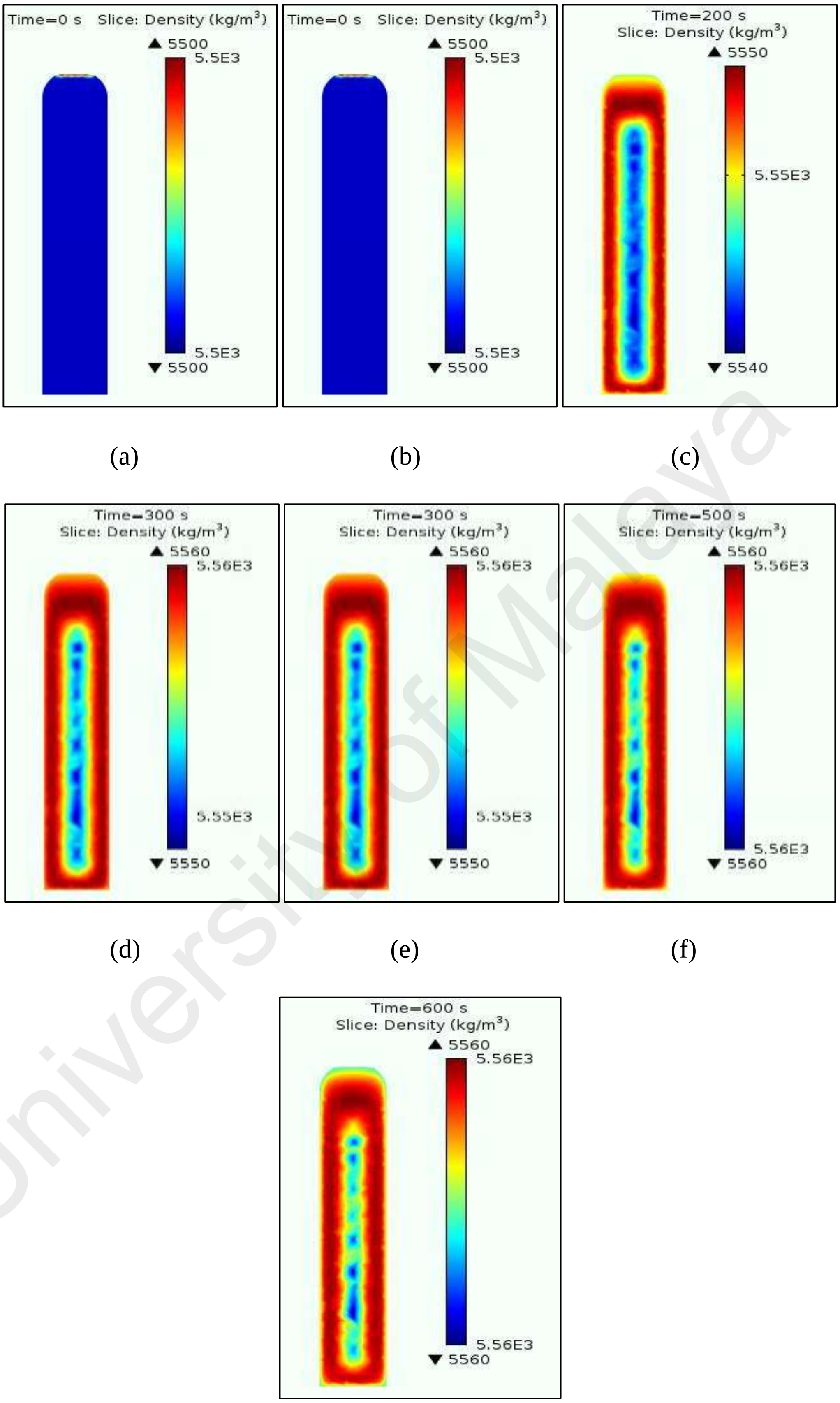

(a) (b) (c)

(d) (e) (f)

(g)

Figure 4.12: Density distribution in half of a cross-section of the hydrogen storage vessel at (a) 0 s, (b) 100 s, (c) 200 s, (d) 300 s, (e) 400 s, (f) 500 s and (g)600 s

4.5 Validation of Actual Simulation

As proposed in Section 3.4, the actual simulation results from Section 4.4.2 are being validated with the prior experiment data collected from Hydrogen Fuel Cell laboratory of Universiti Malaya (UM). The objective is not to match exactly the values acquired in both methods but to get the same trend and the same orders of magnitude.

4.5.1 Temperature

A comparison between simulation and experimental data of metal hydride temperature evolution is demonstrated in Figure 4.13. As can be observed, the experimental and simulation results match closely having small deviations which is acceptable given the lack of information about the material's properties. Although there is some error between the simulation and the experimental data, the predictions match the reported data quite well. It is not clear whether the discrepancies between the experimental and the numerical data are due to experimental issues or minor deficiencies during model implementation in COMSOL.

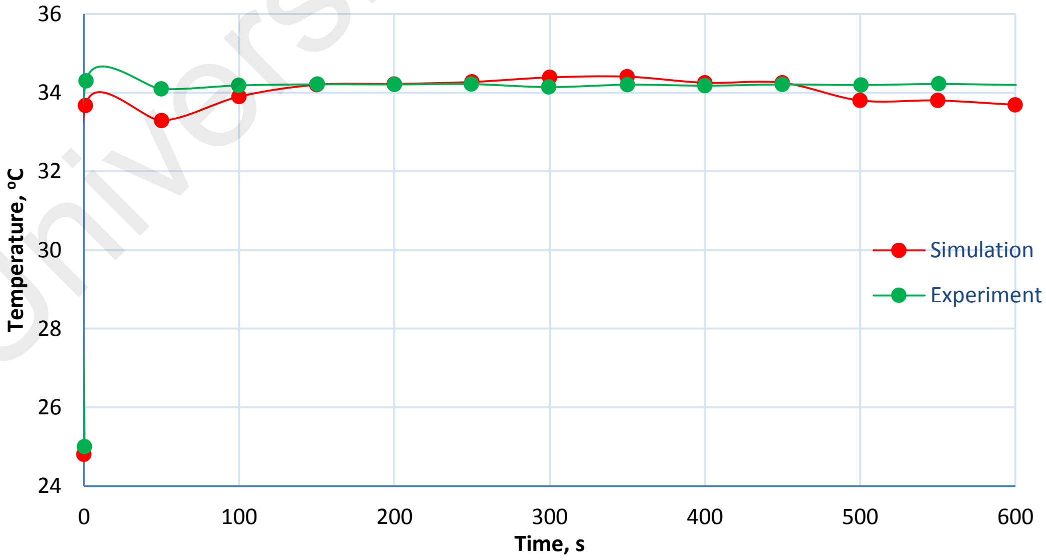

Figure 4.13: Temperature comparison between simulation and experimental data at point r = 0 mm, z = 322 mm

Table 4.4: Temperature comparison between simulation and experimental data at point r = 0 mm, z = 322 mm

Time (s)	Temperature (g)		Deviation (%)
	Simulation	Experimental	
0	24.8019	25.0000	0.79
50	33.2897	34.0929	2.36
100	33.9015	34.1861	0.83
150	34.2027	34.2145	0.03
200	34.2220	34.2119	0.03
250	34.2729	34.2200	0.15
300	34.3887	34.1445	0.72
350	34.4077	34.2057	0.59
400	34.2526	34.1811	0.21
450	33.8024	34.2109	1.19
500	33.6922	34.1976	1.48
550	33.5125	34.2233	2.08
600	33.3601	34.1987	2.45

4.5.2 Mass of Hydrogen Absorbed

In Figure 4.14, a comparison between experimental and simulation results based on the hydrogen mass absorbed can be noticed. It can be seen that the simulation and the experimental data matches closely having small deviations with the percentages varied from 0.0~1.2%. With the decay in temperature being linear, and since the heat transfer coefficient is constant, the rate of heat addition (hydrogen absorption) must also be constant. This is easily seen in the Figure 4.9 since the concentration increases in a linear fashion after the initial opening of the valve. If the experiment was continued it would be expected that the concentration would begin to asymptote as it approaches its concentration limit and the temperature would begin to decrease in a nonlinear fashion.

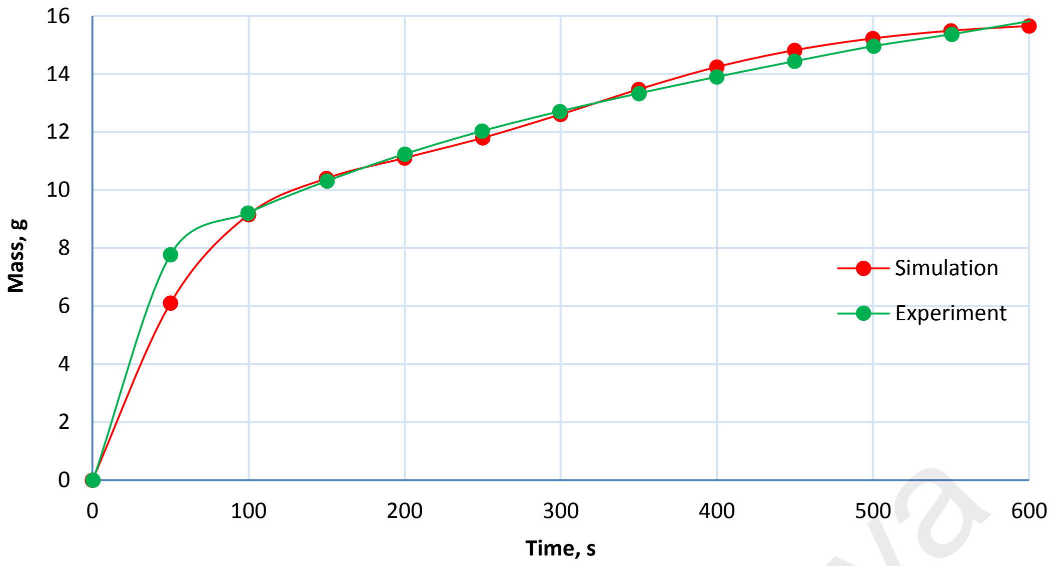

Figure 4.14: Comparison of hydrogen mass absorbed between simulation and experimental data at point r = 0 mm, z = 150 mm

Table 4.5: Comparison of hydrogen mass absorbed between simulation and experimental data at point r = 0 mm, z = 150 mm

Time (s)	**Mass (g)**		**Deviation (%)**
	Simulation	**Experiment**	
0	0.0002	0.0000	0.00
50	6.0991	7.7710	21.51
100	9.1542	9.2090	0.60
150	10.4032	10.3160	0.85
200	11.1065	11.2420	1.21
250	11.7996	12.0330	1.94
300	12.6115	12.7120	0.79
350	13.4740	13.3340	1.05
400	14.2449	13.9020	2.47
450	14.8236	14.4390	2.66
500	15.2287	14.9610	1.79
550	15.4945	15.3720	0.80
600	15.6589	15.8210	1.02

4.6 Sensitivity Analysis

After validating the actual simulation with experimental results, the parametric studies using computational simulation on variation of small and major influence parameters such as porosity (ε), permeability (K), metal thermal conductivity (k_m), hydrogen absorption constant on metal (c_a), activation energy (E_a) and heat transfer coefficient (h)

are conducted. The purpose of this study is to observe the effect of different metal hydrides properties on the behavior of the hydrogen storage system during the absorption process especially in terms of mass and heat transfer. The results are illustrated as the followings.

During analyzing the properties of the material, it is noticed that there are a few parameters that greatly influence the metal hydrides performance by either reducing the absorption time or decreasing the maximum temperature. However, there are also some parameters that do not hold a noticeable effect on the simulation results.

4.6.1 Porosity (ε)

Porosity are one of the parameter that may vary depending on the coating and compaction process of the storage material, which finally morphed into pellets. The void fraction or porosity simply represents the void spaces in the pellets since they are formed by compaction of particles. For the same amount of material, the porosity of the pellets would vary depending on the compaction pressure applied to form the compacts. Assuming that other properties remain the same, increasing porosity would actually increase permeability of hydrogen through the porous space. Thus, the particles will easily come into contact with the hydrogen gas during the sorption process, which would eventually accelerate the reaction process and help reach saturation relatively fast. This is shown in Figure 4.15, where with the increasing of porosity, hydrogen concentration in the hydride also increases at relatively faster rate during the absorption process. Meanwhile, Figure 4.16 shows temperature evolution of metal hydride canister over time at different porosity values. At the beginning, there is sharp growth of temperature curve reaching a peak of maximum temperature for every porosity values and then diminished slowly leading to a temperature plateau. Although the maximum temperature reached by each values were different, the final temperature level is kept more or less similar as the heat produced by exothermic reaction and heat removal due to convection with exterior air are in equilibrium with similar rate of dissipation. As the volume of the canister is fixed, objectively when porosity is high (ε= 0.8), the amount of hydrogen stored is lower as there is less available metal volume within the canister for the hydrogen to be absorbed. Therefore, the absorption process finish faster and the temperature reduced until it reaches ambient temperature sooner. Otherwise, when the porosity is low (ε= 0.1), the absorption process is slower, as there is more metal inside the canister and so more time for hydrogen to completely fill up. Generally, it can be useful in designing a hydrogen storage system on how the porosity can influence the metal hydride behavior, with a trade-off between charge time and storage capacity.

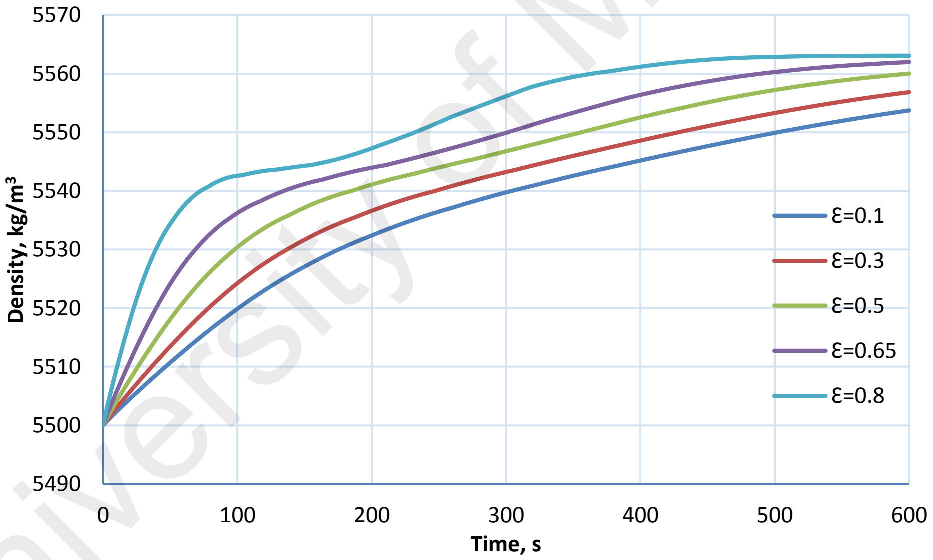

Figure 4.15: Density of metal hydride over time at different porosity values. Point located at r = 0 mm, z = 150 mm

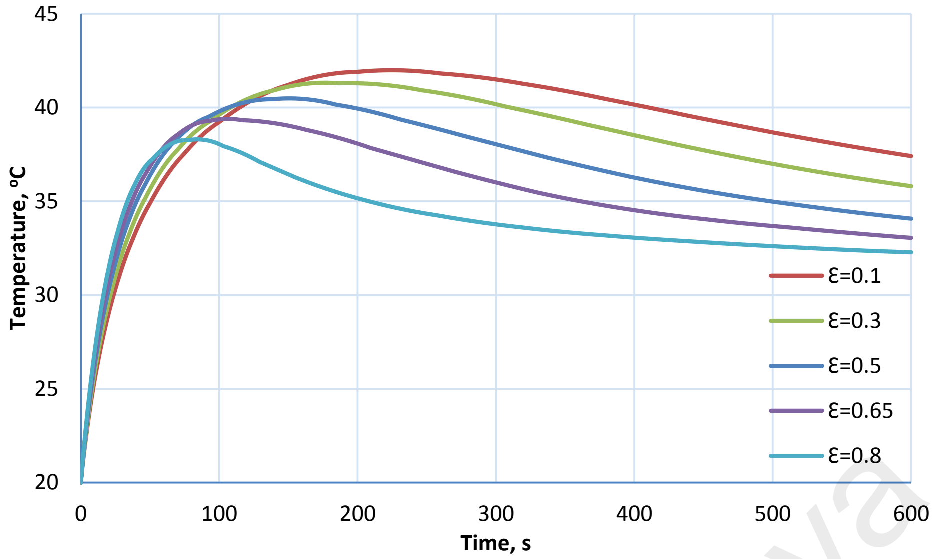

Figure 4.16: Temperature of metal hydride canister over time at different porosity values. Point located r = 33 mm, z = 150 mm

4.6.2 Permeability

The effect of permeability on the density and temperature distribution of metal hydride canister are shown Figure 4.17 and 4.18. It can be observed that there is not much deviation for the metal hydrides density and temperature values with different values of permeability. However, the permeability does influence the results, since this parameter controls the mass transport. When the permeability decreases, hydrogen gas velocity through matrix solid reduces, on the basis of Darcy's law, increasing saturation time. As it can be seen, for permeability below 1 m^2, the system shows a decrease of performance compared to permeability value higher than 1 m^2.

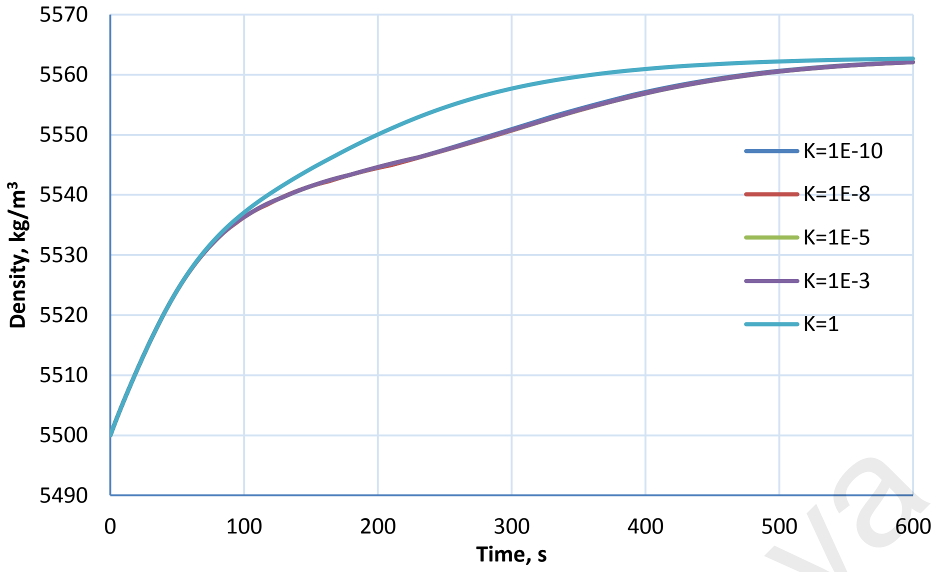

Figure 4.17: Density of metal hydride over time at different permeability values. Point located at r = 0 mm, z = 150 mm

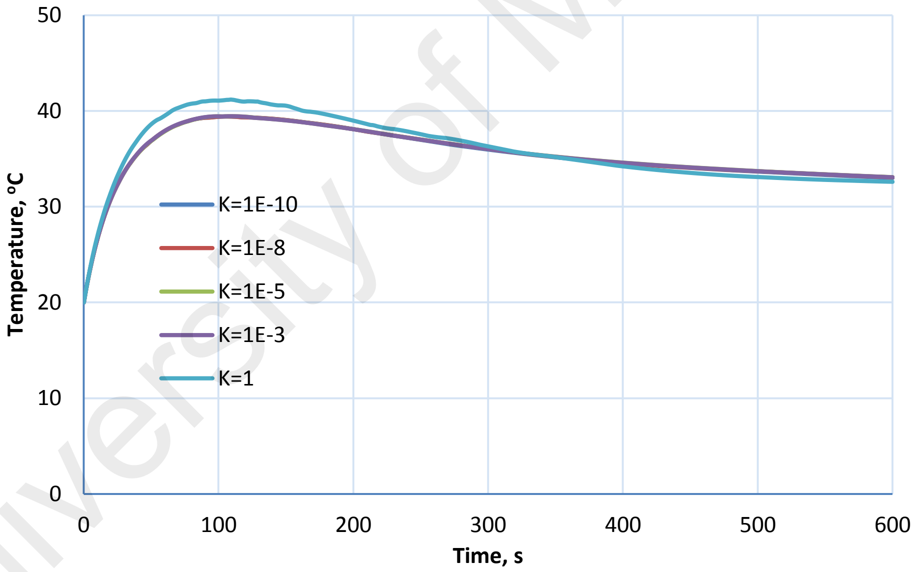

Figure 4.18: Temperature of metal hydride canister over time at different permeability values. Point located r = 33 mm, z = 150 mm

4.6.3 Thermal Conductivity (k_m)

The effect of varying thermal conductivity of the pellets on the density and temperature of metal hydride are displayed in Figure 4.19 and 4.20. The evolution of density for different values of effective thermal conductivity of the material can be seen in Figure 4.19. It is observed that increasing the thermal conductivity value accelerates the reaction kinetics hence rapid absorption of hydrogen. This is because better heat transmission in the hydride bed

It can be seen in Figure 4.20, that for a highly conductive hydride, the heat of reaction is transported to the environment faster result in lower final bed temperature. Although at the beginning, the maximum temperature reached for k_m =10 $\mathrm{W/m.K}$ and k_m = 6.5 $\mathrm{W/m.K}$ is higher compared to others due to faster absorption reaction rate, the temperature quickly slows down as the concentrations becomes saturated, and the heat generated during the reaction process is extracted faster because of better thermal conductivity of the metal hydrides material.

Therefore, it is proven that the improved thermal conductivity of the metal would ensure better heat transmission rate, which eventually translates to faster reaction rate and hence swifter actuation. Thermal conductivity is sensitive to chemical process duration which with both copper encapsulation and compaction to pellet process which can improve overall thermal conductivity of the metal hydrides material. It can be concluded that a conductivity of 6.5 $\mathrm{W/m.K}$ is the best for this system as it provides fastest charging time at the lowest final hydride canister temperature.

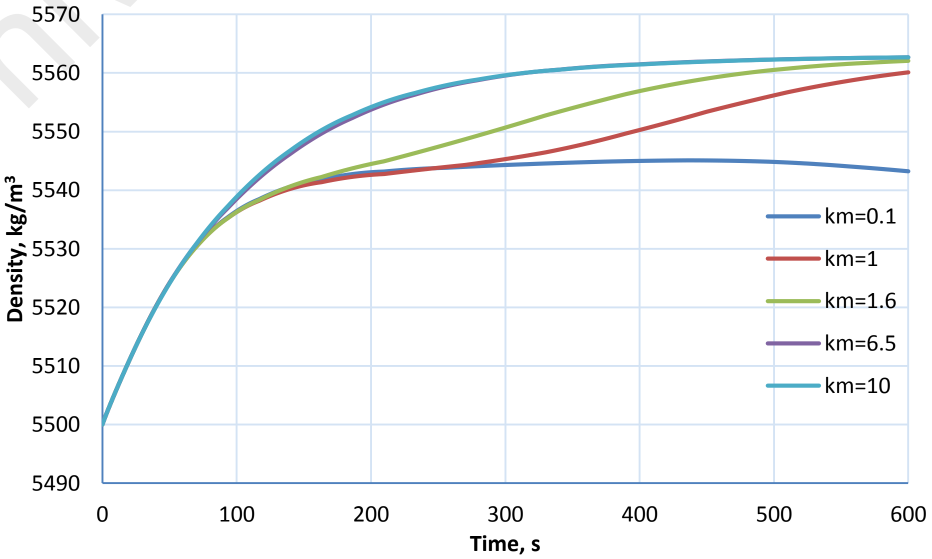

Figure 4.19: Density of metal hydride over time at different thermal conductivity values. Point located at r = 0 mm, z = 150 mm

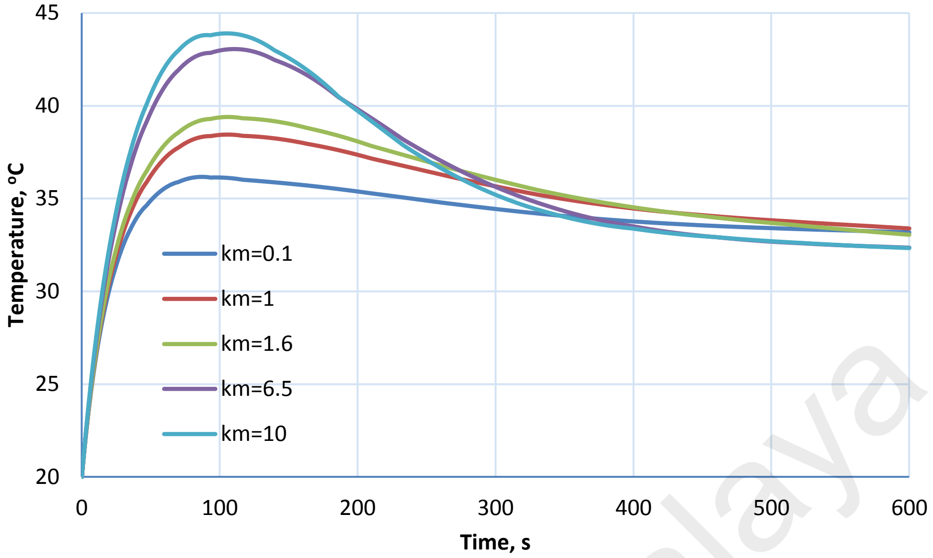

Figure 4.20: Temperature of metal hydride canister over time at different thermal conductivity values. Point located r = 33 mm, z = 150 mm

4.6.4 Hydrogen Absorption Constant on Metal (c_a)

The effect of modifying the absorption rate constant on density and temperature levels are illustrated in Figure 4.21 and Figure 4.22. For a smaller value of absorption rate constant, the temperature evolution by the hydrides bed is lower as the absorption process takes place at slower velocity which generate lower heat from the canister. In other words, to increase the concentration of hydrogen absorbed, the absorption rate constant need to be higher. Therefore, it can be concluded that as the absorption rate constant decrease, the temperature level diminished, as well, but not at a linear rate, as there is a big difference for each absorption rate constant value.

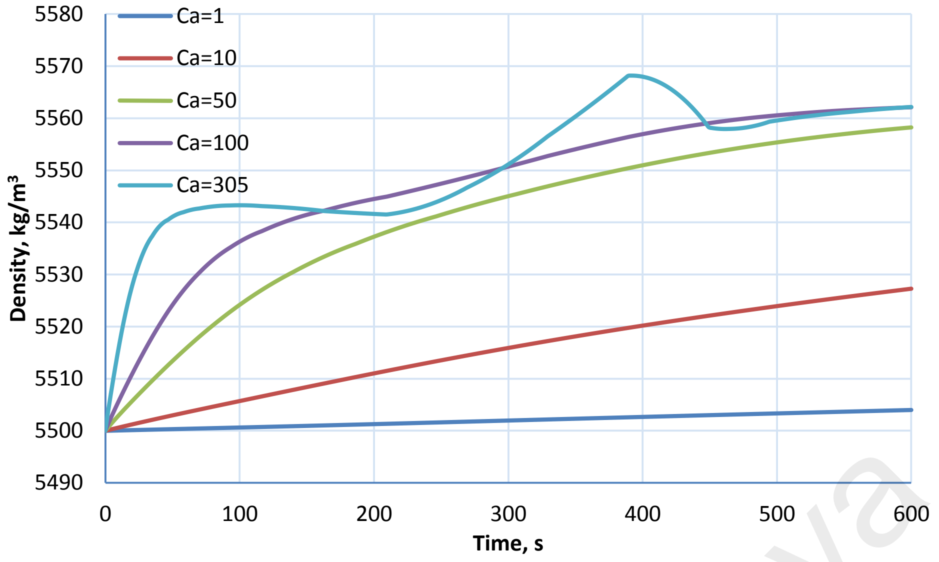

Figure 4.21: Density of metal hydride over time at absorption rate constant values. Point located at r = 0 mm, z = 150 mm

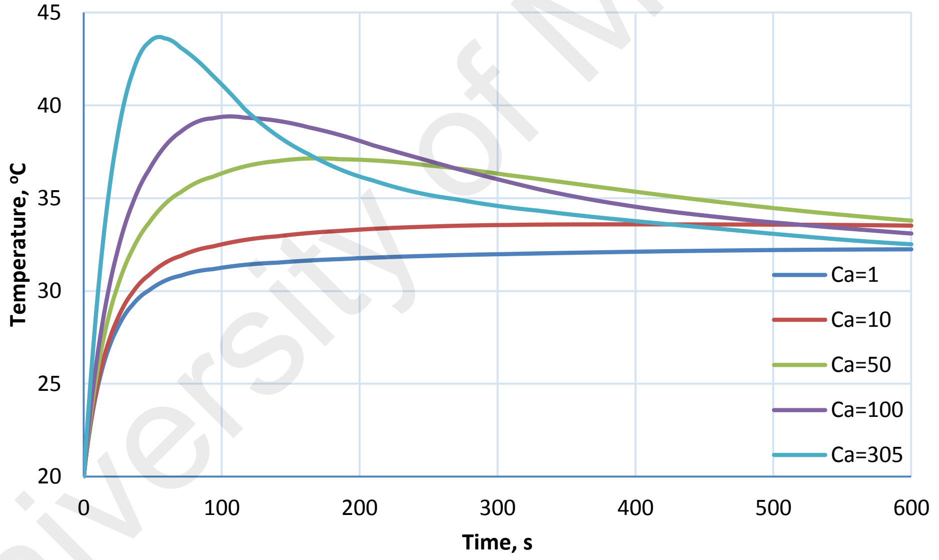

Figure 4.22: Temperature of metal hydride canister over time at different absorption rate constant values. Point located r = 33 mm, z = 150 mm

4.6.5 Activation Energy (E_a)

For a very high value of activation energy, there is no noticeable distinct values in the density and temperature of the metal hydride bed as the density and temperature values for $E_a \geq 50000$ and $E_a \geq 100000$ is the same. Meanwhile, when the activation energy is low a visible difference in the density and temperature evolution is observed. The different effect of different range of activation energy value is due to the obstacle to start any absorption reaction when the activation energy is too high, as seen in Figure 4.23 and Figure 4.24. It is even more difficult to start the absorption when the required heat is not being supplied. For this system, an activation energy of 35000 kg/ m^3 and above are unfavorable. However, it can also been observed that at activation energy of 20000 kg/ m^3, the density level fluctuate greatly due to the system become unstable at too low activation energy.

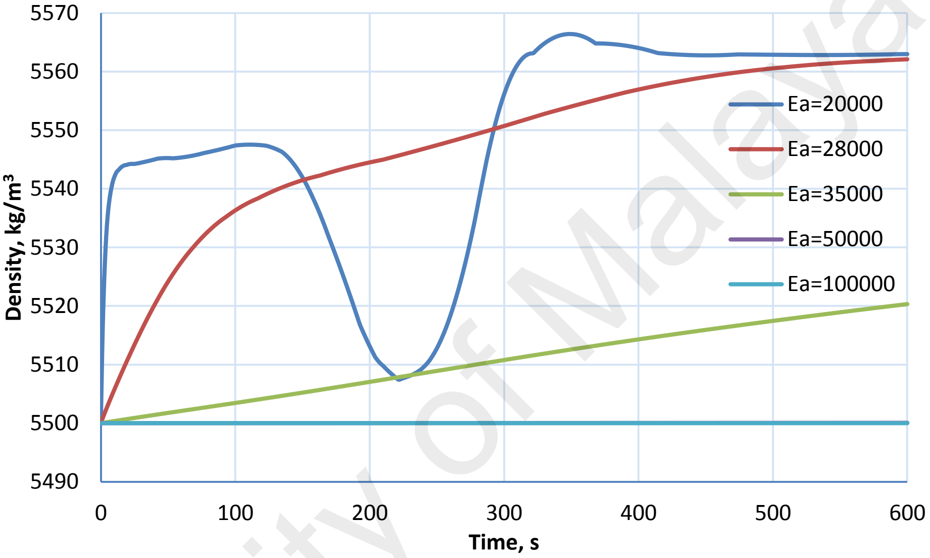

Figure 4.23: Density of metal hydride over time at different activation energy values. Point located at r = 0 mm, z = 150 mm

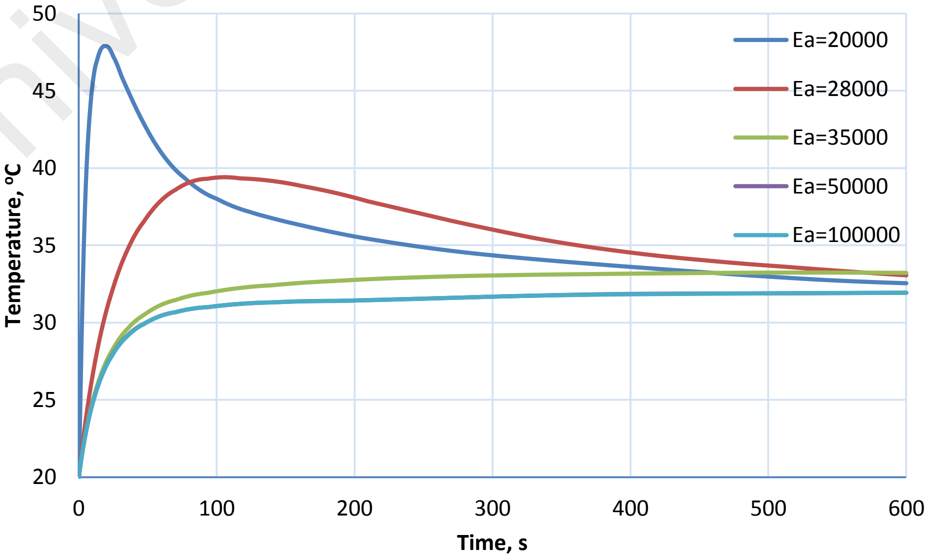

Figure 4.24: Temperature of metal hydride canister over time at different activation energy values. Point located r = 33 mm, z = 150 mm

4.6.6 Heat Transfer Coefficient (h)

Absorption reaction can occurs faster due to the heat transfer coefficient. This is because heat transfer coefficient determines the rate of heat removal from the metal hydride canister and allows a faster hydrogen mass flow rate into the canister. To study the effect of heat transfer coefficient on the hydrogen absorption rate, the value of heat transfer coefficient is varied from 10 to 1000 $\mathrm{W/m^2.K}$ by keeping the other operating parameters as constant. As observed, Figure 4.25 and 4.26 show the effect of different heat transfer coefficient on metal hydrides canister temperature and density distribution for 600 s.

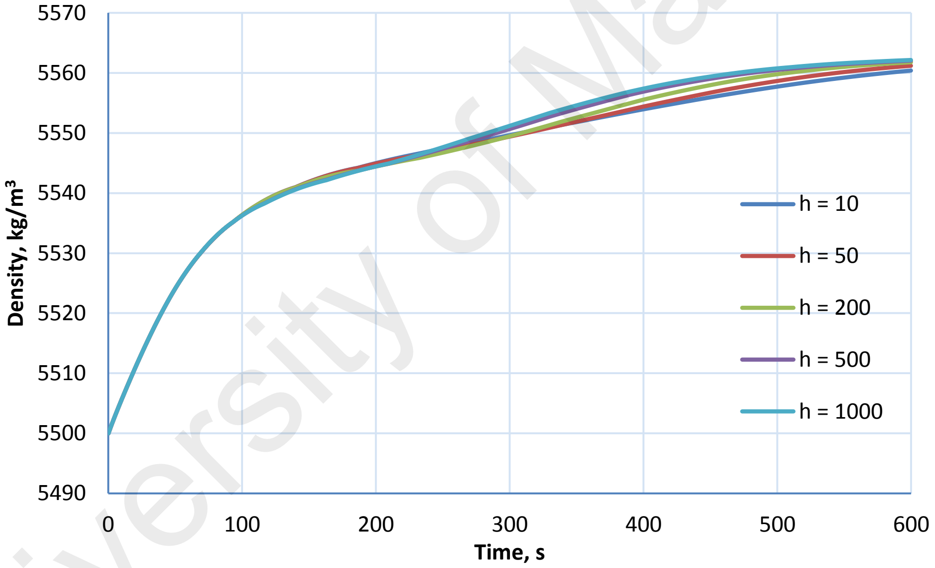

Figure 4.25: Density of metal hydride over time at different heat transfer coefficient values. Point located at r = 0 mm, z = 150 mm

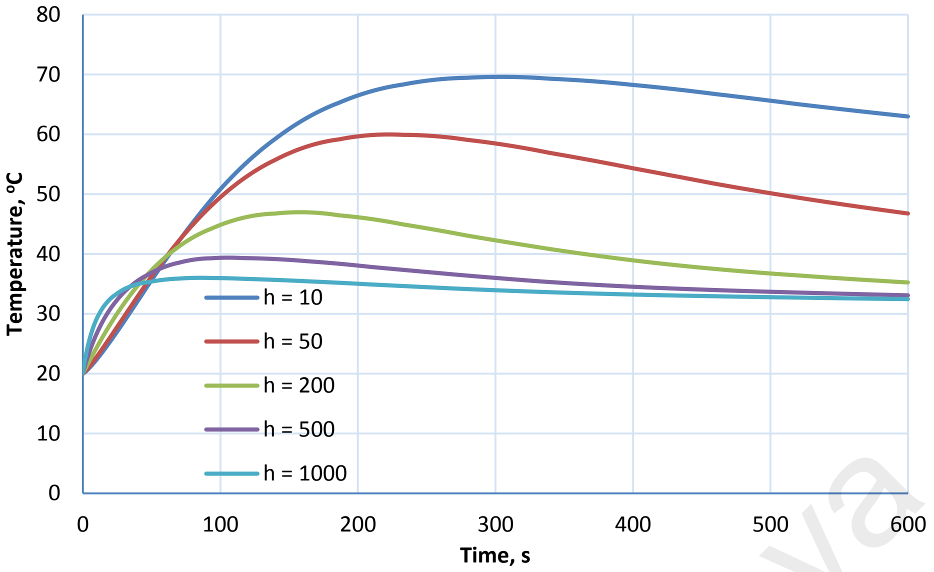

Figure 4.26: Temperature of metal hydride canister over time at different heat transfer coefficient values. Point located r = 33 mm, z = 150 mm

The heat transfer coefficient plays a significant role during absorption process of hydrogen. It is observed from Figure 4.26 that for heat transfer coefficient of 1000W/m^2 K, the reaction bed temperature reaches the canister initial temperature faster, while for the other cases it takes more time. However, as it is noticed from Figure 4.25 that the amount of hydrogen absorbed at different overall heat transfer coefficients is similar without much deviation. Hence, one can conclude that the selection of overall heat transfer coefficient should be based on the optimum value of heat transfer coefficient and not too high as it not give much effect to the hydride density.

4.7 Effect of operating condition

An optimization of the system has been carried out for the operating conditions and thickness of the metal hydrides canister.

4.7.1 Charging pressure

Charging pressure gives significant effect on the absorption process of metal hydride as the difference between equilibrium pressure and pressure within the hydride canister controls the process which effecting the hydration rates. To study the effect of varying charging pressure on the hydrides bed density and temperature, numerical simulation is carried out at five different charging pressures from 10 to 50 bar by keeping the temperature constant. In Figure 4.27 and 4.28, the effect of hydrogen gas pressure on the temperature and density distribution during hydrogen absorption process are shown.

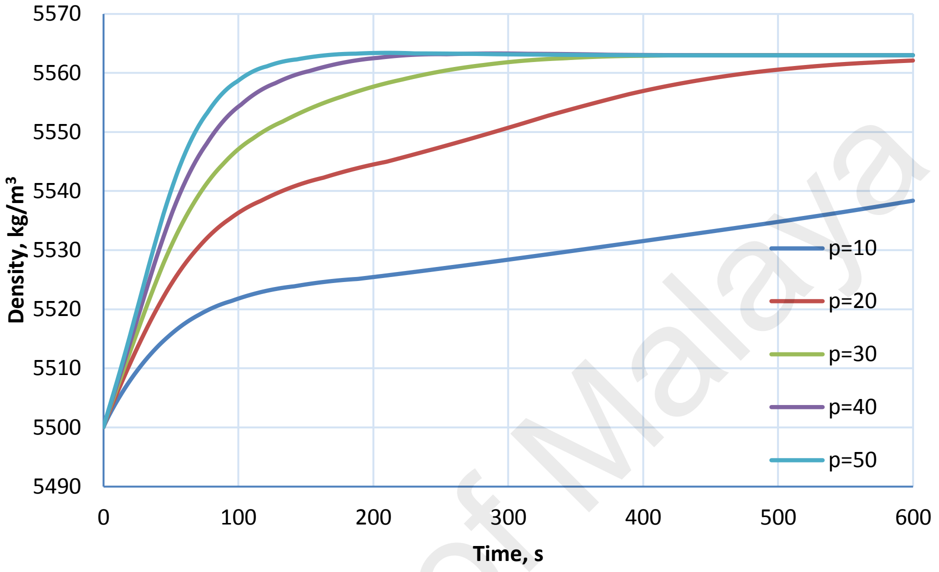

Figure 4.27: Figure 4.27: Density of metal hydride over time at different charging pressure values. Point located at r = 0 mm, z = 150 mm

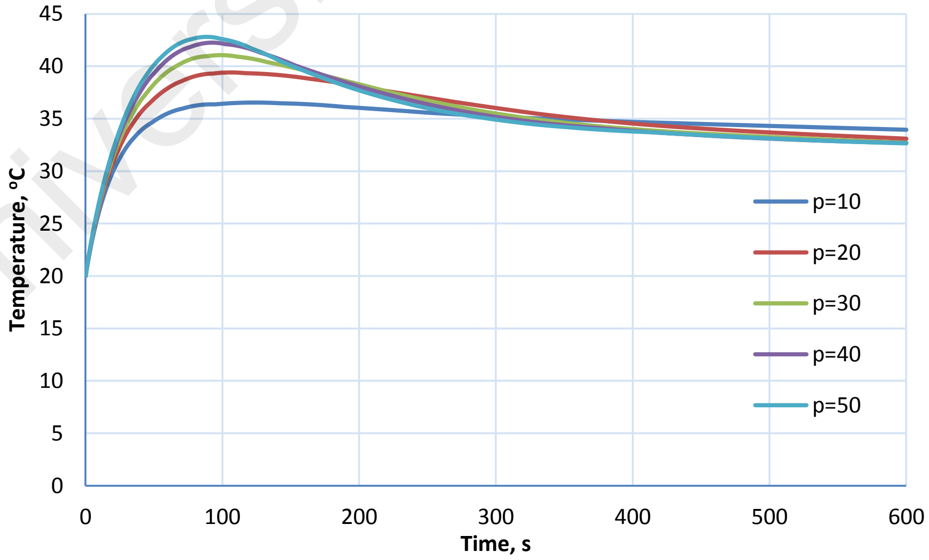

Figure 4.28: Temperature of metal hydride canister over time at different charging pressure values. Point located r = 33 mm, z = 150 mm

As seen in Figure 4.27, a high charging pressure can reduce the time taken for hydrogen gas to completely fill the metal hydrides bed and reaches the saturated density. The increase in the hydrogen absorbent capacity with increasing the supply pressure is due to plateau slope. It can be observed that with high supply pressure, the hydrogen charging time becomes shorter, but there is not much different in the maximum value of hydrogen absorbed except when the charging pressure at 10 bar. So it can be concluded that charging pressure influences the charging time of the hydrides system.

Figure 4.28 shows the temperature evolution of metal hydride bed at different charging pressures during the absorption process. As it can be observed, the temperature value rise sharply at about 50 s in the beginning for a given charging pressure. However, after achieving its maximum temperature, the temperature decreases steadily and approaches the ambient temperature. The sudden increase in the temperature at the initial stage is due to rapid absorption rate of hydrogen into metal hydrides canister. Figure 4.28 also illustrates that for this system, the higher the charging pressure value is, the higher the rise in bed temperature. This is due to the bigger differences between the charging pressure and the equilibrium as well as higher generation of heat. Therefore, improvement in the heat transfer characteristic of the hydrides canister through optimum design can be done in order to reduce the heat generation. The improvement can be done through the development of innovative hydride beds. For example, a new metal hydride bed should be developed with the adoption of graphite matrix or metallic foam, adequate hydrogen porosity and high equivalent thermal conductivity as well as heat transfer coefficient.

4.7.2 Bed Temperature

The density and temperature of metal hydrides bed at different initial bed temperatures are shown in Figures 4.29 and 4.30.

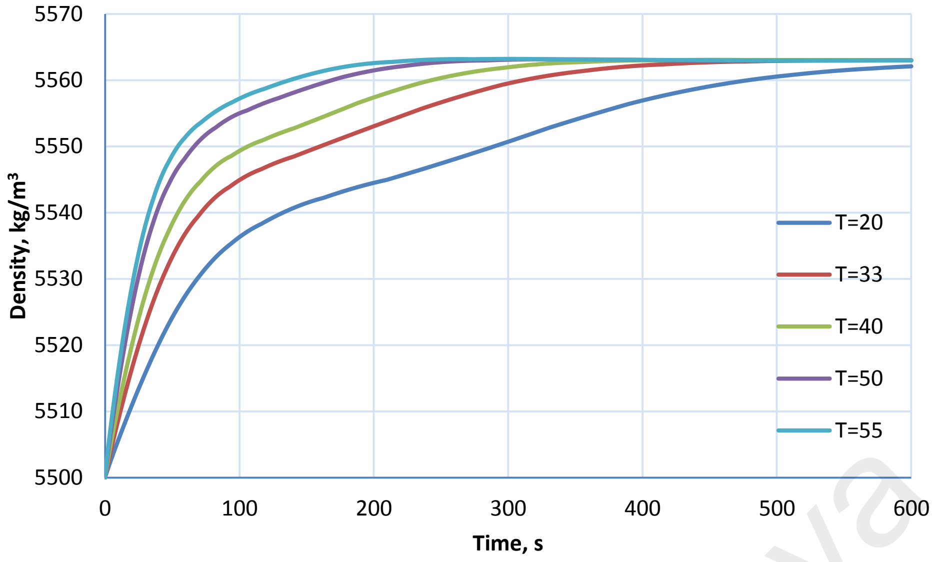

Figure 4.29: Density of metal hydride over time at different bed temperature values. Point located at r = 0 mm, z = 150 mm

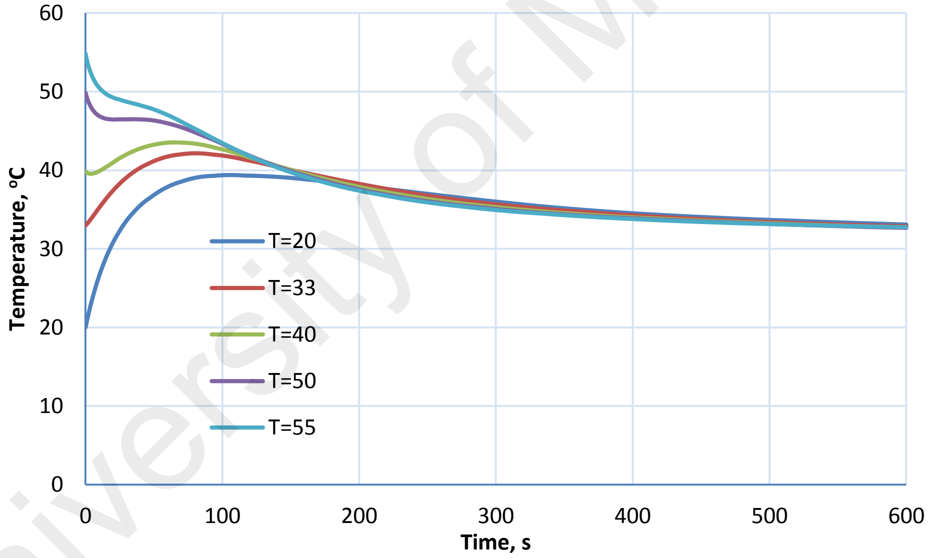

Figure 4.30: Temperature of metal hydride canister over time at different bed temperature values. Point located r = 33 mm, z = 150 mm

As observed in Figure 4.30, increase in initial bed temperature increases the maximum temperature achieved for each given bed temperature value. However, after the peak, the temperature starting to reduce to initial canister temperature and reach the ambient temperature approximately at a similar time as the hydrides density starting to become saturated. Besides, it can be seen in Figure 4.29 that the density of metal hydride also increases faster with higher value of initial bed temperature. This is due to the kinetics of the metal hydrides material which is faster at higher temperature, which indicates faster absorption rates of hydrogen and reduces with charging time. Thus, it can be concluded that the increase in the hydride bed temperature will increase the maximum temperature and decrease the charging time of the hydrides system.

CHAPTER 5: CONCLUSION & RECOMMENDATION

This chapter will conclude the main findings in this thesis and discuss the recommendations for future work.

In this chapter a three-dimensional mathematical model is presented for describing the absorption processes that take place in porous metal hydride

5.1 Conclusion

A three dimensional mathematical model which represent the principle of mass, momentum and energy conversation as well as absorption kinetics is developed to be used in the simulation of hydrogen absorption process within metal hydride canister. The validity of the mathematical model is first tested by comparing it with other author's published work, which later achieved a good agreement between all the data.

The validated model then has been implemented in COMSOL Multiphysics software using an actual metal hydrides canister which utilizes the finite element method to solve the governing equations. The governing equations are numerically solved and the calculated results are compared with the prior experimental data. The simulation and experimental results show agreement with each other having small deviation between 0.0~2.5%.

The simulated actual metal hydrides canister is then be applied to study the behavior of metal hydride canister system. The objectives of the study is to achieve a better metal hydride system while reducing the amount of time-consuming experiments required since simulation is robust and has fast solving time. For this purpose, parametric studies have been conducted. The parametric studies analyze the effect of different metal hydrides properties on the behavior of metal hydrides system in term of heat and mass transfer.

The sensitivity analysis indicated that the effective thermal conductivity was the most sensitive parameters for this system while other parameters such as porosity, permeability and heat transfer coefficient carried little effect on the system. However, the permeability does influence the results, since this parameter controls the mass transport and the effect of the porosity on the metal hydride behavior which can be useful in designing a hydrogen storage system with the study of the porosity can influence on the metal hydride behavior, considering a trade-off between charge time and storage capacity. It can also be observed that at a very high value of activation energy there is no noticeable difference in the density and temperature whereas, in order to increase the concentration of hydrogen absorbed, the absorption rate constant needs to be higher but not exceed the optimum value.

Furthermore, the improvement in the thermal conductivity of the metal would ensure better heat transmission rate, which eventually translates to a faster reaction rate and hence swifter actuation. . It can be concluded that a conductivity of 6.5 $\mathrm{W/m.K}$ is the best for this system as it provides the fastest charging time with the lowest final hydride canister temperature. For heat transfer coefficient, one can conclude that the selection of overall heat transfer coefficient should be based on the optimum value of heat transfer coefficient as increasing of it not give much effect to the hydride density. This is because the heat transfer by convection not a dominant phenomenon during the absorption process.

Lastly, considering the operating condition, it can be concluded that the high charging pressure can reduce the time taken for hydrogen gas to completely fill the metal hydrides bed and the higher the charging pressure value, the higher the rise in bed temperature. Besides, it also can be concluded that increase in the hydride bed temperature will increase the maximum temperature and decrease the charging time of the hydrides system.

5.2 Recommendation

The following suggestion are either plan for the project in the future that are considered to be beyond the scope of this work, or recommendations for future researchers who are planning to study in more details the metal hydride hydrogen storage systems:

1. The major focus for the future can be to develop a mathematical model for heat and mass transfer modelling that will be able to describe kinetics of other complex materials. For now, the developed mathematical model is only applicable to describe the behavior of simple type of material.
2. Further research efforts should be focused on the improvement of the thermal exchange for the storage canister through the development of innovative hydride beds. For example, a new metal hydride bed should be developed with the adoption of graphite matrix or metallic foam, adequate hydrogen porosity and high equivalent thermal conductivity as well as heat transfer coefficient.
3. Lastly, optimum design models for metal hydride storage units is required in order for the metal hydride technology to compete with existence compressed and liquid hydrogen storage which can satisfy the goal for public and efficient energy storage.

REFERENCES

(Aburto, A., & Orgaz, E. (2007). Ab initio structural and electronic investigation of magnetic RNiSn (R=La,Ce,Pr,Nd) intermetallics and their hydrides. *Physical Review B, 75*(4), 045130.

Aceves, S. M., Berry, G. D., Martinez-Frias, J., & Espinosa-Loza, F. (2006). Vehicular storage of hydrogen in insulated pressure vessels. *International Journal of Hydrogen Energy, 31*(15), 2274-2283.

Aceves, S. M., Petitpas, G., Espinosa-Loza, F., Matthews, M. J., & Ledesma-Orozco, E. (2013). Safe, long range, inexpensive and rapidly refuelable hydrogen vehicles with cryogenic pressure vessels. *International Journal of Hydrogen Energy, 38*(5), 2480-2489.

Agrawal, R., Offutt, M., & Ramage, M. P. (2005). Hydrogen economy - an opportunity for chemical engineers? *AIChE Journal, 51*(6), 1582-1589.

Akbarzadeh, A. R., Wolverton, C., & Ozolins, V. (2009). First-principles determination of crystal structures, phase stability, and reaction thermodynamics in the Li-Mg-Al-H hydrogen storage system. *Physical Review B, 79*(18), 184102.

Albanese, E., Kalantzopoulos, G. N., Vitillo, J. G., Pinatel, E., Civalleri, B., Deledda, S., . . . Baricco, M. (2013). Theoretical and experimental study on Mg(BH4)2–Zn(BH4)2 mixed borohydrides. *Journal of Alloys and Compounds, 580, Supplement 1*(0), S282-S286.

Aldas, K., Mat, M. D., & Kaplan, Y. (2002). A three-dimensional mathematical model for absorption in a metal hydride bed. *International Journal of Hydrogen Energy, 27*(10), 1049-1056.

Ananthachar, V., & Duffy, J. J. (2005). Efficiencies of hydrogen storage systems onboard fuel cell vehicles. *Solar Energy, 78*(5), 687-694.

Andreasen, A. (2008). Hydrogenation properties of Mg–Al alloys. *International Journal of Hydrogen Energy, 33*(24), 7489-7497.

Andrews, J., & Shabani, B. (2012). Re-envisioning the role of hydrogen in a sustainable energy economy. *International Journal of Hydrogen Energy, 37*(2), 1184-1203.

Arnbjerg, L. M., Ravnsbæk, D. B., Filinchuk, Y., Vang, R. T., Cerenius, Y., Besenbacher, F., . . . Jensen, T. R. (2009). Structure and Dynamics for LiBH4−LiCl Solid Solutions. *Chemistry of Materials, 21*(24), 5772-5782.

Ashraful, A. M., Masjuki, H. H., Kalam, M. A., Rizwanul Fattah, I. M., Imtenan, S., Shahir, S. A., & Mobarak, H. M. (2014). Production and comparison of fuel properties, engine performance, and emission characteristics of biodiesel from various non-edible vegetable oils: A review. *Energy Conversion and Management, 80*, 202-228.

Baladincz, P., & Hancsók, J. (2015). Fuel from waste animal fats. *Chemical Engineering Journal, 282*, 152-160.

Ball, M., & Wietschel, M. (2009). The future of hydrogen – opportunities and challenges. *International Journal of Hydrogen Energy, 34*(2), 615-627.

Banković-Ilić, I. B., Stojković, I. J., Stamenković, O. S., Veljkovic, V. B., & Hung, Y.-T. (2014). Waste animal fats as feedstocks for biodiesel production. *Renewable and Sustainable Energy Reviews, 32*, 238-254.

Barkhordarian, G., Klassen, T., Dornheim, M., & Bormann, R. (2007). Unexpected kinetic effect of MgB2 in reactive hydride composites containing complex borohydrides. *Journal of Alloys and Compounds, 440*(1–2), L18-L21.

Blackman, J. M., Patrick, J. W., Arenillas, A., Shi, W., & Snape, C. E. (2006). Activation of carbon nanofibres for hydrogen storage. *Carbon, 44*(8), 1376-1385.

Bogdanović, B., Felderhoff, M., & Streukens, G. (2009). Hydrogen storage in complex metal hydrides. *Journal of the Serbian Chemical Society, 74*(2), 183-196.

Borzone, E. M., Baruj, A., Blanco, M. V., & Meyer, G. O. (2013). Dynamic measurements of hydrogen reaction with LaNi5−xSnx alloys. *International Journal of Hydrogen Energy, 38*(18), 7335-7343.

Brouwer, J. (2010). On the role of fuel cells and hydrogen in a more sustainable and renewable energy future. *Current Applied Physics, 10*(2, Supplement), S9-S17.

Busqué Somacarrera, R. (2015). Metal hydride state of charge estimator. Development and experimental validation of the hydrogen storage system model.

Choudhury, P., Srinivasan, S. S., Bhethanabotla, V. R., Goswami, Y., McGrath, K., & Stefanakos, E. K. (2009). Nano-Ni doped Li–Mn–B–H system as a new hydrogen storage candidate. *International Journal of Hydrogen Energy, 34*(15), 6325-6334.

Cipriani, G., Di Dio, V., Genduso, F., La Cascia, D., Liga, R., Miceli, R., & Ricco Galluzzo, G. (2014). Perspective on hydrogen energy carrier and its automotive applications. *International Journal of Hydrogen Energy, 39*(16), 8482-8494.

Ćirić, K. D., Kocjan, A., Gradišek, A., Koteski, V. J., Kalijadis, A. M., Ivanovski, V. N., . . . Stojić, D. L. (2012). A study on crystal structure, bonding and hydriding properties of Ti–Fe–Ni intermetallics–Behind substitution of iron by nickel. *International Journal of Hydrogen Energy, 37*(10), 8408-8417.

de Castro, J. F. R., Santos, S. F., Costa, A. L. M., Yavari, A. R., Botta F, W. J., & Ishikawa, T. T. (2004). Structural characterization and dehydrogenation behavior of Mg–5 at.%Nb nano-composite processed by reactive milling. *Journal of Alloys and Compounds, 376*(1–2), 251-256.

Demirbas, A. (2007). Storage and Transportation Opportunities of Hydrogen. *Energy Sources, Part B: Economics, Planning, and Policy, 2*(3), 287-295.

Denys, R. V., Riabov, B., Yartys, V. A., Delaplane, R. G., & Sato, M. (2007). Hydrogen storage properties and structure of La1−xMgx(Ni1−yMny)3 intermetallics and their hydrides. *Journal of Alloys and Compounds, 446–447*(0), 166-172.

Dornheim, M., Doppiu, S., Barkhordarian, G., Boesenberg, U., Klassen, T., Gutfleisch, O., & Bormann, R. (2007). Hydrogen storage in magnesium-based hydrides and hydride composites. *Scripta Materialia, 56*(10), 841-846.

Eberle, U., Arnold, G., & von Helmolt, R. (2006). Hydrogen storage in metal–hydrogen systems and their derivatives. *Journal of Power Sources, 154*(2), 456-460.

Ehret, O., & Bonhoff, K. (2015). Hydrogen as a fuel and energy storage: Success factors for the German Energiewende. *International Journal of Hydrogen Energy, 40*(15), 5526-5533.

Endo, N., Saitoh, H., Machida, A., & Katayama, Y. (2013). Formation of BCC TiFe hydride under high hydrogen pressure. *International Journal of Hydrogen Energy, 38*(16), 6726-6729.

Falahati, H., & Barz, D. P. J. (2013). Evaluation of hydrogen sorption models for AB5-type metal alloys by employing a gravimetric technique. *International Journal of Hydrogen Energy, 38*(21), 8838-8851.

Freni, A., Cipitì, F., & Cacciola, G. (2009). Finite element-based simulation of a metal hydride-based hydrogen storage tank. *International Journal of Hydrogen Energy, 34*(20), 8574-8582.

Garland, N. L., Papageorgopoulos, D. C., & Stanford, J. M. (2012). Hydrogen and Fuel Cell Technology: Progress, Challenges, and Future Directions. *Energy Procedia, 28*, 2-11.

Gasiorowski, A., Iwasieczko, W., Skoryna, D., Drulis, H., & Jurczyk, M. (2004). Hydriding properties of nanocrystalline Mg2−xMxNi alloys synthesized by mechanical alloying (M=Mn, Al). *Journal of Alloys and Compounds, 364*(1–2), 283-288.

Georgakis, M., Stavropoulos, G., & Sakellaropoulos, G. P. (2007). Predictions for molecular hydrogen adsorption in microporous carbons via molecular dynamics simulations and a suggestion for a hydrogen storage medium. *International Journal of Hydrogen Energy, 32*(15), 3465-3470.

George, L., & Saxena, S. K. (2010). Structural stability of metal hydrides, alanates and borohydrides of alkali and alkali- earth elements: A review. *International Journal of Hydrogen Energy, 35*(11), 5454-5470.

Georgiadis, M. C., Kikkinides, E. S., Makridis, S. S., Kouramas, K., & Pistikopoulos, E. N. (2009). Design and optimization of advanced materials and processes for efficient hydrogen storage. *Computers & Chemical Engineering, 33*(5), 1077-1090.

Gross, K. J., Sandrock, G., & Thomas, G. J. (2002). Dynamic in situ X-ray diffraction of catalyzed alanates. *Journal of Alloys and Compounds, 330–332*(0), 691-695.

He, G., Jiao, L.-F., Yuan, H.-T., Zhang, Y.-Y., & Wang, Y.-J. (2008). Preparation and electrochemical properties of MgNi–MB (M = Co, Ti) composite alloys. *Journal of Alloys and Compounds, 450*(1–2), 375-379.

Ho, S. H., & Rahman, M. M. (2008). Three-dimensional analysis for liquid hydrogen in a cryogenic storage tank with heat pipe–pump system. *Cryogenics, 48*(1-2), 31-41.

Hoel, M., & Kverndokk, S. (1996). Depletion of fossil fuels and the impacts of global warming. *Resource and Energy Economics, 18*(2), 115-136.

Hong, S.-H., & Song, M. Y. (2013). Hydrogen desorption and absorption properties of Pd and MgO or nano-sized Ni-added MgH2 + LiBH4 composites. *Materials Research Bulletin, 48*(9), 3453-3458.

Huang, Z. G., Guo, Z. P., Calka, A., Wexler, D., Lukey, C., & Liu, H. K. (2006). Effects of iron oxide (Fe2O3, Fe3O4) on hydrogen storage properties of Mg-based composites. *Journal of Alloys and Compounds, 422*(1–2), 299-304.

Hwang, H. T., Al-Kukhun, A., & Varma, A. (2010). Hydrogen for Vehicle Applications from Hydrothermolysis of Ammonia Borane: Hydrogen Yield, Thermal Characteristics, and Ammonia Formation. *Industrial & Engineering Chemistry Research, 49*(21), 10994-11000.

Ichikawa, T., Hanada, N., Isobe, S., Leng, H., & Fujii, H. (2005). Composite Materials based on Light Elements for Hydrogen Storage. *MATERIALS TRANSACTIONS, 46*(1), 1-14.

Iosub, V., Matsunaga, T., Tange, K., & Ishikiriyama, M. (2009). Direct synthesis of Mg(AlH4)2 and CaAlH5 crystalline compounds by ball milling and their potential as hydrogen storage materials. *International Journal of Hydrogen Energy, 34*(2), 906-912.

Islam, M. T., Huda, N., Abdullah, A. B., & Saidur, R. (2018). A comprehensive review of state-of-the-art concentrating solar power (CSP) technologies: Current status and research trends. *Renewable and Sustainable Energy Reviews, 91*, 987-1018.

Issariyakul, T., & Dalai, A. K. (2014). Biodiesel from vegetable oils. *Renewable and Sustainable Energy Reviews, 31*, 446-471.

Jain, I. P., Lal, C., & Jain, A. (2010). Hydrogen storage in Mg: A most promising material. *International Journal of Hydrogen Energy, 35*(10), 5133-5144.

Jain, R. K., Jain, A., Agarwal, S., Lalla, N. P., Ganesan, V., Phase, D. M., & Jain, I. P. (2007). Hydrogenation behaviour of Ce-based AB5 intermetallic compounds. *Journal of Alloys and Compounds, 440*(1–2), 84-88.

Jemni, A., & Nasrallah, S. B. (1995). Study of two-dimensional heat and mass transfer during absorption in a metal-hydrogen reactor. *International Journal of Hydrogen Energy, 20*(1), 43-52.

Jeon, E., & Cho, Y. (2006). Mechanochemical synthesis and thermal decomposition of zinc borohydride. *Journal of Alloys and Compounds*, *422*(1–2), 273-275.

Kalisvaart, W. P., Harrower, C. T., Haagsma, J., Zahiri, B., Luber, E. J., Ophus, C., . . . Mitlin, D. (2010). Hydrogen storage in binary and ternary Mg-based alloys: A comprehensive experimental study. *International Journal of Hydrogen Energy, 35*(5), 2091-2103.

Kang, X.-D., Luo, J.-H., & Wang, P. (2012). Efficient and highly rapid hydrogen release from ball-milled 3NH3BH3/MMgH3 (M = Na, K, Rb) mixtures at low temperatures. *International Journal of Hydrogen Energy, 37*(5), 4259-4266.

Klindtworth, E., Delidovich, I., & Palkovits, R. (2018). Borohydride in ionic liquids for tailored hydrogen release. *International Journal of Hydrogen Energy, 43*(45), 20772-20782.

Kontorovich, A. E., Epov, M. I., & Eder, L. V. (2014). Long-term and medium-term scenarios and factors in world energy perspectives for the 21st century. *Russian Geology and Geophysics, 55*(5–6), 534-543.

Kumar, S., Sonak, S., & Krishnamurthy, N. (2013). Hydrogen solid solution thermodynamics of V1−xAlx (x: 0, 0.18, 0.37, 0.52) alloys. *International Journal of Hydrogen Energy, 38*(23), 9928-9934.

Latroche, M., & Percheron-Guégan, A. (2003). Structural and thermodynamic studies of some hydride forming RM3-type compounds (R=lanthanide, M=transition metal). *Journal of Alloys and Compounds, 356–357*(0), 461-468.

Laversenne, B. B. L. Hydrogen storage using borohydrides *Entropy, 184*, 183.183-242.183.

Lee, T. B., & McKee, M. L. (2009). Mechanistic Study of LiNH2BH3 Formation from (LiH)4 + NH3BH3 and Subsequent Dehydrogenation. *Inorganic Chemistry, 48*(16), 7564-7575.

Ley, M. B., Jepsen, L. H., Lee, Y.-S., Cho, Y. W., Bellosta von Colbe, J. M., Dornheim, M., . . . Jensen, T. R. (2014). Complex hydrides for hydrogen storage – new perspectives. *Materials Today, 17*(3), 122-128.

Liang, G. (2004). Synthesis and hydrogen storage properties of Mg-based alloys. *Journal of Alloys and Compounds, 370*(1–2), 123-128.

Liu, T., Wang, C., & Wu, Y. (2014). Mg-based nanocomposites with improved hydrogen storage performances. *International Journal of Hydrogen Energy, 39*(26), 14262-14274.

López González, E., Isorna Llerena, F., Silva Pérez, M., Rosa Iglesias, F., & Guerra Macho, J. (2015). Energy evaluation of a solar hydrogen storage facility: Comparison with other electrical energy storage technologies. *International Journal of Hydrogen Energy, 40*(15), 5518-5525.

M. Martin, C. Gommel, C. Borkhart, & Fromm, E. (1996). Absorption and desorption kinetics of hydrogen storage alloys. *Journal of Alloys and Compounds, 238*(1-2), 193-201.

Ma, L.-J., Jia, J., Wu, H.-S., & Ren, Y. (2013). Ti–η2-(C2H2) and HCC–TiH as high capacity hydrogen storage media. *International Journal of Hydrogen Energy, 38*(36), 16185-16192.

Maeda, T., Fuura, T., Matsumoto, I., Kawakami, Y., & Masuda, M. (2013). Cyclic stability test of AB2 type (Ti, Zr)(Ni, Mn, V, Fe)2.18 for stationary hydrogen storage in water contaminated hydrogen. *Journal of Alloys and Compounds, 580, Supplement 1*(0), S255-S258.

Mao, J. (2011). Light metal hydrides for reversible hydrogen storage applications.

Mao, J., Guo, Z., & Liu, H. (2012). Enhanced hydrogen storage properties of NaAlH 4 co-catalysed with niobium fluoride and single-walled carbon nanotubes. *Rsc Advances, 2*(4), 1569-1576.

Marchenko, O. V., & Solomin, S. V. (2015). The future energy: Hydrogen versus electricity. *International Journal of Hydrogen Energy, 40*(10), 3801-3805.

Mohr, S. H., Wang, J., Ellem, G., Ward, J., & Giurco, D. (2015). Projection of world fossil fuels by country. *Fuel, 141*, 120-135.

Mori, D., & Hirose, K. (2009). Recent challenges of hydrogen storage technologies for fuel cell vehicles. *International Journal of Hydrogen Energy, 34*(10), 4569-4574.

Mosher, D. A., Arsenault, S., Tang, X., & Anton, D. L. (2007). Design, fabrication and testing of NaAlH4 based hydrogen storage systems. *Journal of Alloys and Compounds, 446–447*(0), 707-712.

Nakamori, Y., & Orimo, S.-i. (2004). Destabilization of Li-based complex hydrides. *Journal of Alloys and Compounds, 370*(1–2), 271-275.

Nam, J., Ko, J., & Ju, H. (2012). Three-dimensional modeling and simulation of hydrogen absorption in metal hydride hydrogen storage vessels. *Applied Energy, 89*(1), 164-175.

Nasrallah, S. B., & Jemni, A. (1997). Heat and mass transfer models in metal-hydrogen reactor. *International Journal of Hydrogen Energy, 22*(1), 67-76.

Nath, K., Najafpour, M. M., Voloshin, R. A., Balaghi, S. E., Tyystjärvi, E., Timilsina, R., . . . Allakhverdiev, S. I. (2015). Photobiological hydrogen production and artificial photosynthesis for clean energy: from bio to nanotechnologies. *Photosynthesis Research, 126*(2-3), 237-247.

Nickels, E. A., Jones, M. O., David, W. I. F., Johnson, S. R., Lowton, R. L., Sommariva, M., & Edwards, P. P. (2008). Tuning the Decomposition Temperature in Complex Hydrides: Synthesis of a Mixed Alkali Metal Borohydride. *Angewandte Chemie International Edition, 47*(15), 2817-2819.

Okada, M., Kuriiwa, T., Kamegawa, A., & Takamura, H. (2002). Role of intermetallics in hydrogen storage materials. *Materials Science and Engineering: A, 329–331*(0), 305-312.

Orgaz, E. (2001). The electronic structure of the Laves phase intermetallics LnM2 (Ln=Y, La–Lu, M=Mg, Al) and the LaMg2H7 and CeMg2H7 hydrides. *Journal of Alloys and Compounds, 322*(1–2), 45-54.

Orhan, M. F., & Babu, B. S. (2015). Investigation of an integrated hydrogen production system based on nuclear and renewable energy sources: Comparative evaluation of hydrogen production options with a regenerative fuel cell system. *Energy, 88*, 801-820.

Ouyang, L. Z., Cao, Z. J., Yao, L., Wang, H., Liu, J. W., & Zhu, M. (2014). Comparative investigation on the hydrogenation/dehydrogenation characteristics and hydrogen storage properties of Mg3Ag and Mg3Y. *International Journal of Hydrogen Energy, 39*(25), 13616-13621.

Paggiaro, R., Bénard, P., & Polifke, W. (2010). Cryo-adsorptive hydrogen storage on activated carbon. I: Thermodynamic analysis of adsorption vessels and comparison with liquid and compressed gas hydrogen storage. *International Journal of Hydrogen Energy, 35*(2), 638-647.

Palewski, T., Tristan, N. V., Drulis, H., & Ćwik, J. (2005). Hydrogenation process of the Gd3M (M = Ni or Co) intermetallics compound. *Journal of Alloys and Compounds, 404–406*(0), 584-587.

Pan, H., Liu, Y., Gao, M., Zhu, Y., & Lei, Y. (2003). The structural and electrochemical properties of La0.7Mg0.3(Ni0.85Co0.15)x (x=3.0–5.0) hydrogen storage alloys. *International Journal of Hydrogen Energy, 28*(11), 1219-1228.

Patil, S. D., & Ram Gopal, M. (2013). Analysis of a metal hydride reactor for hydrogen storage. *International Journal of Hydrogen Energy, 38*(2), 942-951.

Ponthieu, M., Fernández, J. F., Cuevas, F., Bodega, J., Ares, J. R., Adeva, P., & Sánchez, C. (2014). Thermodynamics and reaction pathways of hydrogen sorption in Mg6(Pd,TM) (TM = Ag, Cu and Ni) pseudo-binary compounds. *International Journal of Hydrogen Energy, 39*(32), 18291-18301.

Prigent, J., & Gupta, M. (2007). Ab initio study of the hydrogenation properties of Mg-based binary and ternary compounds Mg2X (X = Ni, Si) and YMgNi4. *Journal of Alloys and Compounds, 446–447*(0), 90-95.

Prigent, J., Joubert, J. M., & Gupta, M. (2012). Modification of the hydrogenation properties of LaNi5 upon Ni substitution by Rh, Ir, Pt or Au. *Journal of Alloys and Compounds, 511*(1), 95-100.

Principi, G., Agresti, F., Maddalena, A., & Lo Russo, S. (2009). The problem of solid state hydrogen storage. *Energy, 34*(12), 2087-2091.

Ravnsbæk, D., Filinchuk, Y., Cerenius, Y., Jakobsen, H. J., Besenbacher, F., Skibsted, J., & Jensen, T. R. (2009). A Series of Mixed-Metal Borohydrides. *Angewandte Chemie International Edition, 48*(36), 6659-6663.

Ross, D. K. (2006). Hydrogen storage: The major technological barrier to the development of hydrogen fuel cell cars. *Vacuum, 80*(10), 1084-1089.

Sai Raman, S. S., Davidson, D. J., Bobet, J. L., & Srivastava, O. N. (2002). Investigations on the synthesis, structural and microstructural characterizations of Mg-based K2PtCl6 type (Mg2FeH6) hydrogen storage material prepared by mechanical alloying. *Journal of Alloys and Compounds, 333*(1–2), 282-290.

Sakintuna, B., Lamaridarkrim, F., & Hirscher, M. (2007). Metal hydride materials for solid hydrogen storage: A review☆. *International Journal of Hydrogen Energy, 32*(9), 1121-1140.

Satheesh, A., & Muthukumar, P. (2010). Performance investigation of double-stage metal hydride based heat pump. *Applied Thermal Engineering, 30*(17–18), 2698-2707.

Schuth, F., Bogdanovic, B., & Felderhoff, M. (2004). Light metal hydrides and complex hydrides for hydrogen storage. *Chemical Communications*(20), 2249-2258.

Shao, H., Liu, T., Wang, Y., Xu, H., & Li, X. (2008). Preparation of Mg-based hydrogen storage materials from metal nanoparticles. *Journal of Alloys and Compounds, 465*(1–2), 527-533.

Sharma, S., & Ghoshal, S. K. (2015). Hydrogen the future transportation fuel: From production to applications. *Renewable and Sustainable Energy Reviews, 43,* 1151-1158.

Sharma, V. K., & Anil Kumar, E. (2014). Effect of measurement parameters on thermodynamic properties of La-based metal hydrides. *International Journal of Hydrogen Energy, 39*(11), 5888-5898.

Sherif, S. A., Barbir, F., & Veziroglu, T. N. (2005). Towards a Hydrogen Economy. *The Electricity Journal, 18*(6), 62-76.

Shinnar, R. (2003). The hydrogen economy, fuel cells, and electric cars. *Technology in Society, 25*(4), 455-476.

Smythe, N. C., & Gordon, J. C. (2010). Ammonia Borane as a Hydrogen Carrier: Dehydrogenation and Regeneration. *European Journal of Inorganic Chemistry, 2010*(4), 509-521.

Srinivasa Murthy, S., & Anil Kumar, E. (2014). Advanced materials for solid state hydrogen storage: "Thermal engineering issues". *Applied Thermal Engineering, 72*(2), 176-189.

Effects of catalysts doping on the thermal decomposition behavior of Zn(BH4)2. *International Journal of Hydrogen Energy, 33*(9), 2268-2272.

Srinivasan, S. S., Brinks, H. W., Hauback, B. C., Sun, D., & Jensen, C. M. (2004). Long term cycling behavior of titanium doped NaAlH4 prepared through solvent mediated milling of NaH and Al with titanium dopant precursors. *Journal of Alloys and Compounds, 377*(1–2), 283-289.

Tang, X., Opalka, S. M., Laube, B. L., Wu, F.-J., Strickler, J. R., & Anton, D. L. (2007). Hydrogen storage properties of Na–Li–Mg–Al–H complex hydrides. *Journal of Alloys and Compounds, 446–447*(0), 228-231.

Thomas, G. J., Gross, K. J., Yang, N. Y. C., & Jensen, C. (2002). Microstructural characterization of catalyzed NaAlH4. *Journal of Alloys and Compounds, 330–332*(0), 702-707.

Tietze, V., & Stolten, D. (2015). Comparison of hydrogen and methane storage by means of a thermodynamic analysis. *International Journal of Hydrogen Energy, 40*(35), 11530-11537.

Trevisani, L., Fabbri, M., Negrini, F., & Ribani, P. L. (2007). Advanced energy recovery systems from liquid hydrogen. *Energy Conversion and Management, 48*(1), 146-154.

Truskey, G. A., Yuan, F., & Katz, D. F. (2004). *Transport Phenomena in Biological Systems*: Pearson/Prentice Hall.

Varin, R. A., Czujko, T., & Wronski, Z. (2006). Particle size, grain size and γ-MgH 2 effects on the desorption properties of nanocrystalline commercial magnesium hydride processed by controlled mechanical milling. *Nanotechnology, 17*(15), 3856.

Vittetoe, A. W., Niemann, M. U., Srinivasan, S. S., McGrath, K., Kumar, A., Goswami, D. Y., . . . Thomas, S. (2009). Destabilization of LiAlH4 by nanocrystalline MgH2. *International Journal of Hydrogen Energy, 34*(5), 2333-2339.

Wang, K., Zhang, J.-G., & He, P. (2013). Theoretical study on the structure and dehydrogenation mechanism of mixed metal amidoborane, Na[Li(NH2BH3)]2. *Journal of Alloys and Compounds, 581*(0), 59-65.

Wang, P., & Kang, X.-d. (2008). Hydrogen-rich boron-containing materials for hydrogen storage. *Dalton Transactions*(40), 5400-5413.

Wang, Y., Adroher, X. C., Chen, J., Yang, X. G., & Miller, T. (2009). Three-dimensional modeling of hydrogen sorption in metal hydride hydrogen storage beds. *Journal of Power Sources, 194*(2), 997-1006.

Wang, Y., Zhao, M., & Wang, L. (2009). Effect of La–Mg-based alloy addition on structure and electrochemical characteristics of Ti0.10 Zr0.15V0.35Cr0.10Ni0.30 hydrogen storage alloy. *International Journal of Hydrogen Energy, 34*(6), 2646-2653.

Wiench, J. W., Balema, V. P., Pecharsky, V. K., & Pruski, M. (2004). Solid-state 27Al NMR investigation of thermal decomposition of LiAlH4. *Journal of Solid State Chemistry, 177*(3), 648-653.

Winter, C.-J. (2009). Hydrogen energy — Abundant, efficient, clean: A debate over the energy-system-of-change. *International Journal of Hydrogen Energy, 34*(14, Supplement 1), S1-S52.

Wu, Z., Yang, F., Bao, Z., Nyamsi, S. N., & Zhang, Z. (2013). Improvement in hydrogen storage characteristics of Mg-based metal hydrides by doping nonmetals with high electronegativity: A first-principle study. *Computational Materials Science, 78*(0), 83-90.

Xiong, Z., Wu, G., Hu, J., Liu, Y., Chen, P., Luo, W., & Wang, J. (2007). Reversible Hydrogen Storage by a Li–Al–N–H Complex. *Advanced Functional Materials, 17*(7), 1137-1142.

Yang, J., Sudik, A., Wolverton, C., & Siegel, D. J. (2010). High capacity hydrogen storage materials: attributes for automotive applications and techniques for materials discovery. *Chemical Society Reviews, 39*(2), 656-675.

Yang, S. J., Jung, H., Kim, T., & Park, C. R. (2012). Recent advances in hydrogen storage technologies based on nanoporous carbon materials. *Progress in Natural Science: Materials International, 22*(6), 631-638.

Yermakov, A. Y., Mushnikov, N. V., Uimin, M. A., Gaviko, V. S., Tankeev, A. P., Skripov, A. V., . . . Buzlukov, A. L. (2006). Hydrogen reaction kinetics of Mg-based alloys synthesized by mechanical milling. *Journal of Alloys and Compounds*, *425*(1–2), 367-372.

Young, M., Chang, S., Young, K., & Nei, J. (2013). Hydrogen storage properties of ZrVxNi3.5−x (x = 0.0–0.9) metal hydride alloys. *Journal of Alloys and Compounds, 580, Supplement 1*(0), S171-S174.

Zhang, J., Yan, S., Yu, L. P., Zhou, X. J., Zhou, T., & Peng, P. (2018). Enhanced hydrogen storage properties and mechanisms of magnesium hydride modified by transition metal dissolved magnesium oxides. *International Journal of Hydrogen Energy, 43*(48), 21864-21873.

Zhao, X., Zhou, J., Shen, X., Yang, M., & Ma, L. (2012). Structure and electrochemical hydrogen storage properties of A 2 B-type Ti–Zr–Ni alloys. *International Journal of Hydrogen Energy, 37*(6), 5050-5055.

Zheng, J., Liu, X., Xu, P., Liu, P., Zhao, Y., & Yang, J. (2012). Development of high pressure gaseous hydrogen storage technologies. *International Journal of Hydrogen Energy, 37*(1), 1048-1057.

Zhou, L., Zhou, Y., & Sun, Y. (2006). Studies on the mechanism and capacity of hydrogen uptake by physisorption-based materials. *International Journal of Hydrogen Energy, 31*(2), 259-264.

Zhu, Y., Yang, C., Zhu, J., & Li, L. (2011). Structural and electrochemical hydrogen storage properties of Mg2Ni-based alloys. *Journal of Alloys and Compounds, 509*(17), 5309-5314.

Züttel, A. (2003). Materials for hydrogen storage. *Materials Today, 6*(9), 24-33.

LIST OF PUBLICATIONS AND PAPERS PRESENTED

1. Rusman, N. A. A., & Dahari, M. (2016). A review on the current progress of metal hydrides material for solid-state hydrogen storage applications. *International Journal of Hydrogen Energy*, *41*(28), 12108-12126.